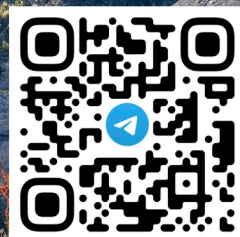


Mining Science and Technology

Горные науки
и технологии

Vol. **10** №4
Том **10** №4
2025



<https://mst.misis.ru/>

<https://t.me/MinSciTech>



Activities of the Mining Science and Technology (Russia) (Gornye nauki i tekhnologii) international journal are aimed at developing international scientific and professional cooperation in the field of mining.

The journal target audience comprises researchers, specialists in the field of mining, representatives of academic and professional communities.

The journal publishes original papers describing research findings, experience in the implementation of projects in mining industry, review publications.

The journal seeks to develop interdisciplinary areas that contribute to progress in mining, for example, technological and environmental safety, project organization and management in mining industry, development of territories, legal aspects of natural resource use, and other areas studied by researchers and practitioners. The journal always welcomes new developments. Papers are accepted in English or Russian.

EDITOR-IN-CHIEF

Vadim L. Petrov, Prof., Dr.Sci.(Eng.), University of Science and Technology MISIS, Moscow, Russian Federation

DEPUTIES EDITOR-IN-CHIEF

Oleg I. Kazanin, Prof., Dr.Sci.(Eng.), Empress Catherine II Saint Petersburg Mining University, St. Petersburg, Russian Federation

Svetlana A. Epshtein, Dr.Sci.(Eng.), University of Science and Technology MISIS, Moscow, Russian Federation

EDITORIAL BOARD

Zach Agioutantis, Prof., Ph.D., University of Kentucky, Lexington, Kentucky, USA

Maksim A. Bogdasarou, Prof., Dr.Sci.(Geol. and Min.), Brest State A. S. Pushkin University, Brest, Belarus

Grigory Yu. Boyarko, Prof. Dr. Sci. (Econ.), Cand. Sci. (Geol. and Miner.), National Research Tomsk Polytechnic University, Tomsk, Russian Federation

Xuan Nam Bui, Prof., Dr.Sci., Hanoi University of Mining and Geology, Duc Thang – Bac Tu Liem, Hanoi, Vietnam

Carsten Drebenstedt, Prof., Ph.D., Freiberg University of Mining and Technology, Freiberg, Germany

Faramarz Doulati Ardejani, Prof., Ph.D., Collodge of Engineering, University of Tehran, Tehran, Iran

Mikhail S. Ershov, Prof., Dr.Sci.(Eng.), National University of Oil and Gas "Gubkin University", Moscow, Russian Federation

Alexandr N. Evdokimov, Dr.Sci. (Geol. and Min.), Empress Catherine II Saint Petersburg Mining University, St. Petersburg, Russian Federation

Akper A. Feyzullaev, Prof., Dr.Sci.(Geol. and Min.), Institute of Geology and Geophysics of the National Academy of Sciences of Azerbaijan, Baku, Azerbaijan

Ochir Gerel, Prof., Dr.Sci.(Geol. and Min.), Geoscience Center, the Mongolian University of Science and Technology, Ulaanbaatar, Mongolia

Zoran Gligorić, Prof., Dr.Sci. (Mining-Underground Mining), University of Belgrade, Belgrade, Republic of Serbia

Monika Hardygora, Prof., Ph.D., Wroclaw University of Technology, Wroclaw, Poland

Nikolae Ilias, Prof., Dr.Sci.(Eng.), University of Petrosani, Petrosani, Romania

Ilya M. Indrupskiy, Prof., Dr. Sci. (Eng.), Oil and Gas Research Institute of the Russian Academy of Sciences (OGRI RAS), Moscow, Russian Federation

Vladislav Kecojevic, Prof., Ph.D., Benjamin M. Statler College of Engineering and Mineral Resources, West Virginia University, Morgantown, West Virginia, USA

Aleksey A. Khoreshok, Prof., Dr.Sci.(Eng.), Gorbachev Kuzbass State Technical University, Kemerovo, Russian Federation

Vladimir I. Klishin, Prof., Dr.Sci.(Eng.), Institute of Coal, Siberian Branch, Russian Academy of Sciences, Kemerovo, Russian Federation

Vladimir N. Koshelev, Prof., Dr.Sci.(Chem.), National University of Oil and Gas "Gubkin University" (Gubkin University), Moscow, Russian Federation

Jyant Kumar, Prof., Ph.D.-Geotech.Eng., Indian Institute of Science, Bengaluru, India

Vladimir A. Makarov, Prof., Dr.Sci.(Geol. and Min.), Siberian Federal University, Krasnoyarsk, Russian Federation

Sergey I. Malafeev, Prof., Dr.Sci.(Eng.), Vladimir State University named after Alexander and Nikolay Stoletovs, Vladimir, Russia

Oleg S. Misnikov, Prof., Dr.Sci.(Eng.), Tver State Technical University, Tver, Russian Federation

Valery V. Morozov, Prof., Dr.Sci.(Eng.), University of Science and Technology MISIS, Moscow, Russian Federation

Igor M. Petrov, Dr.Sci.(Eng.), Infomine Research Group LLC, Moscow, Russian Federation

Bakhadirzhan R. Raimzhanov, Prof., Dr.Sci.(Eng.), University of Science and Technology MISIS (branch), Almalyk, Uzbekistan

Bayan R. Rakishhev, Prof., Dr.Sci.(Eng.), Kazakh National Research Technical University named after K.I. Satpayev, Alma-Ata, Kazakhstan

Oscar Jaime Restrepo Baena, Prof., Ph.D., National University of Colombia, Medellín, Colombia

Alexander N. Shashenko, Prof., Dr.Sci.(Eng.), National Mining University, Dnipro, Ukraine

Vadim P. Tarasov, Prof., Dr.Sci.(Eng.), University of Science and Technology MISIS, Moscow, Russian Federation

Denis P. Tibilov, Prof., Dr.Sci.(Econ.), Moscow State Institute of International Affairs (University) under the Ministry of Foreign Affairs of Russia, Moscow, Russian Federation

Niyaz G. Valiev, Prof., Dr.Sci.(Eng.), The Ural State Mining University, Ekaterinburg, Russian Federation

Natalia Zhuravleva, Prof., Dr.Sci.(Eng.), West Siberian Testing Center JSC (WSTCenter JSC), Novokuznetsk, Russian Federation

Vera V. Yurak, Assoc. Prof., Dr. Sci. (Econ.), Ural State Mining University, Yekaterinburg; Institute of Economics, Ural Branch of the Russian Academy of Sciences, Yekaterinburg, Russian Federation

EDITORIAL COUNCIL

Yuri G. Agafonov, Assoc. Prof., Cand.Sci.(Eng.), University of Science and Technology MISIS, Moscow, Russian Federation

Michael R. Filonov, Prof., Dr.Sci.(Eng.), University of Science and Technology MISIS, Moscow, Russian Federation

Leonid A. Plaschansky, Prof., Cand.Sci.(Eng.), University of Science and Technology MISIS, Moscow, Russian Federation

Yuri I. Razorenov, Prof., Dr.Sci.(Eng.), Empress Catherine II Saint Petersburg Mining University, Saint Petersburg, Russian Federation

EXECUTIVE SECRETARY

Daria P. Galushka, University of Science and Technology MISIS, Moscow, Russian Federation

QUARTERLY

FOUNDED in 2016

REGISTRATION

The journal science and applied research journal is registered by the Federal Service for Communication, IT and Mass Communication Control on August 10, 2015.
Registration Certificate E-No. ФC77-62652

INDEXATION

Scopus, CAS, EBSCO, DOAJ, РИНЦ, ВИНТИ РАН, Dimensions, BASE, J-Gate, Jisc Library Hub Discover.

FOUNDER AND PUBLISHER



MISIS UNIVERSITY
MISIS University of Science and Technology

CONTACT

4 Leninsky Prospect, Moscow 119049, Russian Federation
Phone: +7 (495) 955-00-77
e-mail: send@misis.ru



This work is licensed under a
[Creative Commons Attribution 4.0 License](https://creativecommons.org/licenses/by/4.0/).



Деятельность научно-практического журнала «Горные науки и технологии» (Mining Science and Technology (Russia)) направлена на развитие международного научного и профессионального сотрудничества в области горного дела.

Целевая аудитория журнала – исследователи, специалисты в области горного дела, представители академического и профессионального сообществ.

В журнале публикуются оригинальные статьи, описывающие результаты исследований, опыт реализации проектов в горнопромышленном комплексе, обзорные публикации.

Журнал стремится развивать такие междисциплинарные направления, как технологическая и экологическая безопасность, организация и управление проектами в горной промышленности, развитие территорий, правовые аспекты использования природных ресурсов и другие, которые способствуют прогрессу в горном деле и реализуются исследователями и практиками.

ГЛАВНЫЙ РЕДАКТОР

Петров Вадим Леонидович, проф., д.т.н., Университет науки и технологий МИСИС, г. Москва, Российская Федерация

ЗАМЕСТИТЕЛИ ГЛАВНОГО РЕДАКТОРА

Казанин Олег Иванович, проф., д.т.н., Санкт-Петербургский горный университет императрицы Екатерины II, г. Санкт-Петербург, Российская Федерация

Эпштейн Светлана Абрамовна, д.т.н., Университет науки и технологий МИСИС, г. Москва, Российская Федерация

РЕДАКЦИОННАЯ КОЛЛЕГИЯ

Агиутантис Зак, проф., д-р наук, Университет Кентукки, г. Лексингтон, Кентукки, США

Богдасаров Максим Альбертович, проф., д.г.-м.н., Брестский государственный университет им. А.С. Пушкина, г. Брест, Беларусь

Боярко Григорий Юрьевич – проф., д.э.н., к.г.-м.н., Национальный исследовательский Томский политехнический университет, г. Томск, Российская Федерация

Буи Суан Нам, проф., д-р наук, Ханойский университет горного дела и технологии, г. Ханой, Вьетнам

Валиев Нияз Гадым оглы, проф., д.т.н., Уральский государственный горный университет, г. Екатеринбург, Российская Федерация

Герел Очир, проф., д.г.-м.н., Центр геолого-геофизических исследований, Монгольский университет науки и технологии, г. Улан-Батор, Монголия

Глигорич Зоран, проф., д-р наук, Белградский университет, г. Белград, Республика Сербия

Дребенштедт Карстен, проф., д-р наук, Технический университет Фрайбергская горная академия, г. Фрайберг, Германия

Дулати Ардежани Фарамарз, проф., д-р наук, Инженерный колледж, Тегеранский университет, г. Тегеран, Иран

Евдокимов Александр Николаевич, проф., д.г.-м.н., Санкт-Петербургский горный университет императрицы Екатерины II, г. Санкт-Петербург, Российская Федерация

Ершов Михаил Сергеевич, проф., д.т.н., Российский государственный университет нефти и газа (национальный исследовательский университет) им. И.М. Губкина, г. Москва, Российская Федерация

Журавлева Наталья Викторовна, проф., д.т.н., АО «Западно-Сибирский испытательный центр» (АО «ЗСИЦентр»), г. Новокузнецк, Российская Федерация

Илиаш Николае, проф., д.т.н., Университет Петрошани, г. Петрошани, Румыния

Индрупский Илья Михайлович, проф., д.т.н., Институт проблем нефти и газа Российской академии наук, г. Москва, Российская Федерация

Кецоджевич Владислав, проф., д-р наук, Институт инженерного дела и минеральных ресурсов им. Бенджамина М. Статлера Университета Западной Вирджинии, г. Моргантаун, Западная Вирджиния, США

Клишин Владимир Иванович, проф., д.т.н., Институт угля Сибирского отделения Российской академии наук, г. Кемерово, Российская Федерация

Кошелев Владимир Николаевич, проф., д.х.н., Российский государственный университет нефти и газа им. И.М. Губкина, г. Москва, Российская Федерация

Кумар Джьянт, проф., д-р наук (геотехнический инжиниринг), Индийский институт науки (Indian Institute of Science), г. Бангалор, Индия

Макаров Владимир Александрович, проф., д.г.-м.н., Сибирский федеральный университет, г. Красноярск, Российская Федерация

Малафеев Сергей Иванович, проф., д.т.н., Владимирский государственный университет имени А.Г. и Н.Г. Столетовых, г. Владимир, Российская Федерация

Мисников Олег Степанович, проф., д.т.н., Тверской государственный технический университет, г. Тверь, Российская Федерация

Морозов Валерий Валентинович, проф., д.т.н., Университет науки и технологий МИСИС, г. Москва, Российская Федерация

Петров Игорь Михайлович, д.т.н., ООО «Исследовательская группа «Инфомай»», г. Москва, Российская Федерация

Раимжанов Бахадиржан Раимжанович, проф., д.т.н., филиал Университета науки и технологий МИСИС, г. Алматы, Узбекистан

Ракишев Баян Ракишевич, проф., д.т.н., Казахский национальный исследовательский технический университет им. К.И. Сатпаева, г. Алма-Ата, Казахстан

Рестрепо Баэна Оскар Хайме, проф., д-р наук, Национальный университет Колумбии, г. Медельин, Колумбия

Тарасов Вадим Петрович, проф., д.т.н., Университет науки и технологий МИСИС, г. Москва, Российская Федерация

Тибилов Денис Петрович, проф., д.э.н., Московский государственный институт международных отношений (Университет) Министерства иностранных дел России, г. Москва, Российская Федерация

Фейзуллаев Акпер Акпер оглы, проф., д.г.-м.н., Институт геологии и геофизики (ИГГ) Национальной Академии Наук Азербайджана, г. Баку, Азербайджан

Хорешок Алексей Алексеевич, проф., д.т.н., Кузбасский государственный технический университет им. М.С. Горбачева, г. Кемерово, Российская Федерация

Шашенко Александр Николаевич, проф., д.т.н., Национальный горный университет, г. Днепр, Украина

Хардигора Моника, проф., д-р наук, Вроцлавский технологический университет, г. Вроцлав, Польша

Юрак Вера Васильевна, доц., д.э.н., Уральский государственный горный университет, г. Екатеринбург; старший научный сотрудник, Институт экономики Уральского отделения Российской академии наук (ИЭ УрО РАН), г. Екатеринбург, Российская Федерация

РЕДАКЦИОННЫЙ СОВЕТ

Агафонов Юрий Григорьевич, доц., к.т.н., Университет науки и технологий МИСИС, г. Москва, Российская Федерация

Плещанский Леонид Александрович, проф., к.т.н., Университет науки и технологий МИСИС, г. Москва, Российская Федерация

Разоренов Юрий Иванович, проф., д.т.н., Санкт-Петербургский горный университет императрицы Екатерины II, г. Санкт-Петербург, Российская Федерация

Филонов Михаил Рудольфович, проф., д.т.н., Университет науки и технологий МИСИС, г. Москва, Российская Федерация

ОТВЕТСТВЕННЫЙ СЕКРЕТАРЬ

Галушка Дарья Петровна, Университет науки и технологий МИСИС, г. Москва, Российская Федерация

ПЕРИОДИЧНОСТЬ 4 раза в год

ОСНОВАН в 2016 году

РЕГИСТРАЦИЯ

Зарегистрирован Федеральной службой по надзору в сфере связи, информационных технологий и массовых коммуникаций 10 августа 2015 года.

Свидетельство о регистрации Эл № ФС77-62652.

ИНДЕКСИРОВАНИЕ

Scopus, CAS, EBSCO, DOAJ, РИНЦ, ВИНТИ РАН, Dimensions, BASE, J-Gate, Jisc Library Hub Discover.

OPEN ACCESS Журнал открытого доступа.

УЧРЕДИТЕЛЬ И ИЗДАТЕЛЬ



МИСИС
УНИВЕРСИТЕТ
НАУКИ И ТЕХНОЛОГИЙ

Университет науки и технологий
МИСИС

АДРЕС УЧРЕДИТЕЛЯ И ИЗДАТЕЛЯ

119049, г. Москва, Ленинский проспект, д. 4

КОНТАКТЫ РЕДАКЦИИ

Адрес: 119049, г. Москва, Ленинский проспект, д. 4

телефон: +7 (495) 955-00-77

e-mail: send@misis.ru



Контент доступен под лицензией
Creative Commons Attribution 4.0 License.



CONTENTS

MINERAL RESOURCES EXPLOITATION

Justification of the prospects for developing gas-bearing sites in the Karaganda coal basin 321

R. A. Mussin, N. A. Nemova, D. R. Akhmatnurov, N. M. Zamaliyev, E. D. Reshetnyakov, A. V. Reznik

Justification of the rational scope and technology for the use of hydraulic excavators
in surface mining..... 338

V. A. Khakulov, V. A. Shapovalov, V. N. Ignatov, Zh. V. Karpova, M. V. Ignatov, I. A. Nogerov

Identification of remaining oil reserves at the late stage of development
of the Gilbert field using integrated geophysical data 346

I. I. Bosikov, R. V. Klyuev, I. V. Silaev

DIGITAL TECHNOLOGIES AND ARTIFICIAL INTELLIGENCE

Comprehensive study of the anisotropy of microstructural and filtration properties
of a gas condensate field reservoir based on digital core analysis 357

V. V. Khimulia

ENVIRONMENTAL PROTECTION

Impact of tin ore mining on the streamflow of small rivers in mining regions 369

N. K. Rastanina, D. A. Golubev, N. A. Kayumov, P. L. Rastanin, I. A. Popadyev

BENEFICIATION AND PROCESSING OF NATURAL AND TECHNOGENIC RAW MATERIALS

Regulation of the oil receptivity of the surface of diamonds and kimberlite minerals
using various classes of regulating agents..... 379

V. A. Chanturiya, V. V. Morozov, E. L. Chanturiya, A. L. Samusev

POWER ENGINEERING, AUTOMATION, AND ENERGY PERFORMANCE

Integration of digital technologies into the design process of power supply systems
for mining enterprises 393

V. L. Petrov, E. K. Burmatova, A. V. Pichuev



СОДЕРЖАНИЕ

РАЗРАБОТКА МЕСТОРОЖДЕНИЙ ПОЛЕЗНЫХ ИСКОПАЕМЫХ

- Обоснование перспективности отработки газоносных участков
Карагандинского угольного бассейна 321
Р.А. Мусин, Н.А. Немова, Д.Р. Ахматнуров, Н.М. Замалиев, Э.Д. Решетняков, А.В. Резник

ГЕОЛОГИЯ МЕСТОРОЖДЕНИЙ ПОЛЕЗНЫХ ИСКОПАЕМЫХ

- Обоснование рациональной области и технологии применения
гидравлических экскаваторов на открытых горных работах 338
В.А. Хакулов, В.А. Шаповалов, В.Н. Игнатов, Ж.В. Карпова, М.В. Игнатов, И.А. Ногеров
- Локализация остаточных запасов нефти на поздней стадии разработки
Гильбертского месторождения по данным комплекса геофизических исследований 346
И.И. Босиков, Р.В. Клюев, И.В. Силаев

СВОЙСТВА ГОРНЫХ ПОРОД. ГЕОМЕХАНИКА И ГЕОФИЗИКА

- Комплексное исследование анизотропии микроструктурных и фильтрационных свойств
коллектора газоконденсатного месторождения на базе цифрового анализа керна 357
В.В. Химуля

ОХРАНА ОКРУЖАЮЩЕЙ СРЕДЫ

- Влияние добычи оловорудного сырья на речной сток малых рек
горнопромышленных районов 369
Н.К. Растанина, Д.А. Голубев, Н.А. Каюмов, П.Л. Растанин, И.А. Попадъёв

ОБОГАЩЕНИЕ, ПЕРЕРАБОТКА МИНЕРАЛЬНОГО И ТЕХНОГЕННОГО СЫРЬЯ

- Регулирование олеофильности поверхности алмазов и минералов кимберлита
добавками реагентов-регуляторов различных классов 379
В.А. Чантурия, В.В. Морозов, Е.Л. Чантурия, А.Л. Самусев

ЭНЕРГЕТИКА, АВТОМАТИЗАЦИЯ И ЭНЕРГОЭФФЕКТИВНОСТЬ

- Интеграция цифровых технологий в процесс проектирования систем электроснабжения
горнопромышленных предприятий 393
В.Л. Петров, Е.К. Бурматова, А.В. Пичуев



MINERAL RESOURCES EXPLOITATION

Review paper

<https://doi.org/10.17073/2500-0632-2025-06-425>

UDC 622.271




Justification of the prospects for developing gas-bearing sites in the Karaganda coal basin

R. A. Mussin¹  , N. A. Nemova²   , D. R. Akhmatnurov¹  , N. M. Zamaliyev¹ ,
E. D. Reshetnyakov¹ , A. V. Reznik² 

¹ Abylka Saginov Karaganda Technical University, Karaganda, Republic of Kazakhstan

² N. A. Chinalak Institute of Mining of the Siberian Branch of the Russian Academy of Sciences, Novosibirsk, Russian Federation

 fpvgn@misd.ru

Abstract

The relevance of this study is due to the current need to meet energy resources demand. A promising option worth considering is the production of methane gas from unconventional resources, whose reserves significantly exceed those of conventional deposits. Objective: to evaluate gas-bearing sites and justify the principles for rating their prospects based on an analysis of geological and technological factors affecting the process of gas release from coal seams. To achieve this goal, the study examined the Karaganda coal basin as a promising district for methane gas extraction, divided into five sites: Tenteksky, Saransky, Promyshlenny, Sherubainurinsky, Taldykudusky. The most gas-bearing seams (reservoirs), with depth of occurrence ranging from 420 to 635 m, were studied. As a result of the study, first- and second-level coal seam zones were identified for methane extraction from coal seams. The parameters used to identify these zones were: depth of occurrence, permeability, and desorption of coal in a seam. At a depth of 250–300 m, gas permeability of the seams was recorded within the range of 10–15 millidarcy (mD). It was established that gas permeability decreases with increasing depth, and at a depth of 600–700 m, it amounts to hundredths and thousandths of a millidarcy. To determine the gas content of coal seams, representative samples were taken to characterize the gas content of coal seams from K_{20} to K_1 across the entire area of the mining allotment under investigation. Sites in fault zones were not considered. They are classified as unrepresentative due to gas losses exceeding 30%. It has been established that the increase in gas content (methane content) in the Karaganda basin follows the ascending branch of a S-shaped curve and is described by the Langmuir equation. Methane resources in all host rocks have been determined based on a minimum methane content of 1 m³/t, and in claystones and siltstones with disseminated coal inclusions, based on a methane content of 4–5 m³/t of rock. At the same time, it has been established that in order to make a rough estimate of the resources, it is necessary to have data on total and effective porosity, water saturation of sandstones, and other factors. For the first time in the Karaganda coal basin, an integrated system for assessment of sites in terms of the potential of methane extraction has been implemented, incorporating more than 10 factors. Unlike previous studies, where assessments were made based on individual characteristics (depth, gas content, permeability), this paper proposes a generalized scoring method that allows for quantitative comparison of sites and prediction of methane production performance. Besides, the study novelty comprises the dependencies of Langmuir coefficients on fusinite content and temperature established in the study, which had not previously been applied to local coals. During the study, first- and second-order zones were identified in terms of methane production prospects; quantitative dependencies of gas content on depth, coal rank (stage of maturation), and petrographic composition were established; sites with the greatest commercial production potential were identified, and a methodology for the criterion-based assessment of sites was developed.

Keywords

coal deposit, coal seams, gas, methane, reserves, methane content, gas content, degassing, permeability, desorption, sorption, testing, samples, experiment, simulation, Langmuir equation, Kazakhstan, Karaganda coal basin

Financing

The research was funded by the Science Committee of the Ministry of Science and Higher Education of the Republic of Kazakhstan as part of targeted funding for the implementation of scientific and technical program IRN No. BR24993009.


For citation

Mussin R. A., Nemova N. A., Akhmatnurov D. R., Zamaliyev N. M., Reshetnyakov E. D., Reznik A. V. Justification of the Prospects for developing gas-bearing sites in the Karaganda coal basin *Mining Science and Technology (Russia)*. 2025;10(4):321–337. <https://doi.org/10.17073/2500-0632-2025-06-425>



РАЗРАБОТКА МЕСТОРОЖДЕНИЙ ПОЛЕЗНЫХ ИСКОПАЕМЫХ

Обзорная статья

**Обоснование перспективности отработки газоносных участков
Карагандинского угольного бассейна****Р.А. Мусин¹  , Н.А. Немова²   , Д.Р. Ахматнуров¹  , Н.М. Замалиев¹ ,
Э.Д. Решетняков¹ , А.В. Резник² **¹ Карагандинский технический университет имени Абылкаса Сагинова, г. Караганда, Республика Казахстан² Институт горного дела имени Н.А. Чинакала СО РАН, г. Новосибирск, Российская Федерация fpvgn@misd.ru**Аннотация**

Актуальность данного исследования обусловлена тем, что в настоящее время есть необходимость восполнения потребностей энергоресурсов. Одним из перспективных вариантов стоит рассматривать добычу газа метана из нетрадиционных источников, запасы которых значительно превышают запасы традиционных месторождений. Цель: провести оценку газоносных участков и обосновать принципы рейтингования их перспективности на основе анализа геолого-технологических факторов, влияющих на процесс газовыделения из угольных пластов. Для достижения указанной цели в исследовании рассмотрен Карагандинский угольный бассейн как перспективный по добыче газа метана, разделенный на 5 участков: Тентекский, Саранский, Промышленный, Шерубайнуринский, Талдыкудукский. Исследованы наиболее газоносные пласты, имеющие глубину залегания от 420 до 635 м. В результате исследования были определены зоны угольных пластов первого и второго уровня для добычи метана из угольных пластов. Обоснованными параметрами выделения этих зон являются: глубина залегания, проницаемость и десорбция угля в пласте. На глубине 250–300 м была зафиксирована газопроницаемость пластов в пределах 10–15 мД, при этом установлено, что с увеличением глубины происходит уменьшение газопроницаемости, и на уровне 600–700 м она составляет сотые и тысячные доли миллидарси. Для определения газоносности угольных пластов были отобраны представительные пробы, характеризующие газоносность углей пластов от K_{20} до K_1 на всей площади исследуемого участка горного отвода. Не рассматривались участки в зоне геологических нарушений. Они отнесены к непредставительным из-за большей, чем 30 %, потери газа. Было установлено, что увеличение газоносности (метаноносности) в Карагандинском бассейне происходит по восходящей ветви S-образной кривой и описывается уравнением Ленгмюра. Определены ресурсы метана во всех вмещающих породах по минимальной метаноносности, равной 1 м³/т, а в аргиллитах и алевролитах с включениями рассеянного угольного вещества – со значением метаноносности 4–5 м³/т породы. При этом установлено, что для примерной оценки ресурсов необходимо иметь данные по общей и эффективной пористости, обводненности песчаников, а также другим факторам. Впервые для Карагандинского угольного бассейна реализована система интегральной оценки перспективности участков по добыче метана, включающая более 10 факторов. В отличие от предыдущих исследований, где оценка проводилась по отдельным признакам (глубина, газоносность, проницаемость), в настоящей работе предложена обобщенная балльная методика, позволяющая количественно сравнивать участки и прогнозировать эффективность метанодобычи. Также новыми являются установленные в исследовании зависимости коэффициентов Ленгмюра от содержания фузинита и температуры, что ранее не применялось для местных углей. В ходе исследования: определены зоны первого и второго порядка по перспективности разработки метана, установлены количественные зависимости газоносности от глубины, стадии метаморфизма, петрографического состава, выявлены участки с наибольшим потенциалом промышленной добычи, разработана методика критериальной оценки участков.

Ключевые слова

угольное месторождение, угольные пласты, газ, метан, запасы, метаноносность, газоносность, дегазация, проницаемость, десорбция, сорбция, испытания, пробы, эксперимент, моделирование, уравнение Ленгмюра, Казахстан, Карагандинский угольный бассейн

Финансирование

Исследование профинансировано Комитетом науки Министерства науки и высшего образования Республики Казахстан в рамках программно-целевого финансирования по реализации научной, научно-технической программы ИРН № BR24993009.

Для цитирования

Mussin R.A., Nemova N.A., Akhmatnurov D.R., Zamaliyev N.M., Reshetnyakov E.D., Reznik A.V. Justification of the Prospects for developing gas-bearing sites in the Karaganda coal basin *Mining Science and Technology (Russia)*. 2025;10(4):321–337. <https://doi.org/10.17073/2500-0632-2025-06-425>

Introduction

Currently, Kazakhstan's fuel and energy sector is facing the problem of depletion of hydrocarbon reserves such as natural gas and oil. In addition to the constantly deteriorating conditions for extraction, the structure of existing reserves is also changing, i.e., the share of hard-to-recover reserves is growing. For example, global natural gas resources are already unable to meet the needs of the population, as the most accessible (easily extractable) deposits are largely depleted. At the same time, China, the United States, and Russia are the leaders in terms of primary energy production (according to Enerdata, 2024). Natural gas, crude oil, uranium, and coal constitute the main share of extracted natural resources. Meanwhile, coal accounts for the largest share, 15.9 billion tonnes of oil equivalent, followed by uranium, 10.3 billion tonnes of oil equivalent, while oil accounts for the smallest share, 5.2 billion tonnes of oil equivalent, followed by natural gas, 3.5 billion tonnes of oil equivalent.

Fig. 1 shows global reserves (a) and production volumes (b) of natural gas at the beginning of 2023, estimated by OPEC at 207.9 trillion m³. At the same time, according to the US Energy Information Administration, global oil reserves amounted to 1.7 trillion barrels as of 2023. However, energy needs can be met by extracting methane gas from unconventional sources, whose reserves significantly exceed those of conventional deposits. According to the International Energy Agency, global coal production in 2033 will amount to 8.7 billion tons, with reserves of hard coal at 9.5 trillion tons and those of lignite at 4.9 trillion tons. The presence of significant reserves indicates the presence of large amounts of methane in the subsoil, which mean that projects for their assessment and subsequent extraction may prove promising (Fig. 1, c, d). At the same time, according to data from the International Energy Agency, global methane production from coal seams could reach 200 billion m³ by 2035.

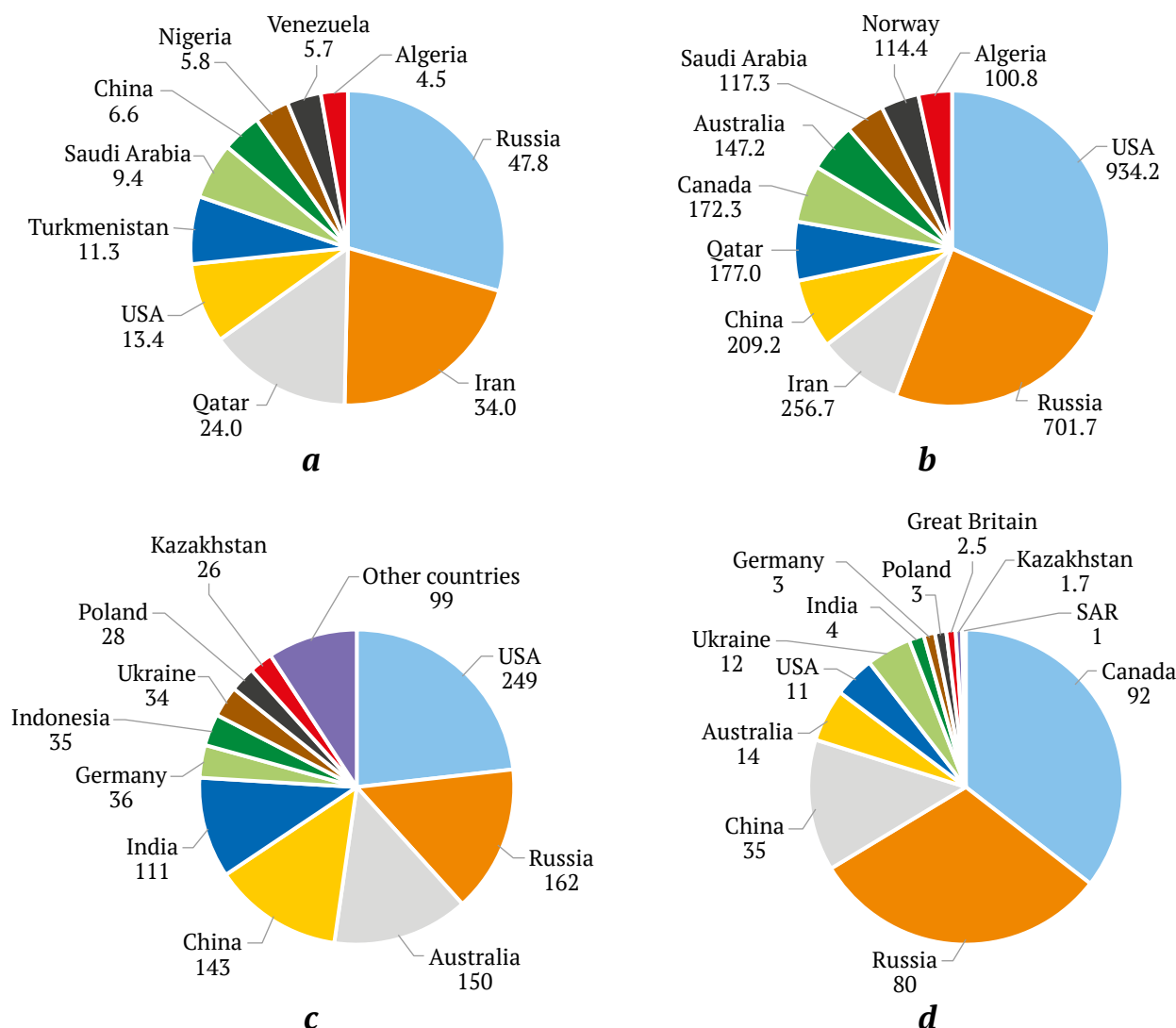


Fig. 1. World reserves as of 2023: a – natural gas, trillion m³; b – natural gas production volumes, billion m³; c – coal, billion t; d – coal seam methane, trillion m³



Statistical reports from IEA¹ also show that global predicted reserves of gas from unconventional sources exceed those in conventional deposits by 2.2 times, with Canada, Russia, and the US leading in terms of the reserves, and the US leading in terms of production².

Unconventional gas reserves significantly exceed those of conventional deposits and, according to data from the International Energy Agency³, amount to 921 trillion m³. Meanwhile, the volume of methane in coal seams worldwide is estimated at 256 trillion m³, which accounts for more than 19% of total gas resources (Table 1).

Various techniques for extracting methane from coal seams are being used quite successfully in certain countries [2, 3]. Practically all over the world, coal seam methane (CSM) extraction has become strategically important both in the context of preliminary (advance) degassing of methane-bearing seams to improve mining safety and as an independent area of subsoil use – the extraction of unconventional hydrocarbons, namely coal seam methane.

Problem definition

For a long time, methane contained in coal seams was considered a harmful factor that reduced the performance of coal mining. A significant portion of the costs associated with organizing coal mining is directed toward creating safe working conditions. This includes the costs of measures to monitor the gas conditions in a mine, ventilate mine workings, purchase equipment to suppress dust and ensure explosion safety, emergency monitoring and warning systems, search and rescue equipment, communication equipment and alarms, as well as degassing of coal-rock mass. Equally important are the costs of operating drainage, electricity, water, and heating systems, purchasing specialized transport, tools, and materials for safe blasting, and other measures. It should be noted that coal seam degassing opens up the feasibility of using methane as a by-product natural resource⁴. To date, in order to improve the environmental situation and reduce methane emissions into the environment,

it is necessary to extract methane from coal seams by means of advance degassing. It should also be noted that methane entering the atmosphere leads to the destruction of the ozone layer, and its annual accumulation in the atmosphere is 1–2%, which exceeds the accumulation rate of other gases. However, methane is a good unconventional energy source and can be considered as a component of the country's fuel and energy raw material base. Given that global predicted reserves of coal seam methane (in coal formations) account for more than 19% of total gas reserves and exceed its availability in conventional deposits by 2.2 times, it is necessary to conduct a resource estimation of the gas-bearing sites of the Karaganda coal basin and justify the rating of the prospectivity of these sites based on an analysis of geological and technological factors affecting the process of gas release from coal seams that is the purpose of this study.

In this regard, the following tasks were set: to analyze the current state and global experience in the field of methane extraction from coal seams; to investigate the methane content of coal seams in the Karaganda basin, taking into account the depth of occurrence, geological structure, and coal rank (stage of coal maturation); to establish dependencies between the geological and petrographic characteristics of coal and methane content parameters based on sorption isotherms; to determine, based on the results of pilot-plant tests, the influence of a number of geological and technological factors characterizing the prospects of the sites on methane recoverability; justify the rating of the prospects of the sites based on the established criteria and a scoring system for key indicators; determine the first and second order sites in terms of methane production prospects, taking into account integral indicators.

Table 1

Structure of global gas resources [1]

Types of gas resources	Volume of gas resources, trillion m ³	Shares of gas resources by type, %
1. Conventional gas resources	405	30.54
2. Unconventional gas resources	921	69.46
2.1. Tight sandstone gas	209	15.76
2.2. Coal seam methane	256	19.31
2.3. Shale gas	456	34.39
Total gas resources	1,326	100.00

¹ International Energy Agency, World Energy Outlook. 2023.

² Coal bed methane: Prospects for the development of unconventional hydrocarbons in the CIS. 2011. URL: <https://gaap.ru/articles/Metan-ugolnyh-plastov/>

³ International Energy Agency, World Energy Outlook. 2023.

⁴ Jaireth S., Huleatt M.B. Australian in situ coal resources. Geoscience Australia, Canberra; 2012. URL: <http://pid.geoscience.gov.au/dataset/ga/74097>

Research methodology and objects

1. Research methodology

This study used a set of methods tested and approved in international and domestic practice for studying the gas content of coal seams, including: direct desorption analysis (canister test) to assess actual gas content, construction of sorption isotherms based on the Langmuir model, and petrographic analysis of coals with the determination of vitrinite and fusinite.

Unlike existing approaches, in which the potential of sites is determined on the basis of individual parameters (depth, gas content, permeability), this study uses an integrated methodology developed earlier by the authors, combining 10 key factors that influence methane content and commercial methane recoverability.

The research methodology includes a comprehensive assessment of the gas content of coal seams based on direct desorption analysis (canister test), determination of sorption kinetic parameters using the Langmuir equation, and petrographic analysis of coal. All methods have been tested and approved in international and domestic practice [4–6] and applied at the pilot-plant testing stage at five sites in the Karaganda basin. The novelty of the approach lies in the integrated criterion-based assessment of sites, taking into account a combination of factors: permeability, moisture content, sorption characteristics, volatile-matter yield, and gas pressure. These parameters were used together for the first time to rank sites for the conditions of this basin.

To determine gas content, the desorption method of investigation was used, the canister test, which is used both internationally and in Russia [7]. This choice was based on the possibility of quantitative determining the volume of desorbable and residual gas under various thermobaric conditions that is particularly important for coals from the Karaganda basin of different stage of maturation (coal rank). This method involves sampling coal core from coal seams using removable KG-55 core gas samplers in exploration wells, using a control calculation method, forecasting the methane content of coal seams based on petrographic composition data. Next, gas was extracted from a gas collector, the core receiver with the coal core sample was separated from the core gas sampler and sealed with plugs. After that, the coal core samples were placed into a thermostat set to a temperature equal to the temperature of the seam from which the samples were taken. The volume of desorbed gas was determined using a measuring cylinder and residual gas in coal under three degassing modes until complete gas extraction: first, at a temperature of 60–90 °C, second, during thermal vacuuming with heating to 60–90 °C, and third, after crushing a sample in a ball mill at 60–90 °C and vacuuming. The total gas content was determined as the sum of the volumes of lost, desorbed, and residual gas. The stages of the workflow for determining the volume of desorbed gas are shown in Fig. 2.

Langmuir isotherms, traditionally used in Coal-Seam Methane (CSM) deposit studies, were used to

**a****b****c**

Fig. 2. Geokrak desorption unit (Poland): *a* – container for collecting samples K01; *b* – installation for creating formation temperature; *c* – gas release recording device

analyze the sorption capacity of coals⁵. The authors' contribution lies in refining the coefficients of the Langmuir equation for coal seams in the Karaganda basin based on laboratory data, taking into account temperature conditions and petrographic composition (in particular, the contents of fusinite and vitrinite). The proposed approach for the first time integrates desorption, permeability, moisture content, maturation, and petrographic parameters of coal into a single scoring system for comprehensive assessment of site potential that is a development of approaches previously described in [8, 9].

2. Sampling

Samples were taken from the study sites with the most gas-bearing seams, which were considered to be representative of the sites. At various depths and several times for the accuracy of the studies conducted to determine the effect of the depth of a seam occurrence on its permeability, samples were taken at the following sites: Tenteksky, with sampling depths of 450, 470, 500 m, Saransky, sampled from 600, 620, 635 m, Promyshlenny, from 460, 480, 500 m, Sherubainurinsky, 420, 435, 440 m, and Taldykudusky, 460, 475, 500 m.

All laboratory studies (analyses and tests) were conducted at the Abylbas Saginov Karaganda Technical University (Karaganda, Kazakhstan).

3. Laboratory research

The whole set of sample processing involved determination of gas composition, technical analysis of samples (A_d , W , V_{daf}), calculation of methane content (CH_4 + heavy hydrocarbons) was carried out in laboratory conditions. A total of 107 representative samples were selected from 59 seam intersections. The largest number of samples came from the thickest seams: K18, K12, K10, and D6. The results of the laboratory investigations are shown in Table 2 and demonstrate the amount of desorbed methane in the selected samples. The highest values were found in the samples from the Dolinskaya formation that is connected with the stage of coal maturation (coal rank).

A detailed description of these methods is not provided in the paper, as they are widely recognized in professional circles. Instead, emphasis is placed on refining the parameters of the Langmuir equation and adapting the methods to the conditions of the Karaganda basin.

⁵ Pashin J.C. Geologic heterogeneity and coalbed methane production – experience from the Black Warrior Basin. In: Selected Presentations on Coalbed Gas in the Eastern United States. U.S. Geological Survey Open-File Report 2004-1273. Pp. 61–92; Jaireth S., Huleatt M.B. Australian in situ coal resources. Geoscience Australia, Canberra; 2012. URL: <http://pid.geoscience.gov.au/dataset/ga/74097>

Table 2

Results of methane desorption from coal seams

Sample number	Seam	Initial pressure, MPa	Volume of desorbed methane, cm ³ /g	Temperature, °C	Time to peak desorption, hours
K ₁₈₋₁	K ₁₈	1.98	5.22	18.8	8.0
K ₁₈₋₂	K ₁₈	1.46	7.62	22.7	9.2
K ₁₈₋₃	K ₁₈	1.94	5.99	18.1	14.1
K ₁₈₋₄	K ₁₈	1.61	6.79	21.1	6.5
K ₁₈₋₅	K ₁₈	2.3	8.29	20.2	8.9
K ₁₂₋₁	K ₁₂	1.4	7.05	18.8	14.8
K ₁₂₋₂	K ₁₂	2.48	6.04	22.5	13.1
K ₁₂₋₃	K ₁₂	2.02	6.91	20.2	12.2
K ₁₂₋₄	K ₁₂	2.03	7.65	20.2	12.2
K ₁₂₋₅	K ₁₂	1.53	7.09	20.8	11.7
K ₁₀₋₁	K ₁₀	1.38	6.01	21.1	12.4
K ₁₀₋₂	K ₁₀	1.66	5.52	20.0	6.0
K ₁₀₋₃	K ₁₀	2.42	5.72	18.5	13.6
K ₁₀₋₄	K ₁₀	2.34	8.37	22.6	9.5
K ₁₀₋₅	K ₁₀	1.98	5.82	22.8	11.7
D ₆₋₁	D ₆	1.75	5.08	21.9	12.7
D ₆₋₂	D ₆	2.1	5.05	20.5	10.4
D ₆₋₃	D ₆	2.04	7.65	20.9	14.6
D ₆₋₄	D ₆	2.18	8.45	21.6	10.6
D ₆₋₅	D ₆	1.36	6.18	22.8	11.8

Analysis of methods for identifying promising sites in countries around the world which extract methane

Many different approaches are proposed for identifying promising sites for methane extraction, one of which is computer modeling of a deposit. For these purposes, a deposit is divided into small areas, which then are compared with each other in a number of characteristics. This method is discussed in more detail in [10]. Its essence lies in a multi-stage analysis of the prospectivity of territories for coal seam methane extraction. The method includes the following main stages: *division* of a deposit into sites – geological and structural zoning of the territory is carried out, with identifying blocks with different geological and geophysical characteristics; *determination* of site parameters – assessment of gas content, permeability, coal seam thickness, depth, degree of fracturing, and other criteria affecting methane recoverability; *selection* of sites suitable for commercial development based on a combination of technical, technological, and economic parameters; *ranking* by level of prospectivi-



ty – sites are classified according to drilling priority based on an integral prospectivity index; *making drilling decisions* – based on the assessments obtained, operating procedure for drilling methane producing wells is formed and their key characteristics (depth, design, flow rate, etc.) are determined; *assessment* of integral methane recoverability – potential methane extraction volumes are calculated by mine field; *analysis* of financial viability – the economic effects of planned coal seam methane production are assessed, taking into account capital and operating costs. This approach allows for well-founded planning of degassing measures, increased performance of commercial methane production, and minimization of geological and economic risks.

In [11], a method for identifying promising sites (“gas domes”) is proposed, which includes geodynamic zoning of the territory under consideration, conducting geophysical surveys to verify the results of geodynamic studies, drilling of exploratory wells to confirm the presence of gas domes, their delineation using wells data, and drilling of directional inclined-horizontal wells for early degassing of the mine field with the feasibility of using the methane obtained. The use of this method allows confirming the boundaries of gas domes identified on the surface during geodynamic zoning and determining the preliminary volume of methane gas resources.

Another method is to evaluate sites based on key factors that affect methane production. For example, they take into account the depth of occurrence, faulting, permeability, and methane content of coal seams. Each assessed site is assigned a score from 10 to –10, where 10 is the best indicator, while negative values are assigned to indicators that have a negative impact. Gas saturation and critical gas desorption pressure indicators are also used to determine the prospects for methane extraction from coal seams. This method is described in paper [12].

In foreign countries, such as the United States, a comprehensive method of identifying “sweet spots” is used to determine promising methane extraction sites: geological, technological, geophysical, and petrophysical studies to determine the permeability and porosity, physical and mechanical properties, elemental and material composition of coal and coal-bearing rocks; coal seam assessment, which is carried out based on the analysis of well log survey data, core and slurry studies, geological and technological studies, hydrodynamic studies, and seismic surveys, during which petrophysical relationships are established, fractured zones and regional faults are identified, and the data is linked to coal horizons; core samples are taken to determine the amount of

gas and the permeability of coal in a given site⁶ [1]. To increase the performance of methane extraction from coal seams (up to 80%), a process was developed and implemented based on the application of pneumatic and hydrodynamic actions on a coal mass, which contribute to the intensification of desorption and increased gas recovery [13]. Similar approaches have been successfully applied in Australia⁷ [1] and China [14], where they have proven their effectiveness for low-permeability and complex coal seams.

Studies [7, 10] present various methods used in Russia to determine the potential of sites for methane extraction at different stages of coal-gas deposit development. For example, at the regional stage, geological data is obtained after coal exploration, and, based on this data, the most promising sites for exploration for gas are selected. During the exploration and appraisal stage, structural wells are drilled and seismic surveys are conducted to clarify the structural and tectonic structure of a deposit, study the geological sequence of a coal-bearing formation, and investigate the permeability and porosity of coal seams. The information presented is a key to identifying the most productive coal seam groups and making informed decisions about positioning of exploration and appraisal wells. In addition, a retrospective method of predicting methane resources based on the analysis of historical data on coal mining and methane release is used to assess the methane content potential of mine fields. The method takes into account: actual coal production volumes and methane release both for mines as a whole and for individual mining sites; the effectiveness of previously used degassing and methane extraction techniques; changes in gas abundance under different mining, geological, and geotechnical conditions. This approach makes it possible to improve the reliability of methane resource forecasts and identify patterns in the spatial distribution of methane-bearing coal seams⁸ [4].

Analysis of coal seams in the Karaganda coal basin

The Karaganda basin is one of the largest in Kazakhstan and is divided into seven formations with balance reserves estimated at 9.5 billion tons, including 0.6 billion tons of brown coal and 8.9 billion tons of hard coal, of which 5.5 billion tons is coking coal. The

⁶ Coal bed methane: Prospects for the development of unconventional hydrocarbons in the CIS. 2011. URL: <https://gaop.ru/articles/Metan-ugolnyh-plastov/>

⁷ Ibid.

⁸ Shevtsov A.G. Geotechnical justification for the use of multilateral horizontal wells in coal seam methane extraction. [Abstract dis. Cand. Eng. Sci.]. Kemerovo; 2021, 123 p. (In Russ.)



Karaganda basin comprises about 80 coal seams with an average total thickness of 110 m, but only 65 seams have a workable thickness (more than 0.6 m). The total thickness of all coal seams averages 110 m. The coal content of individual formations is shown in Table 3.

It should be noted that gas content and methane content are also important factors determining the quality of coal. The average gas content of coals in the Karaganda basin is 20–25 m³/t of combustible mass, which depends on the material composition, coal rank, structural position, and tectonic structure. The

main gas in the basin's subsoil is methane. Research has shown that as the coal rank (degree of maturation) increases, gas content rises from 15–20 m³/t of combustible mass for gas and fat coals to 20–27 m³/t of combustible mass for coking and lean sintering coals. Table 4 shows the characteristics of coal gas content ranges by site of the main formations in the Karaganda basin. The highest values were recorded in the Karadzharo-Shakhansky and Tenteksky sites that was connected with the depth of the seams occurrence and high vitrinite content.

Table 3

Characteristics of the Karaganda coal basin formations

Item No.	Formation name (from bottom to top)	Thickness, m	Seam indices*	Number of seams*	Total thickness of coal seams, m	Coal content
1	Coal Lower-Middle Ashlyarikskaya	585–600	$\frac{A_{1-20}}{A_5, A_{12}}$	$\frac{20-22}{2}$	14–20	2.4–3.7
2	Upper Vizean Serpukhovian and productive Karaganda	695–755	$\frac{K_{1-20}}{K_7, K_{10}, K_{12}, K_{13}, K_{16-17}}$	$\frac{24-26}{6}$	26–42	3.5–6.0
3	Middle Karaganda Productive Dolinskaya	450–550	$\frac{D_{1-11}}{D_6, D_{10}}$	$\frac{10-11}{2}$	14–15	2.9–4.2
4	Coal Tentekskaya	520–560	$\frac{T_{1-17}}{T_3, T_5, T_{12}}$	$\frac{16-18}{3}$	17–18	3.0–3.5

* The denominator represents productive coal seams with an average workable seam thickness of more than 1.5 m.

Table 4

Gas content of the Karaganda basin coals

Karaganda coal basin site, deposit, basin	Depth of flash gas zone H_0	Gas content at a depth of 400 m, m ³ /t of combustible mass	Coal rank	Amount of fusible components (FC), %	
				Raw coal	Concentrate with an actual density of less than 1.4 g/cm ³
Ashlyarikskaya formation					
Promyshlenny	90	20	K ₁	35–54	50–60
Karaganda formation					
Promyshlenny (east)	140	13	Zh ₁	41–66	50–72
Saransky	120	20	K ₁ , K ₂	35–60	45–60
Tsentralny	100	23	K ₂	38–79	50–87
Yuzhny	125	24	K ₃ , OS	40–80	50–88
Manzhinsky	125	22	K ₁ , K ₂	45–80	55–86
Dolinskaya formation					
Dubovsky	–	16	G ₃ , Zh ₁	61–70	69–78
Dolinsky	180	20	Zh ₃ , K ₁	57–80	7–88
Karadzharo-Shakhansky	200	19	Zh ₂	55–80	66–87
Tenteksky (southeast)	180	24	Zh ₃ , K ₁	57–80	65–85
Tenteksky (northwest)	300	17	G ₃ , Zh ₁	57–81	70–85
Samarskoye deposit	150	10	G ₂	65–70	80–85
Zav'yalovskoye deposit	200	16	Zh	60–75	75–85
Tentekskaya formation					
Tenteksky (northwest)	350	15	G ₃	41–71	65–84
Tenteksky (east)	170	21	Zh	40–70	64–84



According to preliminary estimates, 24.3 trillion m^3 of methane formed in the Karaganda basin to a depth of 1,800 m, part of which (about 8%) remained in coal and dispersed matter, part (18%) migrated into the host rocks, and the bulk of the gases (more than 18 trillion m^3) migrated into the atmosphere due to the absence of reliable reservoirs and clayey geological caps. Opening virtually all positive geological structures ruled out the possibility of the formation of independent large natural gas accumulations in the basin.

For example, let us consider the quality characteristics of coal from the Dolinskaya and Karaganda formations in terms of gas content and methane content.

– *Dolinskaya formation*

For seams D_3 and D_4 , the depth of the flash gas zone (H_0) is 252 m. Below this depth, the gas content growth gradient is 1.5 m^3/t of combustible mass per 100 m of depth. Thus, within the boundaries of the field, the gas content of seams D_6 , D_5 , and D_4 will not exceed 13.6 m^3/t of combustible mass. For seams D_2 , D_{1-2} , and D_1 , the depth of the flash gas zone (H_0) is 249 m. The most intense increase in gas content occurs from the surface to a depth of 400 m, and the content reaches 11 m^3/t of combustible mass. Within the range of 400–650 m, the gas content increases by 1.0–0.5 m^3/t of combustible mass per every 100 m of depth, and finally the gas content stabilizes at 13.9 m^3/t of combustible mass.

– *Karaganda formation*

The coal rank (stage of maturation) increases vertically downward and, in plan, in the north-wes-

tern direction, corresponding to the thickness of the Karaganda formation. The average methane content of the seams from the upper boundary of the site (700 m) to the lower boundary (1,400 m) increases by 0.5–2.3 m^3/t of combustible mass and does not exceed 30 m^3/t of combustible mass. The depth of the upper boundary of the methane zone ranges from 61 to 165 m. According to the study, all seams are hazardous in terms of coal burst. In the lower horizons (at depths of 700–1,400 m), compared to the upper horizons, the methane content decreases from 91 to 82% that is compensated by an increase in the percentage of heavy hydrocarbons from 1–2.8 to 9–12%, less frequently up to 17%, which are mainly represented by ethane, propane, butane, and isobutane in a ratio of 155:28:1:3. The effect of maturation is manifested in the fact that the methane content in the seams increases with depth, rising from the upper seam to the lower seam. The coal from the upper seam group (K_{20} – K_{15}) has the lowest methane content, while the coal from the lower subformation of the Karaganda formation (K_5^3 – K_1) has the highest methane content. The changes in methane content downdip of coal seams within deep horizons are illustrated in Table 5. The highest average methane content values were recorded in the K_5^3 – K_1 seams, while the lowest ones, in the K_{20} – K_{15} seams. This is due to the fact that gas pressure increases with depth and the sorption capacity of coal decreases with increasing rock temperature. However, the average methane content in the Karaganda formation seams ranges from 21.6 to 25.6 m^3/t of dry ash-free (daf).

Table 5

Change in methane content downdip of coal seams within the deep horizons of the Karaganda formation

Seam index	Methane content, m^3/t daf, at a depth, m								Average value
	700	800	900	1,000	1,100	1,200	1,300	1,400	
K_{20} – K_{15}	22.4	23.1	23.6	24.0	24.3	24.6	–	–	23.7
	21.6	21.6	–	–	–	–	–	–	21.6
K_{14} – K_{13}	23.0	23.7	24.2	24.6	25.0	25.3	25.5	–	24.5
	23.0	23.8	24.3	–	–	–	–	–	23.7
K_{12}	21.4	21.8	–	–	–	–	–	–	23.7
	23.5	24.2	25.3	25.7	26.0	26.3	–	–	25.1
	24.0	24.4	24.7	24.9	–	–	–	–	24.5
K_{11} – K_9	23.0	23.9	24.7	25.2	25.6	26.0	26.4	26.7	25.2
	22.8	23.2	23.4	23.7	23.9	–	–	–	23.4
K_{7-8}	21.2	–	–	–	–	–	–	–	–
	23.1	23.8	24.3	24.7	25.1	25.4	25.6	25.8	24.8
	22.2	23.5	24.6	25.5	26.5	26.9	–	–	24.9
K_5^3 – K_1	21.6	–	–	–	–	–	–	–	–
	25.6	25.8	26.0	26.1	26.2	26.3	26.4	–	25.6
	23.8	24.4	24.9	25.3	25.6	25.9	26.1	–	25.1



Table 6

Gas content of host rocks

Rock	Gas content, m ³ /t, at depth interval, m						Average Value
	700–800	800–900	900–1,000	1,000–1,100	1,100–1,200	1,200–1,400	
Argillites	2.8	4.2	1.2	2.7	–	–	1.2–4.2
Sandstones	0.03	0.03	0.9	0.08	0.11	0.1	0.03–0.11

Gas content of host rocks

The factors determining the gas content of the deep horizon seams are depth, coal rank, composition, and gas pressure. Among them, the most effective is the depth of seam occurrence, due to which methane content in the depth range of 700–1,400 m increases by 0.8–3.4 m³/t daf. Coals at this depth belong to the K grade and, to a lesser extent, to the OS grade. Due to the fact that coal seams within the site occur deeper than 700 m, factors such as overburden, seam dip angles, and seam disturbance lose their significance for methane redistribution, as at these depths it is in an equilibrated, almost stable state, which can be disturbed by mining operations or degassing of coal seams and rocks.

In the coal-bearing strata, the gas content in an occluded state is extremely negligible and depends mainly on the presence of organic matter in it. The overwhelming volume of free gas fills the pore space in sandstones and siltstones. Therefore, the quantitative content of gas in rocks is directly dependent on their porosity and gas pressure. Table 6 shows the gas content of the host rocks at depths ranging from 700 to 1400 m. The highest values were recorded for argillite at a depth of 800–900 m and for sandstone at a depth of 900–1000 m.

The gas content of the host rocks was determined using samples collected by core gas samplers. The results of the sample analysis showed that the rocks have been degassed to a depth of 250–300 m. Their methane content to a depth of 800 m does not exceed 4 m³/t. The average gas content of the host rocks is 1.3 m³/t. But even if we assume it to be equal to 1 m³/t, the methane amount in the sandstones occurring below 300 m will be about 7.4 billion m³.

In the Karaganda Basin, the dimensions of flash gas zones (FGZ), reaching 400 m from the earth surface, are extremely discontinuous. The average methane content of coal in the basin is 12–15 m³/t, and that of the host rocks is less than 1 m³/t, with maximum methane contents of 25–40 and 4 m³/t, respectively.

When examining issues related to methane extraction, it can be concluded that the Karaganda

coal basin is essentially a coal seam methane deposit⁹ [15–17], with 1 to 4 trillion m³ of gas accumulated at a depth to 1,800 m. It should be emphasized that approximately 500 million m³ of gas is extracted annually through degassing, with only 15% of this volume being used for industrial and production needs, while the rest contributes to emissions into the environment. The lack of a unified and reliable methodology for estimation of methane resources makes it impossible to accurately determine their amount due to different exploration maturity of deposits and different approaches to the estimation. Meanwhile, the recognition of this gas as an alternative energy source is confirmed by the level of capital investment in coal seam methane extraction projects around the world¹⁰ [5, 18].

The influence of geological and technical factors on the prospectivity of sites

The volume of methane resources is determined by the following factors: the total and commercial coal content of a deposit in a basin, gas pressure values, natural methane content, formation temperature depending on depth (from the surface and from the upper boundary of methane gases), coal rank, and, to a lesser extent, the petrographic composition of coal [19].

In the main seams of the Karaganda formation at a depth of 400 m, the content of gas is 22–25 m³/t. Its content increases to 25–27 m³/t in the Sherubainurinsky and Tenteksky sites. The flash gas zone in these sites is located at depths of 120–175 and 130–160 m, respectively. At the same time, the depth of coal seams occurrence has a significant effect on their gas content. Most researchers have concluded that gas

⁹ Coal Washing & power generation from washery rejects. Coal bed methane 2nd Indo-US Coal Working Group meeting. Washington; 2005; Pashin J.C. Geologic heterogeneity and coal-bed methane production – experience from the Black Warrior Basin. In: Selected Presentations on Coalbed Gas in the Eastern United States. U.S. Geological Survey Open-File Report 2004-1273. Pp. 61–92.

¹⁰ Turabaeva Zh. Kazakhstan's methane prospects. Mining and Metallurgical Industry. Almaty; 2019. P. 43. (In Russ.) URL: <https://metallmininginfo.kz/archives/6134>

content increases with depth according to a hyperbolic law and can be described using the Langmuir equation:

$$X = \frac{c(H - H_0)}{1 + b(H - H_0)}, \quad (1)$$

where H is the depth of a seam, m; H_0 is the depth of a methane zone surface, m; c and b are constants for a given seam.

Gas pressure in coal seams was studied by the Institute of Geophysics of the Academy of Sciences of the Kazakh SSR and the former VostNII [18]. The results of these studies showed that methane pressure increases with depth according to the relationship [19], which for depth interval 0 to 800 m can be approximated by a straight line of the form

$$P = 0.1H_c, \text{ kgf/cm}^2, \quad (2)$$

where H_c is the depth of occurrence from a conditional level, m.

For various seams of the Karaganda coal basin, the value of H_y varies between 200 and 800 m. Study [19] shows that gas pressure increases gradually with increasing depth of a seam. This is because a number of factors influences the distribution of gas in a coal-bearing formation, including gas pressure and gas permeability.

The average geothermal gradient in the Karaganda coal basin is 1.6°C per 100 m. This is almost half the average value of this indicator for the upper parts of the Earth's crust, but close to the value of this indicator for the world's carbon basins. In such cases, the porosity of coal is usually around 3–5%.

The ability of coal seams to retain significant volumes of gas even at reduced reservoir pressure is due to their high sorption capacity. This effect is caused by weak intermolecular forces, mainly Van der Waals forces, which ensure the adsorption of methane molecules on the inner surface of the pore space of coal. Significant volumes of gas can be concentrated in coal due to its large area of internal microporosity surface [6, 20, 21]. Through laboratory studies with controlling thermobaric conditions, coal sorption capacity isotherms were constructed. The characteristic dependencies between pressure and sorption capacity of coal obtained as a result of the research are presented in Fig. 3.

The data analysis shows that the Sherubainurinsky site may contain the largest amount of gas, since the coal sorption capacity increases more intensively with increasing pressure, while the Karadzharo-Shakhansky site may contain the least amount.

Based on the results of studying the sorbed methane content of coal seams in the basin, the dependencies of coal gas sorption on gas pressure, temperature, petrographic composition of coal, and moisture content have been determined. The research yielded data indicating that the coals of the Karaganda basin are characterized by insignificant variability of maturation. The established level of carbonification corresponds to stages III–IV of maturation according to accepted classifications [22]. The analysis of the petrographic composition of coals from the Karaganda basin showed that microcomponents of the vitrinite V_t and fusinite F groups dominate in the basin's coals, and their quantitative contents correlate quite closely ($r = 0.84$). The relationship between the main groups of microcomponents in the petrographic composition is described by the following equation:

$$F = 76.7 - 0.849V_t, \%, \quad (3)$$

where F and V_t are fusinite and vitrinite contents, respectively.

Therefore, the petrographic composition is assessed based on one of the main indicator, the fusinite F content, which is calculated based on the organic mass of coal, since the sorption capacity of the mineral part of coal is low.

All isotherms were processed using the Langmuir equation:

$$X_p = \frac{abP}{1 + bP}, \text{ cm}^3/\text{t combustible mass}, \quad (4)$$

where a and b are coefficients of the Langmuir equation, in cm^3/t and cm^2/kg , respectively; P is pressure, kgf/cm^2 .

The determination of a and b coefficients involved the use of the least squares method for the normalized equation:

$$\frac{P}{X_p} = \frac{1}{ab} + \frac{1}{a}P. \quad (5)$$

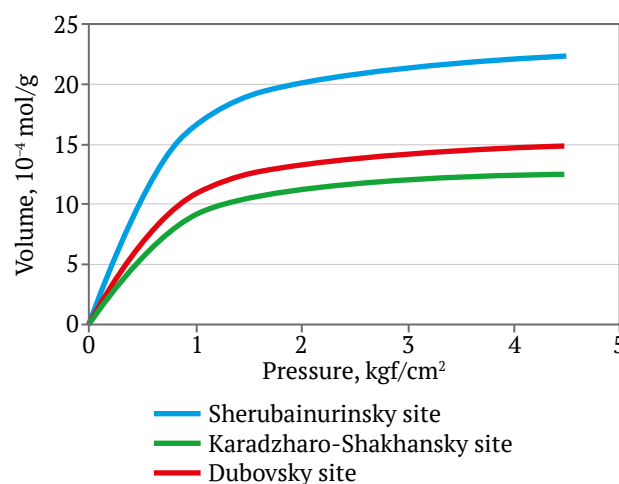


Fig. 3. Methane sorption isotherms at $t = 20^\circ\text{C}$

Next, a criterion method was used to search for specific dependencies for the values of the Langmuir coefficients a and b on temperature and fusinite content, which have the following form:

$$a_t = 33.48 - 0.28t, \text{ m}^3/\text{t combustible mass}; \quad (6)$$

$$b_t = 0.1287e^{-1.4715 \cdot 10^{-4}t}, \text{ cm}^2/\text{kg}; \quad (7)$$

$$a_F = 12.355 + 0.350 \cdot F, \text{ m}^3/\text{t combustible mass}; \quad (8)$$

$$b_F = 0.0956 + 0.000284F, \text{ cm}^2/\text{kg} \quad (9)$$

According to Prof. M.M. Protodyakonov's method, the formula for multifactorial dependence is the product of partial empirical dependencies divided by the general average of the entire data set, raised to a power one less than the number of primary factors. Thus, $a = f(t, F)$ will look as follows:

$$a_{F,t} = a \cdot \frac{a_t}{\bar{a}}, \text{ cm}^2/\text{kg}; \quad (10)$$

similarly, $b = f(t, F)$

$$b_{F,t} = b \cdot \frac{b_t}{\bar{b}}, \text{ cm}^2/\text{kg}, \quad (11)$$

where \bar{a} and \bar{b} are the corresponding general means.

When studying the material composition, it was found that the gas content of host rocks, such as argillites, only in individual cases exceeds $5 \text{ m}^3/\text{t}$, while in the vast majority of cases it is less than $2 \text{ m}^3/\text{t}$. It is characteristic that the stabilization of gas content coincides with the stabilization of their porosity. For instance, in the weathering zone of the Karaganda formation argillites, which extends to a depth of 300 m, the gas content of these rocks is minimal.

The gas content of the siltstones and sandstones, determined from single samples, is $4\text{--}5 \text{ m}^3/\text{t}$. These rocks are characterized by good gas recovery and require almost no thermal vacuum degassing.

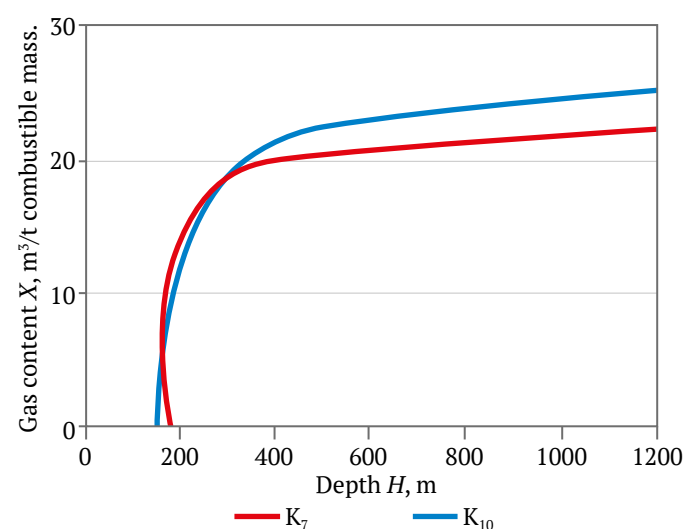


Fig. 4. Gas content of coal seams K_7 and K_{10} as a function of depth

The argillites, on the other hand, are freed from gas only when heated to a temperature of $70\text{--}80^\circ$ and subjected to deep vacuuming. The latter circumstance allows the inflow of methane from the host rocks into wells to be reduced to a negligible amount.

A study of gas (methane) content in the mines of the Promyshlenny and Saransky sites¹¹ [23] showed that as the maturation of coal increases in the western direction (i.e., toward the Sherubainurinsky coal-bearing district), the gas content also increases [24]. An increase in gas abundance with depth has also been established, as clearly demonstrated by the graph in Fig. 4. The total amount of methane formed in the process of coal maturation has approximately the following values by coal rank¹²: G – $212 \text{ m}^3/\text{t}$; Z – $229 \text{ m}^3/\text{t}$; K – $270 \text{ m}^3/\text{t}$; OS – $300 \text{ m}^3/\text{t}$; T – $330 \text{ m}^3/\text{t}$, which does not contradict the data of historical research. Thus, the potential gas resources in the coal-bearing strata of the Sherubainurinsky Syncline are estimated to be significant. At the same time, the current level of methane content is determined primarily not so much by methane generation as by the geological and structural conditions, and porosity and permeability, governing its migration and accumulation. For K_7 seam, gas content increases gradually with depth. In the early stages, gas recovery growth is slow due to significant fractures formed as a result of rock mass deformation (block fragmentation). For K_{10} seam, gas content also increases with depth, but more sharply. This is because the gas content of coal seams depends on the depth of occurrence, the coal rank, and the gas pressure.

Data on the coal and gas content of the Karaganda formation within mining fields 35/36 and 37/38 are provided in geological report¹³, where they are classified as fields not covered by gas sampling. Their gas resources were estimated by analogy with the Stepnya mine field and summarized in comparative Table 7, which shows that despite the identical estimated gas content of these the Karaganda formation fields based on balance reserves, the total methane resources of mine field 35/36 are significantly less and amounts to less than 0.75 billion ethane³, as compared to mine field 37/38 with more than 1 billion m^3 .

¹¹ Natura V.G., Sirotsky R.G., Ozhogina T.V. Russian Federation Patent No. 2601205 Method for determining gas content of coal seams. Appl. on 07.08.2015. Publ. on 27.10.2016.

¹² Akhmaturov D.R. Research into methods for intensifying gas recovery from unloaded coal seams. [PhD dis.]. Karaganda: Karaganda State Technical University; 2018. pp. 142–149. URL: <https://www.kstu.kz/o-zashhite-doktorskoj-dissertatsii-ahmaturova-denisa-ramilevicha/?lang=ru> (Date accessed: 08.09.2025).

¹³ Yermekov M.A. Gas Content of coal-bearing deposits and gas abundance of mines in the Karaganda Basin. [Abstract dis. ... Cand. Geol. and Min. Sci.]. Alma-Ata: Kazakh Polytechnic Institute; 1963. 63 p.

Table 7

**Gas content of coal seams and carbonaceous rocks of the Karaganda formation within mine fields 35/36 and 37/38
(According to the 1989 Geological Report)**

Indicator		Mine field 35/36	Mine field 37/38
		550	570
Average gas content, m ³ /t		14.53	14.69
Depth of level 10 m ³ /t, m		318	318
For balance reserves	total thickness, m	3.7	3.7
	Reserve category	A+B+C	A+B+C
	Coal reserves, kt	28,427	39,508
	Estimated gas content, m ³ /t	12.27	12.35
	Gas resource category	P ₁	P ₁
	Coal reserves, kt	348,799	487,924
For off-balance reserves	Coal reserves, kt	10,423	13,886
	Gas resource category	P ₂	P ₂
	Gas resources, thousand m ³	127,890	171,492
For non-workable coal seams	Total thickness, m	2.24	2.24
	Gas resource category	P ₃	P ₃
	Gas resources, thousand m ³	211,165	295,392
For carbonaceous rocks	Total thickness, m	1.4	1.4
	Gas resource category	P ₃	P ₃
	Gas resources, thousand m ³	65,989	92,310
Total coal reserves, kt		38,850	53,394
Total methane resources, thousand m ³		753,843 (0.75 billion m ³)	1,047,118 (1.0 billion m ³)

According to available data for the Northern site¹⁴, located southeast of the designed site, the seams have been degassed to a depth of 140–150 m that is explained by their rather steep dipping. It has been established that intensive growth in gas content occurs in the first 100 m from the surface of the methane zone, i.e., to a depth of 250 m from the surface. Within this short interval, which is characteristic of steeply dipping strata, the gas content of the seams increases from 2 to 20 m³/t of combustible mass. The gradient of its growth does not exceed 1 m³/t combustible mass per 100 m of depth, and at a depth of 1,000 m, the gas content reaches 24 m³/t combustible mass. The described trend in gas content is characteristic of all seams starting from K₁₀ and downward.

The total methane resources in the Karaganda formation in mine fields 35/36 and 37/38 amount to 1.75 billion m³. The gas content of the Ashlyarikskaya formation coal seams at a depth of 135–140 m is 15–20 m³/t daf. Downward this depth, the Kirovskaya mine is classified as super-category in terms of gas, and from a depth of 180–200 m downward, A₅ and A₇

seams undergo preliminary degassing. There were no sudden coal and gas outbursts. Within the projected site, the gas content of the Ashlyarikskaya formation coals, like those of the Karaganda formation, has not been studied.

The determination of a site's prospectivity (potential) is based on the development of geological assessment criteria, comprising analyzing the depth of occurrence, faulting (disturbance), permeability, and methane content of coal seams to identify the most gas-saturated sites, which can be considered promising for methane extraction from coal seams [10]. The criteria-based rating of a site's prospectivity consisted in assessing coal seams based on 10 key factors and took into account the influence of moisture content, volatile-matter yield, methane desorption, and seam permeability at various depths. Fig. 5 shows the coal content of the formations, taking into account the total and workable number of seams, as well as their total thickness.

The paper [10] presents the results of determining the permeability of the most gas-bearing formations in the studied sites depending on depth. With a small difference in depth, a decrease in formation permeability is observed with increasing depth. The results of processing the obtained permeability data as a function of a depth of occurrence are presented in Fig. 6.

¹⁴ Akhmaturov D.R. Research into methods for intensifying gas recovery from unloaded coal seams. [PhD dis.]. Karaganda: Karaganda State Technical University; 2018. pp. 142–149. URL: <https://www.kstu.kz/o-zashhite-doktorskoj-dissertatsii-ahmaturova-denisa-ramilevicha/?lang=ru> (Date accessed: 08.09.2025).

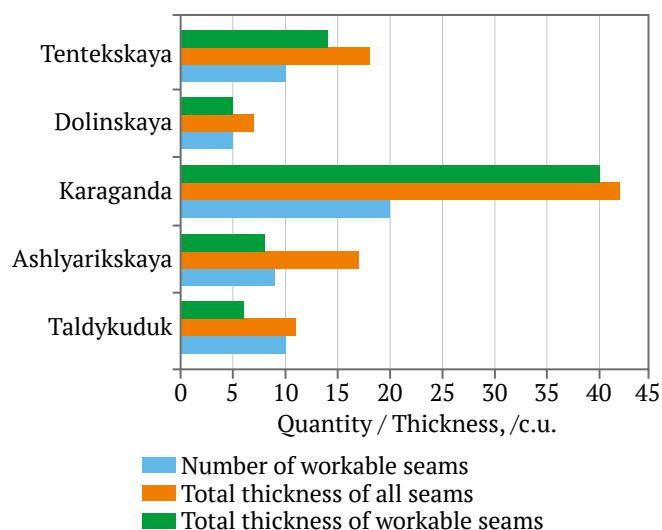


Fig. 5. Coal content of coal seams in the Karaganda basin

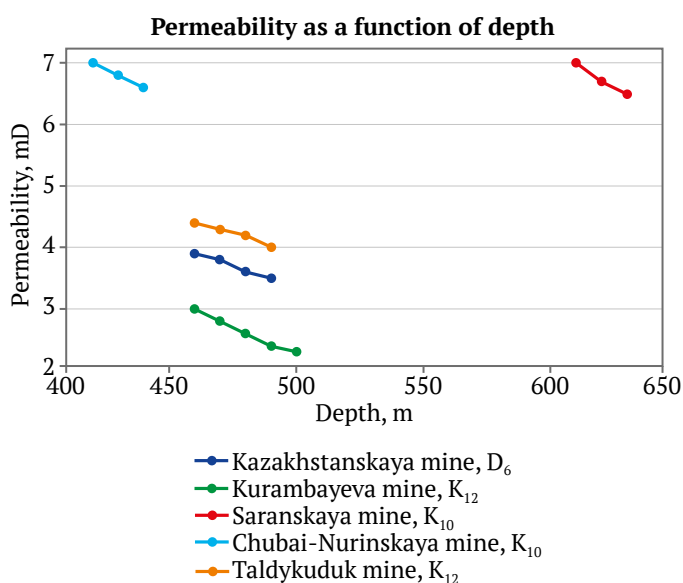


Fig. 6. The Effect of coal seam depth on its permeability

Source: Gurevich Yu. S. Extraction of commercial methane during underground coal mining and process solutions for its use. [Doctoral thesis in Eng. Sci.] Moscow: MGI; 1990. 531 p. (In Russ.)

The data analysis (Fig. 6) shows a stable negative correlation between depth and permeability of seams ($r \approx -0.85$), which is explained by increased rock pressure and compaction of rock. This, in turn, affects the permeability and desorption capacity of coal. A correlation between gas content and coal rank has also been identified: as the fusinite content increases, methane content increases too that is confirmed by the regression equation (see formula (3)). The data indicate the priority role of petrographic composition in the formation of methane resources.

The methodology for assessing the studied sites is as follows: for a comprehensive comparative characterization of gas-bearing coal sites, a factor-point assessment method was used, in which points were assigned to each site according to a number of key parameters reflecting its prospectivity (potential) in terms of methane content and degassing. Each parameter is rated on a scale from 10 to –10 points, where 10 corresponds to the most favorable value and –10 to the least favorable one. A negative value is assigned to an indicator that has an adverse impact. The parameters evaluated comprised permeability (gas permeability), which characterized the ability of a coal mass to allow gas to pass through. The higher the permeability is, the higher the degassing efficiency. The parameters also involved desorption capacity, reflecting the intensity of adsorbed methane release from coal; resource density, which estimates the potential volume of gas contained in the coal mass per unit area or volume; methane content, showing the actual methane content in a coal mass, determined on the basis of direct measurements; volatile-matter yield, reflecting the content of organic components in coal and indirectly indicating the potential for methane formation; moisture, characterizing the moisture content in coal and rock. Since increased moisture hinders gas desorption, this factor is considered negative and its value is taken into account in the calculations with a minus sign.

Table 8

Factor-point assessment of the sites under investigation

Sites under investigation	Points assigned for various factors						Summary score indicators
	Permeability	Desorption	Resource density	Methane content	Volatile-matter yield	Moisture	
Sherubainurinsky	9	7.5	10	9	9	–6.5	38
Saransky	8	5	10	9	9	–7	34
Taldykudusky	5	7	10	10	10	–10	32
Promyshlenny	5	6	10	9.5	9.4	–8	31.9
Tenteksky	5	7	6	10	10	–9	29



The final score (summary indicator) for each site is determined by adding up all the points assigned, taking into account the sign for moisture content.

Interpretation of results: the higher the final value, the more promising a site is in terms of potential gas recovery, degassing feasibility, and conditions for effective methane extraction. For example, the Sherubainurinsky site has the highest integral score (38 points), making it a priority site for degassing measures and pilot-plant operations.

The criterion rating for each site, taking into account fundamental geological and technical factors based on the results of the studies conducted (Table 8), showed that the Sherubainurinsky site is characterized by good resource density, methane content, and volatile-matter yield, but lags behind the other sites in terms of desorption and moisture content. The most promising sites proved to be Sherubainurinsky, Saransky, and Taldykudusky, while the Tenteksky site demonstrated the lowest indicators.

Unlike approaches available in the literature, which are based on a limited set of geological parameters (depth, gas content, permeability), the methodology developed in this study uses an expanded list of factors, 10 key characteristics, including petrographic and thermodynamic characteristics of coals. This allows for a more complete and objective assessment of the prospectivity of sites.

Thus, a distinctive feature of this study is an integration of the methods of desorption analysis, petrographic evaluation, and parametric permeability, combined into a unified evaluation algorithm suitable for implementation in degassing design practice.

An analysis of existing solutions [8, 9] shows that most of them do not take into account:

- sorption and structural properties of coals (Langmuir isotherms);
- the influence of microcomponent composition (fusinite, vitrinite);
- desorption characteristics and rock moisture content.

The advantage of the proposed approach is the multifactorial nature of the assessment, its universal applicability, high practical applicability, and increased forecast accuracy due to the refinement of Langmuir equations and the introduction of the correlations with fusinite content and temperature.

Thus, the scientific novelty of the research is expressed in the development and experimental confirmation of an integrated methodology for assessing coal seam sites, which makes it possible to replace expert, poorly formalized approaches with a quantitative, scientifically sound methodological system with verifiable parameters.

Conclusions

An analysis of the current state and global experience in the field of coal seam methane extraction has shown that some countries are quite successfully applying various processes for extracting methane from coal seams.

The Karaganda coal basin is conditionally divided into five sites based on the potential for methane gas production. Research was conducted covering the most gas-bearing seams at each of these sites. It has been established that the gas content of coal in the Karaganda basin increases regularly with depth along the ascending branch of an *S-shaped* curve, with methane content reaching 25–27 m³/t at depths of over 600 m. As a result of the research, first- and second-order zones have been identified for assessing the prospects of methane extraction from coal seams. The main parameters for classifying these zones are: depth of occurrence, permeability, and desorption characteristics. Gas permeability of up to 10–15 mD can be recorded at a depth of 250–300 m.

Based on an analysis of the sorption capacity of coal seams in the Karaganda basin with respect to methane, parameters were established for models of correlation between coal sorption and factors such as gas pressure, temperature regime, petrographic composition, and moisture content. The results obtained during the research indicate that the Karaganda basin coals are characterized by insignificant variability in the stage of maturation (coal rank). Laboratory studies have established that methane content increases from 21.6 to 26.4 m³/t with increasing seam depth. For the first time for the Karaganda basin, quantitative dependencies of the Langmuir equation coefficients on fusinite content and temperature have been obtained, allowing the parameters of sorption isotherms to be refined and the accuracy of coal gas capacity estimates to be improved.

Based on the results of pilot-plant tests and experimental research, geological and technological factors characterizing the potential of sites for methane extraction were scientifically substantiated, such as: the depth of coal seams, disturbance, permeability, and methane content. The prospectivity rating was based on an assessment of coal seams based on 10 key factors and took into account the effect of moisture content, volatile-matter yield, methane desorption, and seam permeability at different depths. The final score (summary indicator) for each site was determined by adding up all the points assigned, taking into account the sign for moisture content. Interpretation of the results showed that the higher the final value, the more promising a site is in terms of potential gas



recovery, degassing feasibility, and conditions for effective methane extraction. The application of a criterion-based approach made it possible to rank sites based on a scientific approach and quantitative assessments. The most promising areas were recognized to be Sherubainurinsky (38 points), Saransky (34 points), and Taldykudusky (32 points).

The research objective has been achieved: a system has been developed that not only allows assessing the current prospectivity of the mining allotment sites, but also predicting the performance of methane production at an early stage of planning. The results of the study are of practical importance both for the design of new coal mines and for existing mines too.

References

1. Parmuzin P.N. *Foreign and domestic experience in the development of coalbed methane resources: A Monograph*. Ukhta: USTU; 2017. 109 p. (In Russ.)
2. Golitsyn M.V., Golitsyn A.M., Pronina N.V. et al. *Gas-coal basins of Russia and the world*. Ed. by V.F. Cherepovskiy. Moscow: Lomonosov Moscow State University, Russian Academy of Natural Sciences; 2002. 249 p. (In Russ.)
3. Qin Y., Ye J. A review on development of CBM industry in China. In: *AAPG Asia Pacific Region, Geoscience Technology Workshop. Opportunities and Advancements in Coal Bed Methane in the Asia Pacific*. February 12–13, 2015, Brisbane, Australia. Tulsa: AAPG; 2015.
4. Drizhd N.A., Kamarov R.K., Akhmatnurov D.R. et al. Coal bed methane Karaganda basin in the gas balance Republic of Kazakhstan: status and prospects. *Naukovyi Visnyk Natsionalnoho Hirnychoho Universytetu*. 2017;(1):12–20.
5. Kiryaeva T.A. Evaluation of methane resources in Kuzbass in the context of new ideas on methane occurrence in coal bed. 2012;(5):67–75. *Fiziko-Tekhnicheskiye Problemy Razrabotki Poleznykh Iskopayemykh*. (In Russ.)
6. Kirin B.F., Zhuravlev V.P., Ryzhikh L.I. *Dust control in Mines*. Moscow: Nedra; 1983. 213 p. (In Russ.)
7. Nazarova L.A., Nazarov L.A., Karchevsky A.L. Method of “canister test” data interpretation for determination of coal bed diffusion and capacity parameters based on inverse problem solution. *Mining International and Analytical Bulletin*. 2014;(3):56–68. (In Russ.)
8. Veleseovich S.V., Shek V.M. Analysis of the prospects of coal-gas field areas for methane production (case study of the Vorkuta field). *Mining Informational and Analytical Bulletin*. 2005;(5):132–137. (In Russ.)
9. Koryaga M.G., Sychev I.I. A seArch technique for detection of methane accumulation and identification of potential sites for industrial methane mining in southern Kuzbass. *Mining Informational and Analytical Bulletin*. 2015;(3):380–385. (In Russ.)
10. Musin R.A., Asanova Zh.M., Khalikova E.R. et al. Development of technological evaluation criteria for the selection of promising coal methane production sites. *Ugol'*. 2024;(4):102–108. (In Russ.) <https://doi.org/10.18796/0041-5790-2024-4-102-108>
11. Gresov A.I., Obzhairov A.I., Shakirov R.B. *Methane resource base of the coal basins of the Russian Far East and prospects for its industrial development*. Vol. I. Coal-methane basins of Primorye, Sakhalin and Khabarovsk Krai. Vladivostok: Dalnauka; 2009. 247 p. (In Russ.)
12. Lu Ya. Methodology for geological selection of coal deposits for methane extraction from coal seams in China. In: *International Scientific Conference of Students, Postgraduates and Young Scientists “Lomonosov – 2018”*. April 10–11, 2018, Moscow, Russia, 2018. (In Russ.)
13. Yan I., Chen H., Wang H. et al. Influence of tectonic structure on methane recovery in QD site in the Qinshui coal basin in China. *Fiziko-Tekhnicheskiye Problemy Razrabotki Poleznykh Iskopayemykh*. 2021;(3):85–95. (In Russ.) <https://doi.org/10.15372/FTPRPI20210309>
14. Ruban A.D., Zaburyaev V.S. Experience in the extraction and utilization of mine methane in Russia and the Federal Republic of Germany. *Mining Informational and Analytical Bulletin*. 2004;(9):153–158. (In Russ.)
15. Zaburyaev V.S. Coalbed methane: resources, emission volumes, extraction and utilization. *Gornyy Vestnik*. 1994;(1):34–39. (In Russ.)
16. Zolotikh S.S., Arnautov V.S., Surin E.V. *From the depths of Kuzbass storerooms – combustible gas methane*. *Gazprom Dobycha Kuznetsk*. Kemerovo: Kuzbassvuzizdat; 2015. 247 p. (In Russ.)
17. Legotin F.Ya., Akhmetova A.B. The analysis of state and trends of development of the coal mining industry in the Karaganda oblast. *Journal of the Ural State University of Economics*. 2012;(4):50–53. (In Russ.)
18. Volpova L.S., Tokareva S.G. On the error in determining natural gas content by the core gas sampler KA-61. *Izvestiya Vuzov. Geologiya i Razvedka*. 1973;(5):92–94. (In Russ.)



19. *Gas content of coal basins and deposits of the USSR. Vol. 2. Coal Basins and Deposits of Siberia, Kazakhstan and the Far East.* Ed. by A.I. Kravtsov. Moscow: Nedra; 1979. 454 p. (In Russ.)
20. Drizhd N.A., Musin R.A., Aleksandrov A.Yu., Rabatuly M. Experience in drilling a directional well for coalbed methane production. *Gornyy Zhurnal Kazakhstana*. 2019;(12):19–23. (In Russ.)
21. Pashchenkov P.N. Method to determine parameters of Langmuir isotherm and gas permeability of dispersed coal particles. *Mining Informational and Analytical Bulletin*. 2018;(3):120–128. (In Russ.)
22. Slastunov S.V. Problems of coal methane production and promising technological solutions. *Mining Informational and Analytical Bulletin*. 1997;(6):25–31. (In Russ.)
23. Shubina E.A., Lukyanov V.G. Study of natural gas content for the development of coal seam methane production on an industrial scale. *Vestnik KuzGTU*. 2016;(1):3–12. (In Russ.)
24. Drizhd N.A., Rabatuly M., Aleksandrov A.Yu. et al. The results of the development of pilot wells in the Sherubainurinsky site of the Karaganda coal basin. *Ugol'*. 2020;(6):36–40. (In Russ.) <https://doi.org/10.18796/0041-5790-2020-6-36-40>

Information about the authors

Ravil A. Mussin – Associate Professor of the Department of Mineral Deposits Development, Abylkas Saginov Karaganda Technical University, Karaganda, Republic of Kazakhstan; ORCID [0000-0002-1206-6889](https://orcid.org/0000-0002-1206-6889), Scopus ID [7005446397](https://orcid.org/7005446397); e-mail R.A.Mussin@mail.ru

Natalia A. Nemova – Senior Researcher of the Open-Pit Mining Laboratory, N.A. Chinakal Institute of Mining of the Siberian Branch of the Russian Academy of Sciences, Novosibirsk, Russian Federation; Associate Professor of the Department of Engineering Geodesy and Mine Surveying, Siberian State University of Geosystems and Technologies, Novosibirsk, Russian Federation; ORCID [0000-0002-5050-611X](https://orcid.org/0000-0002-5050-611X), Scopus ID [56995813200](https://orcid.org/56995813200); e-mail fpvgn@misd.ru

Denis R. Akhmatnurov – Head of the Laboratory, Abylkas Saginov Karaganda Technical University, Karaganda, Republic of Kazakhstan; ORCID [0000-0001-9485-3669](https://orcid.org/0000-0001-9485-3669), Scopus ID 57194187849; e-mail d_akhmatnurov@mail.ru

Nail M. Zamaliyev – Associate Professor of the Department of Mineral Deposits Development, Abylkas Saginov Karaganda Technical University, Karaganda, Republic of Kazakhstan; ORCID [0000-0003-0628-2654](https://orcid.org/0000-0003-0628-2654); e-mail Nailzamaliyev@mail.ru

Edvard D. Reshetnyakov – Engineer of the Department of Mineral Deposits Development, Abylkas Saginov Karaganda Technical University, Karaganda, Republic of Kazakhstan; ORCID [0009-0000-1128-2056](https://orcid.org/0009-0000-1128-2056); e-mail vip_red2001@gmail.com

Alexander V. Reznik – Senior Researcher of the Open-Pit Mining Laboratory, N.A. Chinakal Institute of Mining of the Siberian Branch of the Russian Academy of Sciences, Novosibirsk, Russian Federation; ORCID [0000-0002-0077-3404](https://orcid.org/0000-0002-0077-3404); e-mail a-reznik@mail.ru

Received 26.06.2025

Revised 31.07.2025

Accepted 01.08.2025



MINERAL RESOURCES EXPLOITATION

Research paper

<https://doi.org/10.17073/2500-0632-2025-09-460>

UDC 622.271.4

**Justification of the rational scope and technology
for the use of hydraulic excavators in surface mining**

V.A. Khakulov¹ , V.A. Shapovalov¹ , V.N. Ignatov² , Zh.V. Karpova³ ,
M.V. Ignatov¹ , I.A. Nogerov¹

¹ Kabardino-Balkarian State University, Nalchik, Russian Federation

² Platov South-Russian State Polytechnic University (NPI), Novocherkassk, Russian Federation

³ NIPI Nedra LLC, Novocherkassk, Russian Federation

vkh21@yandex.ru

Abstract

The constrained conditions of deep-pit mining and the rigid technological interdependence between operations on lower and upper horizons significantly complicate the performance of loading and haulage systems and, in particular, hinder the efficient use of large rope shovels. At the same time, due to a limited service life and a sharp decline in reliability after 7–10 years of operation, mobile hydraulic excavators cannot compete with mechanical shovels when excavating hard rock formations. Based on research and industrial experiments, combined solutions have been developed and tested for the use of rope and hydraulic excavators within their respective optimal application areas to improve the efficiency of mining operations. The proposed priority application zone for hydraulic excavators is defined in areas with a planned low concentration of drilling-and-blasting operations, where the utilisation factor of rope shovels is below 0.5, while that of mobile hydraulic excavators – with appropriate geomechanical support – is at least 0.7. At the same time, hydraulic excavators cannot directly compete with large mechanical shovels in the development of hard rock. Therefore, a specialised technology for within-block differentiation of drilling and blasting parameters is proposed to ensure the geomechanical conditions necessary for the effective integration of hydraulic excavators into mining operations.

Keywords

stripping ratio, pit slope angle, loading and haulage systems, differentiation of drilling and blasting parameters, excavation process monitoring, intelligent monitoring systems, rock mass loading uniformity, rope shovel, hydraulic excavator, backhoe

For citation

Khakulov V.A., Shapovalov V.A., Ignatov V.N., Karpova Zh.V., Ignatov M.V., Nogerov I.A. Justification of the rational scope and technology for the use of hydraulic excavators in surface mining. *Mining Science and Technology (Russia)*. 2025;10(4):338–345. <https://doi.org/10.17073/2500-0632-2025-09-460>

РАЗРАБОТКА МЕСТОРОЖДЕНИЙ ПОЛЕЗНЫХ ИСКОПАЕМЫХ

Научная статья

**Обоснование рациональной области и технологии применения
гидравлических экскаваторов на открытых горных работах**

В.А. Хакулов¹ , В.А. Шаповалов¹ , В.Н. Игнатов² , Ж.В. Карпова³ ,
М.В. Игнатов¹ , И.А. Ногеров¹

¹ Кабардино-Балкарский государственный университет имени Х.М. Бербекова, г. Нальчик, Российская Федерация

² Южно-Российский государственный политехнический университет имени М.И. Платова,
г. Новочеркасск, Российская Федерация

³ ООО НИПИ «Недра», г. Новочеркасск, Российская Федерация

vkh21@yandex.ru

Аннотация

Стеснённые условия отработки глубоких горизонтов карьера и наличие жёсткой технологической связи между продвижением горных работ на нижних и верхних горизонтах существенно усложняют работу погрузочно-транспортных комплексов и, в частности, не позволяют эффективно использовать мощные канатные карьерные экскаваторы. В то же время мобильные гидравлические экскаваторы из-за ограниченного ресурса и резкого падения надёжности после 7–10 лет службы не выдерживают конку-



ренции с карьерными механическими лопатами при разработке тяжелых скальных пород. В результате проведения исследований и промышленных экспериментов были установлены и апробированы комбинированные решения по использованию канатных и гидравлических экскаваторов в своих рациональных областях для эффективного применения на горном производстве. Предлагаемая область приоритетного применения гидравлических экскаваторов определяется в зонах планируемой низкой концентрации буровзрывных работ, где коэффициент использования канатных экскаваторов составляет менее 0,5, а мобильных гидравлических – при условии специального геомеханического обеспечения – не менее 0,7. В то же время гидравлические экскаваторы напрямую не могут конкурировать с мощными карьерными механическими лопатами при отработке тяжёлых скальных пород. Поэтому предлагается специальная технология внутриблоковой дифференциации параметров буровзрывных работ, которая решает задачу геомеханического обеспечения эффективного внедрения гидравлических экскаваторов в горном производстве.

Ключевые слова

коэффициент вскрыши, угол наклона борта карьера, погрузочно-транспортные комплексы, дифференциация параметров буровзрывных работ, мониторинг процесса экскавации, интеллектуальные комплексы мониторинга, ритмичность отгрузки горной массы, канатный экскаватор, гидравлический экскаватор, обратная лопата

Для цитирования

Khakulov V.A., Shapovalov V.A., Ignatov V.N., Karpova Zh.V., Ignatov M.V., Nogerov I.A. Justification of the rational scope and technology for the use of hydraulic excavators in surface mining. *Mining Science and Technology (Russia)*. 2025;10(4):338–345. <https://doi.org/10.17073/2500-0632-2025-09-460>

Introduction

As mining depth increases, the stripping ratio rises sharply, significantly reducing the profitability of open-pit operation [1–3]. The most effective way to partially stabilize stripping volumes with increasing depth [4, 5] is to maintain a relatively steep pit slope angle [6, 7]. However, two major factors limit this approach: the stability of pit walls and the sharp decline in productivity of loading and haulage systems employing large electric rope shovels [8, 9]. To ensure high equipment productivity at deep pit levels while maintaining a low current stripping ratio, mining operations are conducted within working concentration zones that are moved vertically along the pit wall¹ [10]. This technology, which uses relatively wide working benches in concentration zones, enables efficient loading of productive mining systems with blasted rock mass. At the same time, moving these zones vertically along the pit wall requires time-consuming conservation and deconservation procedures. Additional complications arise due to a rigid technological interdependence, whereby progress in lower levels depends on the advancement of upper-level operations. Under such constrained conditions, large electric rope shovels cannot be used efficiently, and mobile hydraulic excavators are employed instead. However, hydraulic excavators cannot directly compete with large mechanical shovels, particularly when excavating hard rock formations [11].

Although mobile, this type of equipment is less suited to harsh mining conditions and has a shorter service life, with reliability declining significantly after 7–10 years of operation. At the same time, amid general trends toward the use of higher-capacity mining equipment in deep open pits, certain operational zones emerge where mobile hydraulic excavators can be used effectively. Therefore, research aimed at defining the rational application areas and technologies for using hydraulic excavators at mining and processing plants remains highly relevant.

A number of approaches have been proposed to improve the efficiency of hydraulic excavator operation. P. Bules² justified the optimal service life of key components and systems of hydraulic mining excavators to extend their operational lifespan. However, this assessment did not address the technological aspects of excavator operation or specific application conditions. Without technological adaptation, hydraulic excavators remain less suited for severe mining environments.

Another line of research focuses on improving mining technology. For example, E. V. Loginov proposed³ a method for controlling the operational stripping ratio when using backhoe-type hydraulic excavators in deepening mining systems. Replacing rope

² Bules P. Ensuring the reliability of hydraulic mining excavators during open-pit operations in Russia [Cand. Sci. (Eng.) diss.]. Moscow: National University of Science and Technology MISIS; 2016.

³ Loginov E. V. Control of the operational stripping ratio when using backhoe-type hydraulic excavators in deepening mining systems [Cand. Sci. (Eng.) diss.]. St. Petersburg: Saint Petersburg Mining University; 2018.

¹ Isaychenkov A. B. Optimization of jointly performed overburden mining processes using modern excavator-truck complexes (on the example of the "Tugnuy" open-pit mine). [Cand. Sci. (Eng.) diss.]. Moscow: IPKON RAS; 2016. 231 p. (In Russ.)



shovels with backhoe-type hydraulic excavators in deep pit levels allows for narrower working benches. As a result, steeper pit slope angles can be formed, which correspond to a 10% reduction in the operational stripping ratio.

Nevertheless, the stripping ratio inevitably increases with depth [12–14]. To maintain mining efficiency, combined use of rope shovels and hydraulic excavators is required, each operating within its optimal application range. It is also necessary to consider that hydraulic excavators are less suited for excavating hard rock formations. The bucket filling efficiency in such conditions is affected by the ratio between bucket width and capacity – a parameter significantly higher for hydraulic excavators than for rope shovels of equivalent capacity. Moreover, the kinematic design of backhoes provides a substantially lower digging force. When comparing front-shovel and backhoe configurations of hydraulic excavators, it should be noted that these types differ in crowding and breakout forces. For instance, models of mining hydraulic excavators manufactured by Komatsu Mining Germany (KMG) with a backhoe configuration have 20–30% lower crowding force and 8–22% lower breakout force⁴.

Research aim and objectives

The aim of this study is to justify the rational scope and technology for the use of hydraulic excavators.

Research objectives:

- to adapt hydraulic excavators for operation in harsh hard-rock mining conditions;
- to define the optimal application areas of hydraulic excavators and improve their reliability and competitiveness compared to rope shovels.

The stated objectives are addressed by implementing continuous monitoring of the excavation process with a focus on geomechanical conditions. The resulting data are used to refine rock blastability zoning, adjust drilling-and-blasting designs and the selection of equipment, optimize preventive maintenance schedules.

Research methods included:

- comparative analysis (evaluating the efficiency of rope and hydraulic excavators);
- analytical modelling (parameter calculations);
- instrumental monitoring (accelerometers, gyroscopes, and GPS sensors for analysing excavation performance);

– field experiments (tests conducted at open pits in the Kabardino–Balkarian Republic and Rostov Region);

- remote sensing (drone-based aerial photography for analyzing rock mass structure);
- machine learning (developing an expert model for predicting borehole capacity based on drill cuttings characteristics).

The central premise of this study is that rope shovels, although less sensitive to geomechanical variability and designed for long service life, are not efficient in all operating contexts. The findings highlight the need for an integrated mining approach in which rope and hydraulic excavators complement each other within their respective optimal application zones. Since hydraulic excavators have a shorter service life and declining reliability over time, their effective use becomes less straightforward. Hard and abrasive rock formations require a higher level of geomechanical support for hydraulic machines. In many cases, the degree of fragmentation sufficient for productive operation of rope shovels proves inadequate for hydraulic backhoes. Thus, although hydraulic excavators are widely used in the construction industry, their effective deployment in large-scale mining requires system-level adaptation that integrates technical, operational, and geomechanical factors. Partial adaptation that focuses only on individual aspects cannot fully resolve the problem. Measures aimed solely at improving reliability – such as more frequent replacement of high-wear components – are ineffective if geomechanical influences are not taken into account. The spatial and temporal variability of the structural and strength properties of the rock mass governs the geomechanical loading on the equipment and, consequently, its wear, which evolves together with operating hours and failure statistics across the excavator fleet. Therefore, to improve mining efficiency on a systematic basis, it is necessary to monitor geomechanical conditions so as to provide information support for revising rock blastability zoning, adjusting mining technology and equipment selection, updating preventive maintenance schedules.

Main theoretical framework

The primary methodological challenge lies in distinguishing between the technological and geomechanical components of equipment productivity losses. This issue was addressed by the authors in earlier studies through the development of an intelligent excavation monitoring module incorporating an accelerometer, gyroscope, barometer, magnetometer, GPS receiver, and temperature sensor. The mod-

⁴ Bules P. ensuring the reliability of hydraulic mining excavators during open-pit operations in Russia [Cand. Sci. (Eng.) diss.]. Moscow: National University of Science and Technology MISIS; 2016.

ule, enclosed in a shock-resistant housing, is magnetically mounted at the junction between the excavator arm and bucket. In particular, the presence of an accelerometer in the measurement module enables recognition of the excavator's primary and auxiliary operational cycles, as well as spatial and temporal tracking of bucket position, by analysing the projections of gravitational force along the coordinate axes. The hardware and methodology of excavation process monitoring were successfully tested at open pits in the Kabardino–Balkaria Republic and Rostov Region during 2019–2022 [15].

Recording the spatial position of each operational cycle, along with changes in bucket filling time and volume, combined with the analysis of actual drilling-and-blasting parameters, provides insight into variations in the structural and strength properties of the rock mass. This technical solution enables excavation process monitoring with identification of the geomechanical component, allowing for refinement of rock blastability zoning, adjustment of mining technology and equipment selection, and optimisation of preventive maintenance schedules.

It is proposed that hydraulic excavators be used primarily in areas with a planned low concentration of drilling-and-blasting operations. As shown in Fig. 1, in zones of low blasting concentration,

with production blast volumes of $20\text{--}40 \times 10^3 \text{ m}^3$, the equipment utilisation factor falls below 0.5, indicating extremely low efficiency of rope shovels.

The proposed combined excavation technology for rope and hydraulic excavators is based on improving technological zoning according to rock blastability categories. The method involves, on one hand, concentrating blasting operations in areas suitable for high-efficiency operation of rope shovels, and on the other, designating zones for hydraulic excavators where concentrated blasting is technologically impractical or impossible.

The greatest challenges are posed by hard, abrasive rock masses, including those disturbed by both underground [16, 17] and surface mining operations, which require a higher level of geomechanical support for effective hydraulic excavator operation. When fragmentation meets the performance criteria for rope shovels but is insufficient for hydraulic backhoes, it becomes necessary to switch to smaller-diameter boreholes with a higher drilling volume. At the same time, it must be considered that fractured rock masses naturally break along joint planes during blasting, and additional explosive consumption does not improve fragmentation quality. For a meaningful comparative analysis of technologies using different drilling and loading equipment, the productivity of drilling rigs should be evaluated in terms of the mass of blasted rock.

Significant difficulties arise in fractured rock masses containing large-block inclusions, where both rock blastability and borehole capacity within a single blast block vary considerably. For example, in fractured rocks with gaping joints, the capacity of boreholes drilled with a 243 mm bit for granular explosives can exceed 59 kg/m, whereas in monolithic rocks this value is about 45–47 kg/m. Increased borehole capacity negatively affects charge column placement [18, 19], shifting it 15–20% downward within the borehole. As a result, the explosive charge becomes concentrated in the overdrilled section, leading to poor fragmentation in the upper part of the bench, disturbance of the floor of the underlying bench, and additional borehole losses due to induced fracturing.

To mitigate random downward displacement of the explosive column, zoning studies are conducted to determine the optimal parameters of drilling-and-blasting operations for fractured and blocky portions of the blast block and to clarify the relationship between borehole capacity and the structural properties of rock masses (Fig. 2). For different rock types, a characteristic particle-size class is defined – representing the lower limit of coarse drill cuttings,

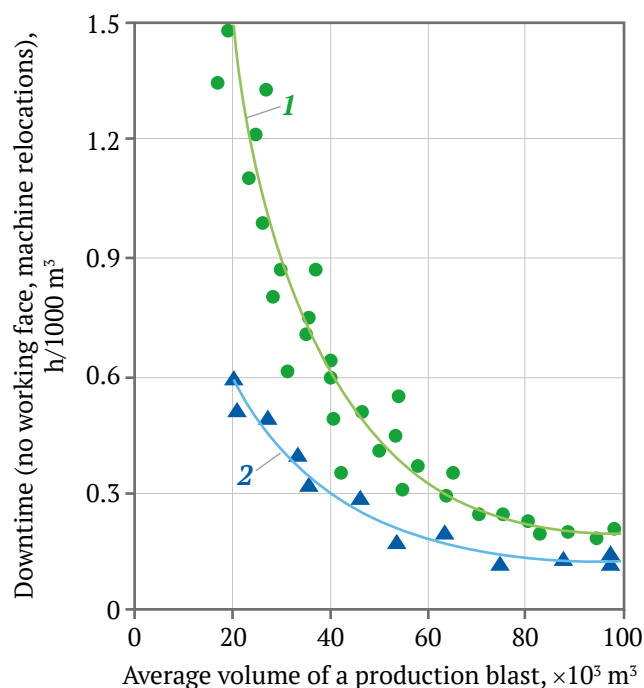


Fig. 1. Comparative analysis of the effect of concentrating drilling-and-blasting operations on downtime of rope and hydraulic excavators: 1, 2 – variation in operational downtime of rope shovel EKG-4.6 and hydraulic excavator Hyundai R520LC-9S associated with relocations and lack of blasted rock, respectively

the yield of which reflects the blockiness of the rock mass. For example, the characteristic particle-size range for hornfels from the Tyrnyauz deposit is 5–10 mm.

Drilling plans are based on parameters relevant to the most fractured portions of a blast block (Fig. 3 – positions 1 and 2). After drilling the planned boreholes, the mass yield and particle-size distribution of the drill cuttings are used to localize poorly fragmentable zones. Boreholes drilled in such strong-rock portions of the massif exhibit smooth, non-sloughing walls and a sharply contrasting cuttings signature (a high yield of cuttings concentrated at the characteristic size). By contrast, boreholes drilled in the fractured parts of the block display irregular walls with spalls and gaping joints and produce a low yield of cuttings, the sizes of which substantially exceed the established characteristic values.

It should be noted that the effectiveness of this relatively simple technology strongly depends on the human factor. In particular, the heavy reliance on visual assessment of borehole condition adversely affects the accuracy of rock-type and blastability zoning and complicates subsequent verification and post-processing. To overcome this limitation, we propose recording the position and condition of borehole collars using an unmanned aerial vehicle to enable automated identification of prospective

zones and differentiation of blasting parameters within a blast block (Fig. 4).

The task of revising rock-mass zoning by blastability is addressed through monitoring supported by intelligent models and by system-level analysis of mining process outcomes, measured parameters and industrial blast indicators tied to the specific rock-mass location under study.

The proposed technology for areas with elevated structural variability in the rock mass is implemented in two stages:

- at the first stage, drilling is carried out according to the design using parameters relevant for the most fractured part of the block;

- at the second stage, within the localized hard-to-blast zones, one or two additional blast holes are drilled at the centre of each group of four previously drilled holes.

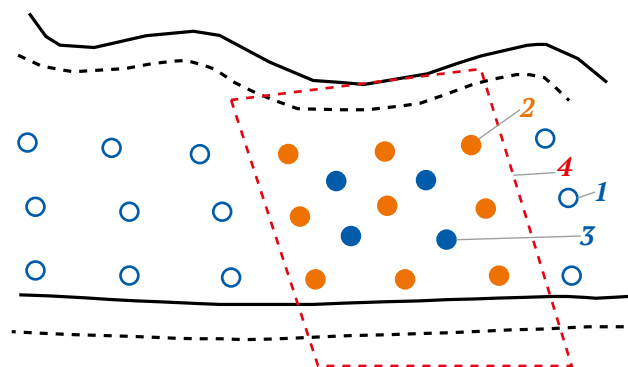


Fig. 3. Technological scheme for differentiating blasting parameters in areas of high variability in rock-mass structure: 1, 2 – boreholes drilled according to the block drilling plan (1 – identified by monitoring as drilled in fractured rock; 2 – identified by monitoring as drilled in massive/monolithic rock); 3 – additional boreholes drilled following corrective calculations; 4 – zone of large-block rock localization identified by monitoring



Fig. 4. Drilled blast block imaged by unmanned aerial vehicle (UAV), with a zone highlighted as prospective for differentiated blasting parameters

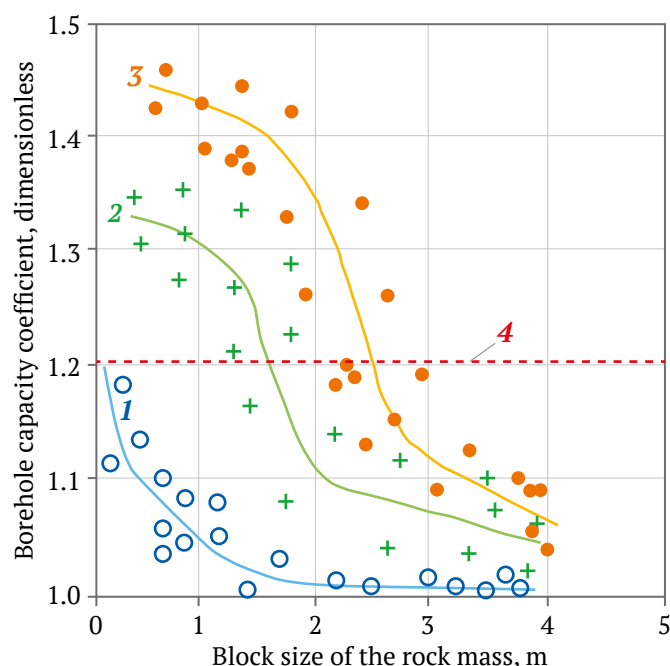


Fig. 2. Dependence of changes in borehole capacity on the structural properties of rock masses:

- 1 – fractured rock masses with closed joints;
- 2 – fractured rock masses with open or infill-filled joints;
- 3 – fractured rock masses with gaping (widely open) joints;
- 4 – boundary of controlled explosive fragmentation



Methodology for calculating drilling and blasting parameters

An increased consumption of explosives required for breaking strong rock masses necessitates additional drilling, the total length of which is determined by the following expression, m [18]:

$$L_{ad} = \frac{(q_{ex} - q_r)V_s}{Pk_u}, \quad (1)$$

where q_{ex} – specific explosive consumption required for breaking the block's coarse-fragmented zone, kg/m³; q_r – specific explosive consumption according to zoning data for the fractured part of the block, kg/m; V_s – volume of the strong-rock portion of the block, m³; k_u – borehole utilisation factor, dimensionless; P – borehole capacity in the coarse-block portion of the block, determined by the following expression, kg/m [18]:

$$P = k_1 + k_2 \frac{V_{ct}}{C_{ch}}, \quad (2)$$

where k_1 and k_2 – proportionality coefficients specific to the rock type; V_{ct} – yield of drill cuttings from boreholes drilled in strong-rock zones, %; C_{ch} – content of the most characteristic particle-size classes in drill fines, %.

To scale up the technology of within-block differentiation of drilling and blasting parameters, preliminary studies must be conducted for various rock types to establish correlations between the characteristics of drill cuttings and the capacity of drilled boreholes. The most labour-intensive operations involve determining such parameters as drill cuttings yield, content of the characteristic particle-size classes, and actual borehole capacity for each block.

It should be noted that reliable prediction of borehole capacity is essential for efficient blast design. To improve reliability and responsiveness, a machine learning-based method has been developed. The model's database includes high-resolution images of block boreholes and experimentally obtained borehole capacities measured during charging. Model training necessarily involves comparing predicted and actual values, followed by testing on data from the next block. A technology has been developed for drone-based imaging and laser scanning of the block, providing information support for a self-improving clustering model that predicts borehole capacity based on the characteristics of drill cuttings. This approach resolves the most labour-intensive component in implementing the within-block differentiation of drilling and blasting parameters.

Conclusion

Based on the conducted research and industrial experiments, combined solutions have been developed and tested for the use of rope and hydraulic excavators within their respective optimal application areas to improve the efficiency of mining operations. The priority application zone for hydraulic excavators is defined as areas with a planned low concentration of drilling-and-blasting operations, where the utilisation factor of rope shovels is below 0.5, while that of mobile hydraulic excavators is at least 0.7. At the same time, hydraulic excavators cannot directly compete with large mechanical shovels, particularly when working in hard rock formations. To address this issue, a specialised technology for within-block differentiation of drilling and blasting parameters is proposed, providing the geomechanical conditions necessary for the effective integration of hydraulic excavators into large-scale mining operations.

References

1. Blom M., Pearce A.R., Stuckey P.J. Short-term planning for open pit mines: a review. *International Journal of Mining, Reclamation and Environment*. 2019;33(5):318–339. <https://doi.org/10.1080/17480930.2018.1448248>
2. Nehring M., Knights P.F., Kizil M. S., Hay E. A comparison of strategic mine planning approaches for in-pit crushing and conveying, and truck/shovel systems. *International Journal of Mining Science and Technology*. 2018;28(2):205–214. <https://doi.org/10.1016/j.ijmst.2017.12.026>
3. Anistratov K. Yu. Feasibility Study of the Efficiency of Using EKG-18 Rack-and-Pinion Crowd Mining Excavators Manufactured by PJSC “Uralmashplant” in Coal Open-Pit Mines. *Russian Mining Industry*. 2016;(5):18–23. (In Russ.)
4. Demirel N., Taghizadeh A., Khouri S., Tyuleneva E. Optimization of the excavator-and-dump truck complex at open pit mines—the case study. In: *IIIrd International Innovative Mining Symposium. E3S Web of Conferences*. 2018;41:01006. <https://doi.org/10.1051/e3sconf/20184101006>



5. Kuznetsov D., Kosolapov A. Dynamic of performance of open-pit dump trucks in ore mining in severe climatic environment. *Transportation Research Procedia*. 2022;63:1042–1048. <https://doi.org/10.1016/j.trpro.2022.06.104>
6. Makarov V.N., Anistratov K.Yu. Achievement of the highest record indicators of the monthly production of EKG-18 excavators at open-pit mines of “StroyService” JSC. *Ugol’*. 2019;(1):20–26. (In Russ.) <https://doi.org/10.18796/0041-5790-2019-1-20-26>
7. Upadhyay S.P., Askari-Nasab H. Simulation and optimization approach for uncertainty-based short-term planning in open pit mines. *International Journal of Mining Science and Technology*. 2018;28(2):153–166. <https://doi.org/10.1016/j.ijmst.2017.12.003>
8. Deryabin S.A., Rzazade U.A., Kondratev E.I., Temkin I.O. Metamodel of autonomous control architecture for transport process flows in open pit mines. *Mining Informational and Analytical Bulletin*. 2022;(3):117–129. (In Russ.) https://doi.org/10.25018/0236_1493_2022_3_0_117
9. Samavati M., Essam D., Nehring M., Sarkeret R. A local branching heuristic for the open pit mine production scheduling problem. *European Journal of Operational Research*. 2017;257(1):261–271. <https://doi.org/10.1016/j.ejor.2016.07.004>
10. Samavati M., Essam D., Nehring M., Sarkeret R. A new methodology for the open-pit mine production scheduling problem. *Omega*. 2018;81:169–182. <https://doi.org/10.1016/j.omega.2017.10.008>
11. Khakulov V.A., Shapovalov V.A., Ignatov V.N. et al. Rational technology and application domain of hydraulic backhoes in open pit mines. *Mining Informational and Analytical Bulletin*. 2023;(8):112–127. (In Russ.) https://doi.org/10.25018/0236_1493_2023_8_0_112
12. Moreno E., Rezakhah M., Newman A., Ferreira F. Linear models for stockpiling in open-pit mine production scheduling problems. *European Journal of Operational Research*. 2017;260(1):212–221. <https://doi.org/10.1016/j.ejor.2016.12.014>
13. Rais K., Kara M., Gadri L. et al. Original approach for the drilling process optimization in open cast mines; case study of Kef Essenoun open pit mine Northeast of Algeria. *Mining Science*. 2017;24:147–159. <https://doi.org/10.5277/msc172409>
14. Brown C. Autonomous vehicle technology in mining. *World of Mining Professionals*. 2012;(1):30–32.
15. Khakulov V.A., Shapovalov V.A., Ignatov V.N. et al. Improvement of geotechnology based on monitoring and zoning of the geomechanical state of rock massifs. *Mining Informational and Analytical Bulletin*. 2023;(9):68–83. (In Russ.) https://doi.org/10.25018/0236_1493_2023_5_1_20
16. Lyashenko V.I., Khomenko O.E., Golik V.I. Friendly and resource-saving methods of underground ore mining in disturbed rock masses. *Mining Science and Technology (Russia)*. 2020;5(2):104–118. <https://doi.org/10.17073/2500-0632-2020-2-104-118>
17. Golik V., Komashchenko V., Morkun V., Irina G. Improving the effectiveness of explosive breaking on the bade of new methods of borehole charges initiation in quarries. *Metallurgical and Mining Industry*. 2015;7(7):383–387.
18. Zhaboev M.N., Khakulov V.A., Bakharev L.V., Ravikovich B.S. Improvement of the blasting technology for complex-structured rock masses. *Gornyi Zhurnal*. 1990;(9):22–23. (In Russ.)
19. Khakulov V.A., Karpova Zh.V., Khatukhova D.V., Shinakhova A.E. Improving drilling and blasting design based on artificial intelligence expert systems. *Gornyi Zhurnal*. 2025;(2):13–18. (In Russ.) <https://doi.org/10.17580/gzh.2025.02.07>

Information about the authors

Viktor A. Hakulov – Dr. Sci. (Eng.), Head of the Department of Information Technologies in Control of Technical Systems, Kabardino-Balkarian State University, Nalchik, Russian Federation; ORCID [0000-0001-9429-1774](https://orcid.org/0000-0001-9429-1774), Scopus ID [57200144748](https://scopus.org/57200144748), ResearcherID [B-2340-2018](https://orcid.org/B-2340-2018); e-mail vk21@yandex.ru

Vitaliy A. Shapovalov – Dr. Sci. (Phys. & Math.), Professor of the Department of Information Technologies in Control of Technical Systems, Kabardino-Balkarian State University, Nalchik, Russian Federation; ORCID [0000-0002-9701-6820](https://orcid.org/0000-0002-9701-6820), Scopus ID [57190966150](https://scopus.org/57190966150), ResearcherID [J-9696-2015](https://orcid.org/J-9696-2015); e-mail vet555_83@mail.ru

Viktor N. Ignatov – Dr. Sci. (Eng.), Professor of the Department of Mining, Platov South-Russian State Polytechnic University (NPI), Novocherkassk, Russian Federation; ORCID [0000-0001-5529-2395](https://orcid.org/0000-0001-5529-2395), Scopus ID [57200148638](https://scopus.org/57200148638); e-mail VNIgnatov@yandex.ru



Zhanna V. Karpova – Cand. Sci. (Eng.), Engineer, NIPi Nedra LLC, Novocherkassk, Russian Federation; ORCID [0000-0001-9664-5863](#), Scopus ID [57204943495](#); e-mail z.karpovaspb@gmail.com

Mikhail V. Ignatov – Cand. Sci. (Eng.), Associate Professor of the Department of Information Technologies in Control of Technical Systems, Kabardino-Balkarian State University, Nalchik, Russian Federation; ORCID [0000-0002-5393-470X](#), Scopus ID [57204758591](#); e-mail Ign_m@mail.ru

Ibragim A. Nogerov – Senior Lecturer of the Department of Information Technologies in Control of Technical Systems, Kabardino-Balkarian State University, Nalchik, Russian Federation; ORCID [0000-0001-8182-7293](#), Scopus ID [57200193883](#); e-mail nogerov.ibragim@mail.ru

Received 07.09.2025

Revised 11.10.2025

Accepted 17.10.2025



MINERAL RESOURCES EXPLOITATION

Research paper

<https://doi.org/10.17073/2500-0632-2024-07-284>

UDC 553.98

**Identification of remaining oil reserves at the late stage of development of the Gilbert field using integrated geophysical data**I. I. Bosikov¹ , R. V. Klyuev² , I. V. Silaev³ ¹ North Caucasus Mining and Metallurgical Institute (State Technological University), Vladikavkaz, Russian Federation² Moscow Polytechnic University, Moscow, Russian Federation³ North Ossetian State University named after K.L. Khetagurov, Vladikavkaz, Russian Federation

igor.boss.777@mail.ru

Abstract

The completeness of oil recovery under elastic water-drive conditions depends on numerous factors, including the geological structure of the reservoir, the properties of the oil-bearing formations, the interaction between the production zone and the peripheral area, the current reservoir pressure relative to the initial level, and the extent to which the productive horizons are swept by waterflooding throughout their thickness and areal distribution. The main objective of this study is to evaluate the remaining oil reserves in the field and to develop technologies for their efficient recovery. The degree of reserve depletion was assessed through a comprehensive analysis of all available data, enabling the identification of the oil-water contact (OWC) front movement and the current energy state of the reservoir. The assessment of recovery completeness was carried out using the results of field-geophysical surveys, the characteristics of oil-displacement by water, and data from hydrodynamic modelling. Geophysical monitoring was performed for each well individually to track the OWC position and identify water-swept zones of the productive reservoir. The Pulsed Neutron–Neutron Logging (PNNL) method was employed for real-time monitoring of oil-water interface movement during field development. It was established that the remaining recoverable reserves (RRR) account for 32.5% of the initial recoverable reserves (IRR). The current oil recovery factor (ORF) is 0.507. The field is currently at the fourth stage of development, characterized by a high water cut (94.8%) and a low annual oil-production rate (1.71–2.32% of the IRR).

Keywords

oil field, borehole, well logging, Pulsed Neutron–Neutron Logging (PNNL), oil-water contact (OWC), horizontal wells, interpretation, reservoir, porosity, collector, oil saturation

For citation

Bosikov I. I., Klyuev R. V., Silaev I. V. Identification of remaining oil reserves at the late stage of development of the Gilbert field using integrated geophysical data. *Mining Science and Technology (Russia)*. 2025;10(4):346–356. <https://doi.org/10.17073/2500-0632-2024-07-284>

РАЗРАБОТКА МЕСТОРОЖДЕНИЙ ПОЛЕЗНЫХ ИСКОПАЕМЫХ

Научная статья

Локализация остаточных запасов нефти на поздней стадии разработки Гильбертского месторождения по данным комплекса геофизических исследованийИ. И. Босиков¹ , Р. В. Ключев² , И. В. Силаев³ ¹ Северо-Кавказский горно-металлургический институт (государственный технологический университет), г. Владикавказ, Российская Федерация² Московский политехнический университет, г. Москва, Российская Федерация³ Северо-Осетинский государственный университет им. К.Л. Хетагурова, г. Владикавказ, Российская Федерация

igor.boss.777@mail.ru

Аннотация

Полнота выработки запасов нефти в условиях упруговодонапорного режима зависит от множества факторов: геологического строения коллектора, свойств нефтяных пластов, характера взаимосвязи зоны отбора с законтурной областью, состояния текущего пластового давления относительно начального уровня, а также степени охвата продуктивных горизонтов процессом заводнения по всей толще



и площади распространения. Основной задачей настоящего исследования является оценка оставшихся запасов нефти на месторождении и разработка технологий для их эффективной эксплуатации. Оценка степени отработки запасов проводится на основании комплексного анализа всех имеющихся данных, позволяющих определить особенности продвижения фронта водонефтяного контакта (ВНК) и энергетическое состояние резервуара. Анализ полноты выработки запасов проводился на основе результатов промысловых геофизических исследований, характеристик процесса вытеснения нефти водой и данных гидродинамического моделирования. Геофизический контроль выполнялся индивидуально по каждой скважине с целью мониторинга положения ВНК и выявления обводнённых участков продуктивного пласта. Метод импульсного нейтрон-нейтронного каротажа применялся для оперативного отслеживания динамики перемещения границы раздела нефть–вода в ходе разработки месторождения. Установлено, что остаточные извлекаемые запасы составляют 32,5% от начально извлекаемых запасов (НИЗ). Текущий коэффициент извлечения нефти составляет 0,507. Установлено, что месторождение находится на четвертой стадии разработки, характеризующейся высокой обводненностью (94,8 %) и низкими темпами отбора нефти (1,71–2,32 % от НИЗ в год).

Ключевые слова

нефтяные месторождения, скважина, каротаж, метод импульсного нейтрон-нейтронного каротажа, водонефтяной контакт, горизонтальные скважины, интерпретация, пласт, пористость, коллектор, нефтенасыщенность

Для цитирования

Bosikov I. I., Klyuev R. V., Silaev I. V. Identification of remaining oil reserves at the late stage of development of the Gilbert field using integrated geophysical data. *Mining Science and Technology (Russia)*. 2025;10(4):346–356. <https://doi.org/10.17073/2500-0632-2024-07-284>

Introduction

The efficiency of oil recovery under elastic water-drive reservoir conditions depends on multiple factors, including the geological structure of the field, reservoir properties, the nature of interaction between the production zones and the peripheral aquifer, the current reservoir pressure relative to the initial level, the areal and vertical sweep efficiency of the waterflooding process, and a number of other conditions.

The Gilbert oil field was discovered as a result of seismic exploration conducted within the northern part of the Sunzha anticline structure in the North Caucasus region, which is known for its Oligocene oil-bearing formations. The exploration activities were carried out by *Geofizinfo LLC* in 1996–1997. Subsequently, the obtained data were verified through detailed Common Depth Point (CDP) processing performed by *Regiongeofizika JSC* from 1997 to 1999. Exploratory drilling began in December 2001 with the spudding of the first prospecting well (No. 1). In the spring of 2002, testing of Middle Cambrian sandstone reservoirs yielded significant inflows of high-quality crude oil, confirming the presence of commercially viable hydrocarbon reserves in the area.

The commercial oil potential of the Gilbert field has been confirmed through a comprehensive suite of studies, including core analysis, well logging data, and successful testing of oil-bearing intervals conducted both during drilling and after geological and technical operations.

The objective of this study is to evaluate the remaining recoverable oil reserves in the field and to

develop technologies for their efficient recovery. This evaluation is based on a complete dataset enabling the assessment of the waterflood front advancement and the overall energy state of the reservoir.

The research methods are based on field and geophysical data, oil displacement characteristics, and hydrodynamic modeling. Geophysical investigations were aimed at monitoring the movement of the oil-water contact (OWC) and identifying water-swept zones within the productive horizon. Control of the OWC position was performed using the Pulsed Neutron-Neutron Logging (PNNL) method [1–3]. This method is among the most effective well logging techniques applied for lithological characterization of formations, determination of porosity, evaluation of hydrogen content, and identification of hydrocarbon-bearing zones [3–5].

The advantages of PNNL compared to other methods include: high sensitivity to hydrogen content; determination of effective porosity; delineation of productive intervals; minimal influence of rock density; environmental safety; and compatibility with modern data processing technologies.

Therefore, PNNL offers several benefits that enable obtaining detailed information on rock properties and effectively identifying productive intervals, providing a reliable basis for planning further exploration and development activities [4–6].

The research design involves monitoring the advancement of the OWC and detecting water-swept intervals of productive formations, along with implementing an integrated approach to studying oil recovery processes and well performance monitoring [6, 7].



The main objectives of the study are as follows:

1. To evaluate the dynamics and spatial characteristics of the OWC advancement and water breakthrough in the productive formations of the Gilbert field based on a comprehensive analysis of PNNL data and other field-geophysical investigations.

2. To determine the degree of depletion and localization of remaining recoverable oil reserves (RRR) through analysis of displacement characteristics, hydrodynamic modeling, and comparison of current and initial oil saturation data.

The scientific novelty of the study lies in the development and validation of an integrated methodology for localizing residual oil reserves at a late stage of field development in geologically complex reservoirs. The methodology includes the following elements:

- quantitative assessment of the contribution of heterogeneous waterflooding mechanisms (layered displacement and OWC rise) to total recovery and their spatial differentiation based on long-term PNNL monitoring data;

- verification of PNNL-based geophysical monitoring results using tracer studies, which made it possible to identify high-permeability channels (“super-reservoirs”) and assess their impact on displacement efficiency;

- integration of refined waterflood boundaries obtained from PNNL and tracer data into the hydrodynamic model, enabling high-confidence mapping of the distribution of residual movable oil reserves and delineation of specific zones for geological and technical interventions (GTI).

Reservoir productivity characteristics and initial development conditions

The data obtained in March 2002 during the testing of the first well indicated that the water-free oil production rate stabilized at 8.07–11.22 m³/day with 2–4 mm chokes and drawdowns of 2.86–3.67 MPa. The lowest point of the perforated interval, from which oil was produced (with flow rates varying from 8.1 to 11.2 m³/day), was located at an absolute elevation of –1988.1 m (approximately 2038–2040 m in measured depth). Due to the complex lithological structure of the reservoir — characterized by thin interbedding of sand and clay layers — precise determination of the oil–water contact (OWC) was challenging. The conditional boundary of the productive interval was established at a depth of 2047.4 m (absolute elevation –1995.3 m). According to the results of testing Well No. 1 conducted in May 2003 (perforation interval 2023–2038 m), the production rate of nearly pure oil ranged from 27.0 to 60.5 m³/day with 3–5 mm chokes

and drawdowns of 1.8–3.7 MPa [7]. The productivity index was estimated at 15.0–16.3 m³/(d·MPa) [8–10]. The first two exploratory wells were drilled within the oil-bearing contour: Well No. 1 located at the central site and Well No. 2 in its immediate vicinity. Additional studies, including detailed seismic data reprocessing and interpretation of all previously acquired information, were carried out after drilling Wells No. 1 and No. 2 in 2002, allowing the structural model of the Sunzha anticline to be refined. Analysis of the production performance of subsequent development wells (Nos. 3–9) showed the highest productivity indices in Wells No. 3 and No. 9 — approximately 40.9 and 53.3 m³/(d·MPa), respectively — with total liquid production (oil + water) ranging from 37.2 to 62.8 m³/day and 55.2 to 132.2 m³/day. The lowest values were recorded in Wells No. 4, No. 7, and No. 8, ranging from 9.0 to 12.9 m³/(d·MPa).

Such a wide variation in productivity parameters clearly indicates pronounced zonal heterogeneity of the reservoir. It is noteworthy that already at the stage of preparing the initial development plan [10–12], based on data from exploration and appraisal wells drilled in the central part of the Sunzha structure, poor reservoir storage and permeability properties were identified, which was reflected in the inflow performance relationship (IPR) curves.

During the hydrodynamic analysis, the reservoir temperature was determined to average approximately 58 °C.

The obtained experimental data made it possible to justify the initial reservoir pressure and to calculate productivity indices. The near-wellbore permeability and hydraulic conductivity were determined using the Dupuit equation [13–15].

The position of the initial oil–water contact was determined based on well test results and field-geophysical investigations.

Measurements by the Pulsed Neutron-Neutron Logging (PNNL) method were interpreted for nine wells. A comprehensive suite of well logging surveys (GIS) — including inflow profiling (thermometry, thermal flowmeter logging, and spinner flowmeter logging) — was performed in six wells.

Nearly all wells, except for horizontal ones, have been surveyed using field-geophysical methods throughout the development history. In total, 17 PNNL surveys were conducted in nine wells and seven inflow profile studies were performed.

Characteristics of oil-water contact rise

The upward movement of the OWC is non-uniform. The main factors controlling the dynamics of this process include the geological structure of the ac-



cumulation, the drilling rate, and the rate of reservoir fluid production. An important role is also played by vertical heterogeneity of the productive formations: the upper part is composed of sandstones with variable grain size; the middle part is characterized by increased heterogeneity and includes sandstones with a high content of silt and clay fractions; the lower part consists predominantly of sandstones [15,16].

Oil saturation was classified according to the following criteria: the reservoir contains essentially pure oil when the oil saturation exceeds 0.7 (70%); the reservoir is considered oil-water saturated with oil prevailing at saturation values from 0.6 to 0.7 (60–70%), including the lower boundary of 0.6; mixed oil–water saturation is characteristic of the interval from 0.3 to 0.6 (30–60%); at values below 0.3 (less than 30%), the pore space is fully saturated with water [16–18].

Interpretation of field-geophysical data

Well No. 1 is located in the near-contour zone in the northern part of the field. The geological section includes both high-capacity reservoir layers with porosity of 10–16% and thin interbeds with porosity of 2–6%. The producing interval at 2038–2040 m was perforated in 2002; testing with a 3 mm choke yielded an oil rate of 9.76 m³/d. The 2023–2038 m interval was perforated later, in 2013. Production from the well started in August 2004. Pulsed Neutron-Neutron Logging (PNNL) was run three times: immediately before the start of production and again in May 2019, when the water cut of the produced fluid was about 3%. Earlier, in 2006, comprehensive hydrodynamic surveys had been carried out at a low water cut (up to 3%), including PNNL, gamma-ray logging (GR), casing-collar locator (CCL), and inflow profiling [18, 19]. According to the 2019 PNNL results, intervals with a mixed “oil + water” fluid composition are identified from a depth of 2035.8 m, while “water + oil” intervals occur from 2038.4 m; clearly water-bearing zones are located below 2040.6 m.

Analysis of the gamma-ray log indicates that the main source of oil inflow is the upper part of the perforated interval (2023–2025 m), whereas water is produced predominantly from the lower perforation shots at 2039–2040 m. The repeated PNNL survey showed that the penetration zone of the “oil + water” mixture is confined to the upper part of the section (2023.6–2024.2 m); below, down to 2025 m, a “water + oil” composition dominates. Intermediate “water + oil” zones are also observed in the 2025.2–2025.8 m and 2032.0–2032.8 m intervals. These intervals are characterized by low oil saturation (0–8%), which confirms progressive layer-by-layer replacement of oil by water [19].

Thus, the low oil saturation in the 2039.8–2040.6 m interval according to the industrial cut-off criteria (oil saturation $S_o = 33\%$) and the appearance of water from deeper zones support the conclusion that the oil-water contact has migrated upward concurrently with layer-by-layer waterflooding of the section penetrated by the well.

Based on this analysis, a well intervention plan was proposed for Well No. 1: upon reaching a critical water cut of 99%, to isolate the currently producing perforation intervals 2038–2040 m (main) and 2023–2038 m (extended) by setting a pressure cement plug, followed by drilling out the cement plug and perforating the upper part of the reservoir in the 2023–2030 m interval.

According to PNNL data obtained from Well No. 2 at the initial stage of production, when the water cut did not exceed 1% (before near-wellbore stimulation), the section was characterized as oil-saturated.

Four months after the stimulation treatment, inflow-profile logging (1–6 December 2005) showed that almost the entire perforated interval contributed to production.

PNNL surveys demonstrated that the decrease in oil saturation was accompanied by a rise in the OWC. The current OWC position in the studied well is approximately two metres higher than the depth recorded during drilling.

In 2012, a further decline in oil saturation to 25–55% was recorded in the 2159.4–2164 m interval, along with evidence of layer-by-layer waterflooding in the lower part of the penetrated reservoir interval.

According to PNNL data acquired at water cuts above 80%, completely swept zones were observed within the perforated intervals. Below the perforated section, both oil-saturated layers and mixed oil-and-water intervals were identified, indicating layer-by-layer waterflooding in the lower unperforated portion of the section. However, no further upward movement of the OWC was detected.

Based on these results, geological and technical interventions were carried out in 2018–2019, including extended perforation of the 2168–2171 m interval combined with isolation of all previously opened zones. According to PNNL data, oil saturation in the newly opened interval reached 76–89%.

The results of PNNL analysis indicate both the upward movement of the OWC and layer-by-layer waterflooding of the productive formations; in some cases, these two processes were observed simultaneously.

Analysis of OWC rise dynamics over time showed that, at the early stage of field development, the rate of OWC movement was non-uniform. As of 2006, the difference in OWC depth among the five monitored

wells reached 13 m. The total fluid production rate in these wells ranged from 15 to 20 t/d, with drawdowns between 1.9 and 3.6 MPa. The greatest OWC displacement was observed in Wells No. 8 and No. 9, where the rise reached approximately 15 m.

Repeat surveys revealed the following changes in OWC level: in Well No. 2, the rise over a five-year period amounted to only 1.4 m; in Well No. 8, an increase of 7.6 m was recorded over seven years of production; whereas in Well No. 9, the OWC rose by 1 m within one year.

According to the trend relationships shown in Fig. 1, the current average OWC level is estimated at an absolute elevation of –1984 m.

The obtained results suggest that layer-by-layer waterflooding predominantly occurs in the peripheral zones of the field, extending from the northeast toward the southeast, whereas upward OWC displacement prevails in the central zones. Based on the interpretation of PNNL data and production history, it can be concluded that the remaining recoverable reserves (RRR) are mainly localized within the central dome-shaped area in the northeastern part of the oil reservoir.

In 2012, tracer tests were carried out at the Gilbert field. A tracer agent was injected into water-injection Well No. 12 to identify hydrodynamic communication between the injection and production wells, determine the actual flow velocities and directions of the injected water and reservoir fluids, and evaluate the influence of the injection well on the performance of the producing wells.

Several wells are characterized by the presence of a dominant permeable layer, distinguished by a pro-

nounced increase in tracer concentration. In Wells No. 4, 5, and 6, this layer was detected at the first tracer breakthrough, whereas in Wells No. 1, 2, 3, 10, and 11 it appeared only at the fourth arrival. The exception was Well No. 8, where tracer concentrations remained stable throughout the observation period.

Tracer concentration is inversely proportional to the number of major conductive layers. A distinctive feature of Well No. 5 is its extremely high tracer concentration, which indicates the presence of a small-volume but highly conductive flow channel. This suggests the existence of a fracture or zones of intensely developed reservoir rock (“super-reservoirs”). At present, this well shows the lowest water cut among comparable deviated wells (about 90%).

Water breakthrough at the Gilbert field began as early as 2007, when several wells exhibited a rapid increase in water cut to 70–80%. During the following thirteen years, the average annual growth rate of water cut ranged from 11 to 14%. After the commissioning of injection Well No. 12 in December 2010, the water cut in most deviated wells ranged from 42 to 82%.

Since 2011, the rate of water-cut increase has gradually declined: the annual growth dropped from 9.2% to negligible values of about 0.1% by 2016. For example, in Well No. 8, the water cut decreased from 90.8% in January 2016 to 84% by the end of December.

Thus, operation of injection Well No. 12 did not cause a significant increase in water cut, which agrees with the results of hydrodynamic modelling, indicating that shutting in Well No. 12 would have a minimal impact on oil-production water cut (less than 1%).

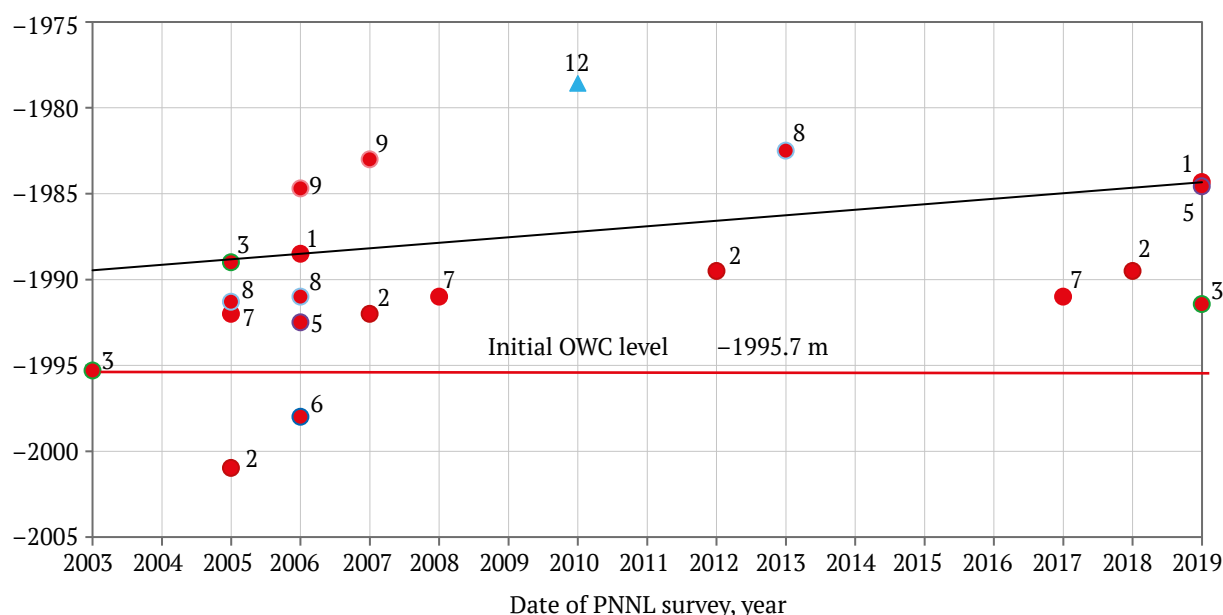


Fig. 1. Evaluation of OWC rise at the Gilbert field based on PNNL data

Analysis of displacement characteristics and evaluation of remaining recoverable reserves

The displacement characteristics provide an integrated representation of the actual oil recovery processes and the associated dynamics of reservoir waterflooding during the late stage of field development. Converting production parameters into displacement characteristics and selecting an appropriate empirical correlation make it possible to estimate the potential volumes of recoverable oil.

It should be noted that the most accurate determination of displacement characteristics is feasible for productive horizons with an extended production history and a water cut exceeding 80–90%. Field data collected over a 16-year period show a consistently high water cut in produced fluids and significant depletion of oil reserves.

The displacement characteristics were used to estimate the RRR under current development conditions, based on established analytical methods. Calculations were performed both using water-cut growth curves and production-rate decline relationships. The resulting values are presented in Table 1.

At a final water cut of 98%, the average RRR value is only slightly below 131 thousand tons. The actual displacement characteristics and forecast indicators derived from them are shown in Fig. 2.

Fig. 2 presents both actual and calculated displacement characteristics used to assess the redevelopment potential of the field. The left-hand graph illustrates the relationship between cumulative oil and liquid production, while the right-hand graph shows the relationship between current oil rate and water cut. The divergence between the actual data (solid

Table 1

Oil recovery factor (ORF) estimates for the Gilbert field based on displacement characteristics (different methods)

Indicator	Water-cut curves			Production decline curves		Average values
	A.M. Pirverdyan's method	S.N.Nazarov–N.V.Sipachev method	G.S. Kambarov's method	A.M. Pirverdyan's method	G.S. Kambarov–A.V. Kopytov method	
Cumulative oil production as of 01.01.2020, thousand tons	682	682	682	682	682	682
Cumulative oil production at the end of development, thousand tons	788	758	749	948	821	813
Incremental oil production as of 01.01.2023, thousand tons	106	76	67	266	139	131
Calculated ORF	0.583	0.560	0.554	0,701	0.607	0.601
Approved ORF	0.605					

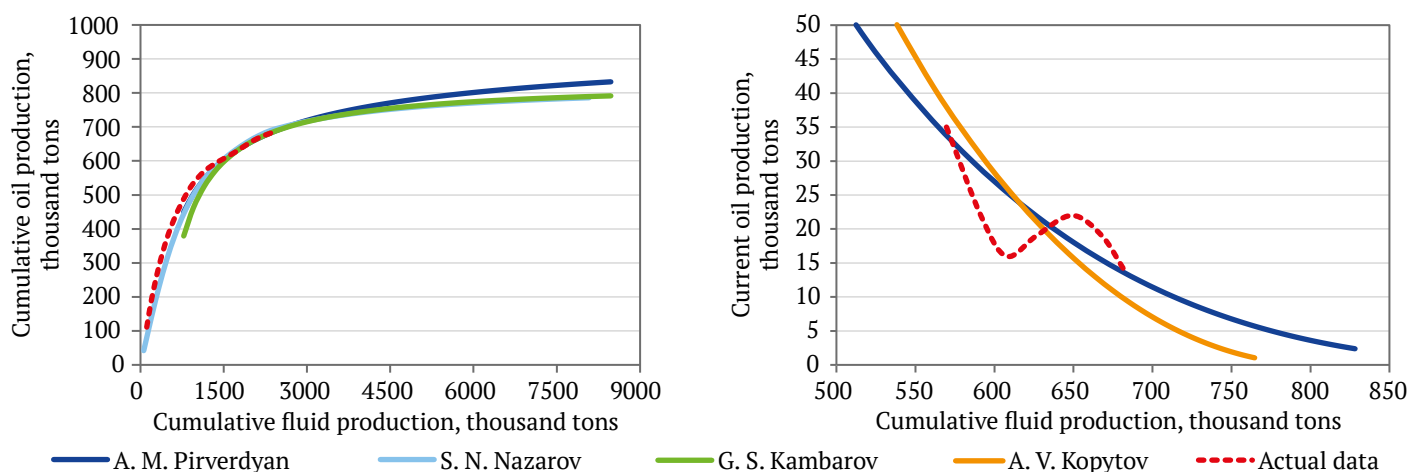


Fig. 2. Displacement characteristics of the Gilbert field

lines) and the predicted curves (dashed lines) in the region of high water cut values ($> 90\%$) and large cumulative liquid production indicates additional recovery potential, estimated at an average of 131 thousand tons of oil. These relationships formed the basis for calculating the oil recovery factor and determining the remaining reserves.

To further evaluate the efficiency of field development, displacement characteristics showing the relationship between water cut and oil recovery degree were constructed (Fig. 3).

The plots illustrate the dynamics of reservoir waterflooding as reserves are depleted. The horizontal axis represents the recovery degree relative to the initial recoverable reserves (IRR, %), while the vertical axis shows the water cut of produced fluids (%). The solid line corresponds to actual field data, whereas the dashed line represents the fitted empirical correlation (displacement characteristic) used to forecast performance parameters up to the economic limit water cut (98%). Analysis of the curve confirms that the field has entered the final stage of development, with the current water cut at 94.8% and 84.2% of the IRR recovered.

A single Middle Cambrian reservoir (Horizon 2) is currently under development. The recovery degree for this reservoir is 83.4%, which corresponds to the value recorded in the State Reserve Balance as of 1 January 2022. The water cut of produced fluids reaches

94.8%. The slight discrepancy between the recovery degree relative to the IRR and the water cut level indicates that the planned ORF and cumulative production reported in the State Reserve Balance have been achieved as of the specified date.

Analysis of the available data indicates that reservoir water encroachment is driven by two mechanisms: upward movement of the OWC and layer-by-layer waterflooding. Layer-by-layer waterflooding mainly occurs in the peripheral zones of the field, extending from the northeast toward the southwest, whereas upward OWC movement predominates in the central part of the accumulation. Based on the interpretation of PNNL neutron-carbonate logs and production history data, accumulations of remaining unrecovered oil were identified in the northeastern part of the reservoir near the fractured zones around Wells No. 1 and No. 8, as well as in the central area near Wells No. 2 and No. 4.

Analysis of the displacement characteristics made it possible to estimate the expected volume of RRR under current development conditions. The predicted RRR values range from 67 to 266 thousand tons, with an average of approximately 131 thousand tons.

The degree of depletion and the spatial distribution of the remaining oil were verified through hydrodynamic modelling (as of 1 January 2022), which provided a more accurate assessment of the current recovery degree (Table 2).

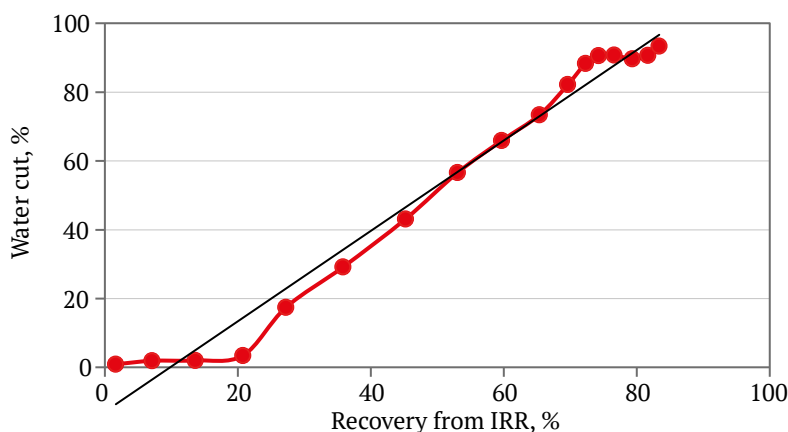


Fig. 3. Relationship between low-viscosity hydrocarbon recovery and reservoir water cut for the Gilbert field

Table 2

Oil recovery performance of the Gilbert field as of 01 January 2022

Field	Reservoir	Reserve category	Initial geological reserves, thousand tons	Approved ORF	Initial recoverable reserves, thousand tons	Cumulative oil production as of 01.01.2022, thousand tons	Recovery from IRR, %	Current ORF	Current water cut, %	Remaining recoverable reserves, thousand tons	Remaining recoverable reserves, %
Gilbert	Middle Cambrian	A	1582	0.609	997	785	84.2	0.507	94.8	185	18.5

Fig. 4 shows the distribution of movable oil reserves in the Middle Cambrian reservoir of the Gilbert field at the initial stage of development (as of 01 January 2019, the date of project preparation – 2020) and as of 01 January 2022. The density maps indicate that the highest concentrations of movable reserves occur in areas of maximum initial oil-saturated thickness.

Analysis of the obtained data reveals the following:

1. The Middle Cambrian reservoir is at the fourth stage of development, characterised by declining oil production rates, a high water cut in produced fluids, and a reduced recovery rate relative to the initial recoverable reserves.

2. The highest concentrations of movable oil reserves are found in the northern and eastern parts of the accumulation near Wells No. 1 and No. 8, with smaller volumes remaining in the central productive zone near Wells No. 2 and No. 4.

3. The remaining recoverable reserves (185 thousand tons, according to hydrodynamic modelling) can be efficiently produced through the existing wells (Nos. 1–10). To accelerate depletion, it is recommended to perform geological and technical interventions or drill an additional sidetrack from either Well No. 1 or No. 8, depending on which reaches the critical water-cut level first.

Fig. 4 presents spatial distribution maps of movable oil reserve density: (a) at the initial stage of

development (2019) and (b) as of 01 January 2022. Analysis of these maps demonstrates significant reserve redistribution resulting from field depletion. The highest concentration of remaining movable reserves persists in the northeastern part of the accumulation near Wells No. 1 and No. 8 and in the central area near Wells No. 2 and No. 4. Comparison of the maps highlights the zones of most intensive depletion and confirms the localization of residual reserves within near-wellbore areas characterized by the best reservoir storage and permeability properties.

Practical significance

The findings of this study have the following practical implications:

- they enable a shift from extensive to targeted field development by accurately identifying zones of remaining oil reserves, which in turn supports the planning of focused geological and technical interventions;

- they provide a quantitative estimate of the redevelopment potential – about 185 thousand tons of additional oil – which justifies continued operation and effectively extends the field's life cycle;

- they demonstrate that the integrated workflow combining PNNL, tracer testing, and hydrodynamic modeling can be replicated at comparable fields to improve oil recovery.

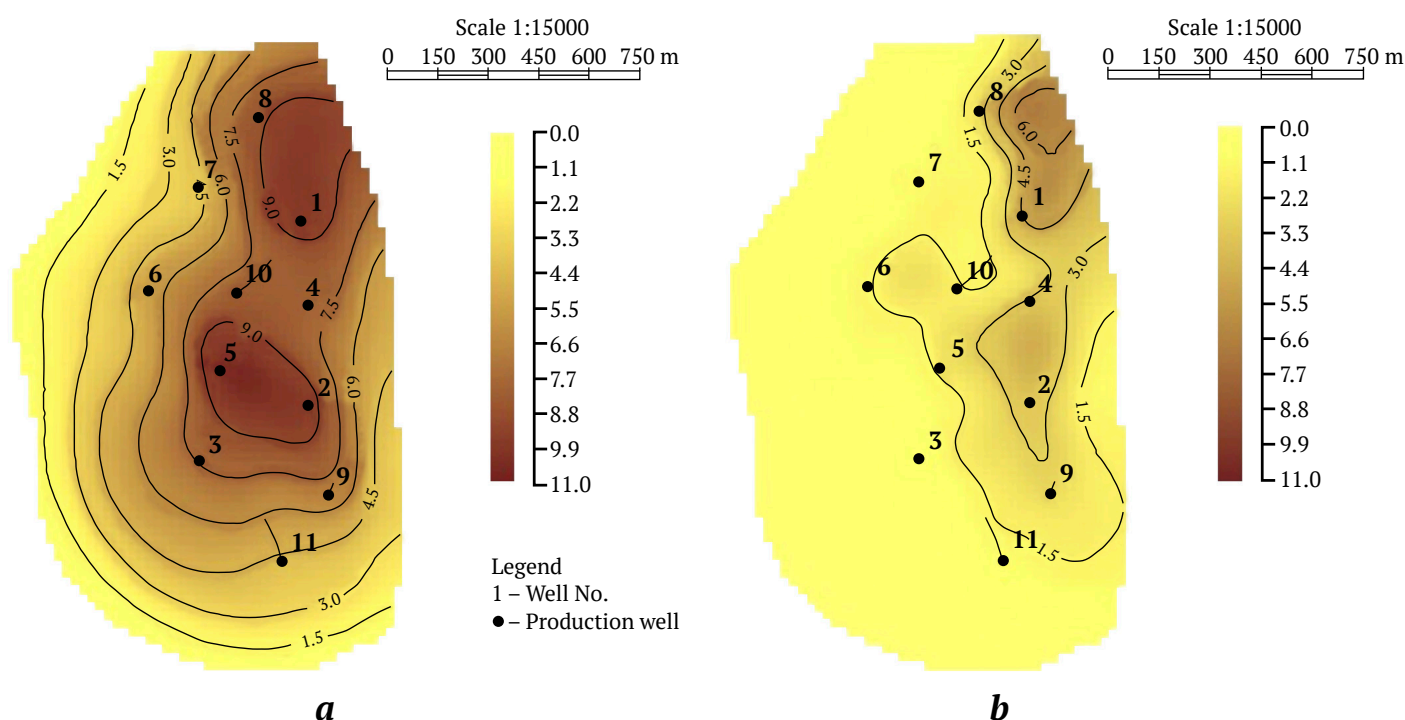


Fig. 4. Map of movable oil reserves in the Gilbert field:
a – at the start of development (2019); b – as of 01 January 2022



Economic efficiency

This study shifts field management at the late stage of development from a predominantly operational focus to a strategic one. The identified redevelopment potential provides a sound basis for economically justified extension of the field's productive life.

Previously, geological and technical interventions were associated with high risk due to uncertainty in the location of productive intervals. The proposed methodology allows operators to move from uniform well servicing to a selective investment strategy. Clear spatial localization of remaining reserves makes it possible to design an optimized program of geological and technical interventions and avoid costly exploratory operations.

Most of the additional oil production can be obtained from the existing well stock, which reduces the need for new capital-intensive infrastructure and significantly improves project profitability. Realizing the identified potential will move the recovery factor closer to the approved target, effectively converting part of the reserves into commercially recoverable volumes. Thus, the economic value of this work lies not only in the direct monetization of additional oil volumes, but also in the development of a management framework that supports a profitable and orderly completion of field development.

Conclusions

Based on a comprehensive analysis of oil recovery performance at the Gilbert field using geographic information systems and field-geophysical data, the following conclusions can be drawn:

1. The main objective of the study has been achieved: the RRR have been quantified and their

main accumulation zones identified. The RRR amount to 18.5% of the initial recoverable reserves. The ORF is 0.507, compared with the approved value of 0.609. The field is at the fourth stage of development, characterized by a high water cut of 94.8%.

2. The dynamics and pattern of OWC movement and reservoir water encroachment have been evaluated. Analysis of PNNL data shows that the OWC rise is non-uniform: in the central part of the reservoir, an upward shift of 2–15 m has been recorded, whereas layer-by-layer waterflooding predominates in the peripheral zones. The current OWC level is estimated at an absolute elevation of –1984 m.

3. The depletion level and spatial distribution of the RRR have been determined. Hydrodynamic modelling combined with displacement characteristic analysis indicates that unrecovered reserves are concentrated in a fault-adjacent zone near Wells No. 1 and No. 8, as well as in the central part of the field near Wells No. 2 and No. 4.

4. The effectiveness of PNNL for development monitoring has been confirmed. In total, 17 surveys were carried out in nine wells, which made it possible to delineate water-swept and oil-saturated intervals and to assess current oil saturation. In waterflooded intervals, saturation has decreased to 25–55%.

In summary, the study has provided a detailed picture of the current state of the Gilbert field, substantiated the volume and distribution of the remaining recoverable reserves, and proposed measures to enhance oil recovery. These results are expected to reduce technological risks and improve the economic efficiency of further field development.

References

1. Bembel R.M., Sukhov V.A., Schetinin I.A. Ways of increasing geological efficiency of hydrocarbon fields development in Western Siberia. *Oil and Gas Studies*. 2017;(6):6–10. (In Russ.) <https://doi.org/10.31660/0445-0108-2017-6-6-10>
2. Bosikov I.I., Klyuev R.V., Khetagurov V.N., Silaev I.V. Comprehensive assessment of hydrodynamic processes in the Klinskoye Quarry with the use of their control methods in rock masses. *Sustainable Development of Mountain Territories*. 2023;15(2):284–297. (In Russ.) <https://doi.org/10.21177/1998-4502-2023-15-2-284-297>
3. Gayduk V.V. The nature of the oil and gas potential of the Tersko-Sunzhensky oiland gas-bearing region. *Geology, Geophysics and Development of Oil and Gas Fields*. 2019;(2):40–46. (In Russ.) <https://doi.org/10.30713/2413-5011-2019-2-40-46>
4. Medvedev N.Y. *Geotechnological basis for the development of oil pools with hard-to-recover reserves*. Moscow: VNIIOENG; 1997. 336 p. (In Russ.)
5. Danilov V.N. Formation of thrusts and hydrocarbon potential of Urals Foredeep. *Russian Oil and Gas Geology*. 2021;(1):57–72. (In Russ.) <https://doi.org/10.31087/0016-7894-2021-1-57-72>



6. Jafarov R.R., Rahimov F.V., Hashimova G.I. Perspectives of upper kirmaki clay suite in Chilov field. *Azerbaijan Oil Industry Journal*. 2020;(12):12–16. (In Russ.) <https://doi.org/10.37474/0365-8554/2020-12-12-16>
7. Ivlev D.A. Method for regional forecast of oil and gas potential territories by machine learning algorithms on the example of the Tyumen formation of Western Siberia. *Bulletin of the Tomsk Polytechnic University. Geo Assets Engineering*. 2021;332(1):41–53. (In Russ.) <https://doi.org/10.18799/24131830/2021/1/2998>
8. Kaukenova A.S. Oil and gas potential of the south Turgay basin. Proceedings of higher educational establishments. *Geology and Exploration*. 2020;(3):38–45. (In Russ.) <https://doi.org/10.32454/0016-7762-2020-63-3-38-45>
9. Kobylinsky D.A. Criteria for determining the oil and gas potential of the territory based on the data of ground geochemical survey performed on the ground and artificial sorbent. *The Eurasian Scientific Journal*. 2020;12(6):1–10. (In Russ.) URL: <https://esj.today/PDF/51NZVN620.pdf>
10. Kuznetsov V.G., Zhuravleva L.M. Reef formations in the West Canada basin and their oil and gas potential. *Lithology and Mineral Resources*. 2018;53(3):236–251. <https://doi.org/10.1134/S0024490218030045> (Orig. ver.: Kuznetsov V.G., Zhuravleva L.M. Reef formations in the West Canada basin and their oil and gas potential. *Litologiya i Poleznye Iskopaemye*. 2018;(3):257–273. (In Russ.) <https://doi.org/10.7868/S0024497X18030047>)
11. Gainanshin R.N., Khafizov S.F., Abramov V.Y. et al. Oil and gas perspective assessment and the choice of the exploration program based on the multivariate geological modeling. *Territoriya Neftegaz*. 2019;(3):12–16. (In Russ.)
12. Bosikov I.I., Klyuev R.V., Revazov V.Ch., Martyushev N.V. Analysis and evaluation of prospects for high-quality quartz resources in the North Caucasus. *Mining Science and Technology (Russia)*. 2023;8(4):278–289. <https://doi.org/10.17073/2500-0632-2023-10-165>
13. Panikarovskii E.V., Panikarovskii V.V., Anashkina A.E. Vankor oil field development experience. *Oil and Gas Studies*. 2019;(1):47–51. (In Russ.) <https://doi.org/10.31660/0445-0108-2019-1-47-51>
14. Sharafutdinov V.F., Cherkashin V.I., Musikhin V.A. et al. Prospects of oil and gas production of michael deposits of Buy-Naks depression of pre-degrenary Daghestan. *Proceedings of the Institute of Geology of the Dagestan Scientific Center of the Russian Academy of Sciences*. 2018;1(72):17–23. (In Russ.) <https://doi.org/10.31161/2541-9684-2018-62-1-17-23>
15. Bronskova E.I. Comprehensive analysis of April field geological structure to provide effective additional exploration and development of Tyumen suite deposits. *Geology, Geophysics and Development of Oil and Gas Fields*. 2016;(8):36–44. (In Russ.)
16. Sevostyanova R.F., Sitnikov V.S. The development of ideas about the structure and oil and gas potential of Nepa-Botuoba anticline and adjacent part of Predpatomskii trough. *Journal of Mining Institute*. 2018;234:599–603. <https://doi.org/10.31897/pmi.2018.6.599>
17. Cherkashin V.I., Sabanaev K.A., Gadzhieva T.R. Tectonic structure and perspectives of oil and gas sedimentary cover of the bottom of the Caspian Sea. *Proceedings of the Institute of Geology of the Dagestan Scientific Center of the Russian Academy of Sciences*. 2018;4(75):24–29. (In Russ.) <https://doi.org/10.31161/2541-9684-2018-62-4-25-30>
18. Ulmasvay F.S., Dobrynina S.A., Sidorchuk E.A. New regularities in the distribution of oil and gas in sedimentary stratum (by the case of Ciscaucasia). *Actual Problems of Oil and Gas*. 2018;1(20):8. <https://doi.org/10.29222/ipng.2078-5712.2018-20.art8>
19. Bosikov I.I., Klyuev R.V., Martyushev N.V. et al. Analysis of the quality of underground mineral waters of terrigenous deposits of the hauterivbarremian aquifer of the lower cretaceous. *News of the National Academy of Sciences of the Republic of Kazakhstan. Series of Geology and Technical Sciences*. 2024;2(464):36–47. <https://doi.org/10.32014/2024.2518-170x.392>

Information about the authors

Igor I. Bosikov – Dr. Sci. (Eng.), Associate Professor, Head of the Department of Oil and Gas Engineering, North Caucasus Mining and Metallurgical Institute (State Technological University), Vladikavkaz, Russian Federation; ORCID [0000-0001-8930-4112](https://orcid.org/0000-0001-8930-4112), Scopus ID [56919738300](https://scopus.org/56919738300); e-mail igor.boss.777@mail.ru



Roman V. Klyuev – Dr. Sci. (Eng.), Associate Professor, Professor of the Department of Low-Temperature Engineering named after P.L. Kapitsa, Moscow Polytechnic University, Moscow, Russian Federation; ORCID [0000-0003-3777-7203](#), Scopus ID [57194206632](#), Research J-8000-2014; e-mail kluev-roman@rambler.ru

Ivan V. Silaev – Cand. Sci. (Eng.), Associate Professor, Head of the Department of Physics and Astronomy, North Ossetian State University named after K.L. Khetagurov, Vladikavkaz, Russian Federation; ORCID [0000-0003-2490-1578](#), Scopus ID [57189031683](#)

Received 16.07.2024

Revised 24.10.2025

Accepted 27.10.2025




DIGITAL TECHNOLOGIES AND ARTIFICIAL INTELLIGENCE

Research paper

<https://doi.org/10.17073/2500-0632-2025-05-413>

UDC 550.8.013:622.276.1/4

**Comprehensive study of the anisotropy of microstructural and filtration properties of a gas condensate field reservoir based on digital core analysis**V. V. Khimulia   *Ishlinsky Institute for Problems in Mechanics of the Russian Academy of Sciences,
Moscow, Russian Federation* khim@ipmnet.ru**Abstract**

Modern technologies based on numerical simulation and X-ray microtomography provide new opportunities for detailed study of a reservoir pore space and prediction of its filtration properties. The paper describes the findings of digital analysis of pore space and filtration characteristics of poorly consolidated sandstones in a pay interval of a gas condensate field located in the northern shelf of the Russian Federation. The study was conducted based on data from X-ray computed microtomography, digital core analysis methods, and numerical simulation. To build digital twins of a core, 3D images of the reservoir rocks were processed and binarized. Calculations of the directional variability of key reservoir properties including open and closed porosity, geodesic tortuosity, and percolation path characteristics were performed, as well as numerical simulation of filtration flow in three orthogonal directions. Special attention was paid to determining the representative elementary volume based on step-by-step averaging of porosity across cubic domains. The results demonstrate a weak but stable anisotropy in the filtration properties of rocks, associated with the directional structure of the pore framework. It has been found that even with similar values of open porosity, the geometry of filtration paths and tortuosity have a significant effect on permeability. The data obtained are of practical importance for geological and hydrodynamic simulations, optimization of horizontal well direction, assessment of sand production risk, and prediction of filtration front stability in offshore field development. The work emphasizes the need for a comprehensive digital approach when assessing the filtration properties of reservoirs in conditions of complex lithology and limited core material.

Keywords


digital core analysis, porosity, permeability, tortuosity, percolation paths, filtration properties, anisotropy, filtration and capacitance properties

For citation

Khimulia V.V. Comprehensive study of the anisotropy of microstructural and filtration properties of a gas condensate field reservoir based on digital core analysis. *Mining Science and Technology (Russia)*. 2025;10(4):357–368. <https://doi.org/10.17073/2500-0632-2025-05-413>

ЦИФРОВЫЕ ТЕХНОЛОГИИ И ИСКУССТВЕННЫЙ ИНТЕЛЛЕКТ

Научная статья

**Комплексное исследование анизотропии
микроструктурных и фильтрационных свойств коллектора
газоконденсатного месторождения на базе цифрового анализа керна**В. В. Химуля   *Институт проблем механики имени А.Ю. Ишлинского РАН,
г. Москва, Российская Федерация* khim@ipmnet.ru**Аннотация**

Современные технологии, основанные на применении методов численного моделирования и рентгеновской микротомографии, предоставляют новые возможности для детального изучения порового пространства коллектора и прогноза его фильтрационно-ёмкостных свойств. В статье описаны результаты цифрового анализа порового пространства и фильтрационных характеристик слабосцементированных песчаников продуктивного интервала газоконденсатного месторождения, расположенного на северном шельфе РФ. Исследование выполнено на основе данных рентгеновской компьютерной микротомографии, методов цифрового анализа керна и численного моделирования. Для построения цифровых двойников керна выполнена обработка и бинаризация 3D-снимков коллектора. Проведены количественные расчёты



направленной изменчивости ключевых коллекторских свойств, включая открытую и закрытую пористость, геодезическую извилистость, характеристики перколяционных путей, а также численное моделирование фильтрационного потока по трём ортогональным направлениям. Отдельное внимание уделено определению репрезентативного элементарного объёма на основе поэтапного усреднения пористости по кубическим доменам. Результаты демонстрируют слабовыраженную, но устойчивую анизотропию фильтрационных свойств пород, связанную с направленной структурой порового каркаса. Выявлено, что даже при близких значениях открытой пористости геометрия фильтрационных путей и извилистость оказывают значительное влияние на проницаемость. Полученные данные имеют практическую значимость для задач геолого-гидродинамического моделирования, оптимизации направления горизонтальных скважин, оценки риска пескопроявлений и прогноза устойчивости фильтрационного фронта при разработке шельфовых месторождений. Работа подчёркивает необходимость комплексного цифрового подхода при оценке фильтрационных свойств коллекторов в условиях сложной литологии и ограниченности кернового материала.

Ключевые слова

цифровой анализ керна, пористость, проницаемость, извилистость, пути перколяции, фильтрационные свойства, анизотропия, ФЕС

Для цитирования

Khimulia V.V. Comprehensive study of the anisotropy of microstructural and filtration properties of a gas condensate field reservoir based on digital core analysis. *Mining Science and Technology (Russia)*. 2025;10(4):357–368. <https://doi.org/10.17073/2500-0632-2025-05-413>

Introduction

Modern technologies based on numerical simulation and X-ray microtomography provide new opportunities for detailed study of a reservoir pore space and prediction of its filtration properties [1, 2]. However, traditional assessment methods (laboratory measurements using a core [3], hydrodynamic well studies, empirical correlations [4]) do not take into account the microstructure of the pore framework and often do not allow reliable prediction of permeability based solely on porosity [4]. This is particularly relevant for poorly consolidated sandstones in gas condensate offshore fields, where reservoir stability and filtration efficiency [5] often depend not only on pore volume, but also on their spatial arrangement [6]. The use of digital core twins based on microtomographic data allows reproducing the topology of the pore space [7, 8] and improving the reliability of productivity forecasts [9].

One of the key tasks of digital analysis is the quantitative characterization of parameters affecting filtration processes, including open and closed porosity [7, 9], tortuosity [10], percolation channel structure [11], and directional (anisotropic) variability of these parameters [12, 13]. This is particularly important when exploiting formations (reservoirs) with horizontal wells, where drainage efficiency can significantly depend on the orientation of the wellbore relative to the textural features of the reservoir [14, 15].

The number and morphology of filtration channels are critical in the development of offshore fields [16], where operational errors can lead to sand production, rock removal, and a sharp drop in permeability [17, 18]. In poorly consolidated rocks, the stability of well walls [19] and local permeability are determined not so much by averaged characteristics [20] as by microstructural parameters of the pore framework, including substructural anisotropy [21, 22]. Despite the increasing

importance of considering the above characteristics, most studies are limited to isotropic models or focus on porosity, without taking into account the complex influence of pore morphology on filtration [23, 24].

The aim of this study is to quantitatively describe the anisotropy of filtration properties, a targeted analysis of morphometric characteristics and their relationship to permeability for poorly consolidated sandstones in a pay interval of a gas condensate field on the northern shelf based on digital core twins, followed by interpretation of the results for hydrodynamic simulation, the propagation of the filtration front in a formation, and designing horizontal well directions. The scientific novelty of the work lies in performing a comprehensive digital assessment of the spatial anisotropy of a pore space, taking into account the morphological and physical characteristics of a reservoir, establishing the fact of stable substructural anisotropy within the bedding plane for the field under consideration, justifying the directions for drilling horizontal wells in conditions of textural heterogeneity of the formation, conclusions about the risks of local pressure accumulation in the formation and capillary isolation of condensate.

To achieve this goal, the following tasks were set:

1. Building digital twins of the core based on high-resolution microtomographic data.
2. Determination of open and closed porosity, tortuosity, percolation path parameters, and assessment of their directional variation.
3. Numerical simulation of filtration flow in three orthogonal directions with permeability calculation.
4. Analysis of the relationship between the geometric characteristics of the pore space and filtration properties.
5. Determination of representative elementary volume (REV) and justification of the reliability of the digital model.

1. Research Technique and Subjects

The subject of the study was the reservoir rocks of a pay intervals of a gas condensate field located on the northern shelf of Russia. The rocks are represented by poorly consolidated sandstones characterized by low strength and high porosity and permeability. This extracted reservoir is characterized by the lack of pronounced visual bedding and is subject to intense sanding. Core fragments were selected from the pay interval, followed by the preparation of more than 10 samples of arbitrary shape with dimensions ranging from 5 to 20 mm. X-ray computed microtomography method was used to study the pore space. The scanning was performed using Procon X-Ray CT-MINI instrument from the Institute of Mechanics Problems of the Russian Academy of Sciences [9]. The obtained tomographic data consisted of sets of slices with a resolution (voxel = cubic pixel size [25]) of 4.995 μm , reconstructed into three-dimensional digital models of core fragments. All samples had a similar structural composition that confirms the representativeness of the sample set, but for subsequent digital analysis, samples with a complete absence of fracturing were selected, which may be the result of the influence of transportation and storage conditions on the fracturing-prone material.

After reconstruction and processing (including Gradient and/or Gaussian Brightness correction [26], filtering with Non-local Means algorithms [27]), segmentation [28] of tomographic images was performed to distinguish two phases: pore space (air) and solid matrix (grains). VGStudio software [29] was used for the reconstruction, as well as proprietary algorithms for processing 3D images. Threshold algorithms based on the analysis of the intensity

distribution histogram were used for the segmentation [28]. As a result, a binary voxel model (a digital twin) was formed, in which each voxel was designated as either porous or matrix. Such models serve as the basis for subsequent calculations. Figure 1 shows the main stages of processing and segmentation of the tomographic data.

Digital analysis of the pore space included:

- assessment of open and closed porosity in three orthogonal directions;
- calculation of geodesic tortuosity (minimum, maximum, and average) based on algorithms for finding the shortest paths from one face of a three-dimensional binary model to the opposite face;
- identification and analysis of percolation paths including calculation of their length and diameter of constrictions (maximum diameter of a particle passing through a channel);
- numerical simulation of filtration flow based on the navier–stokes model using laminar flow conditions to estimate permeability and flow distribution in each direction;
- construction of visual maps of velocities, pressure gradients, and porosity distribution by layers for qualitative interpretation of the spatial structure of the pore framework.

The pore space analysis was performed in GeoDict [30]. Open and closed porosity was calculated by counting the proportions of pore voxels. Open porosity was defined as the proportion of voxels that are connected to one of the outer faces of the model and form a through path. Closed porosity refers to isolated pores that are not connected to external faces. These values were calculated separately for three orthogonal directions.

A voxel size is 4.995 μm

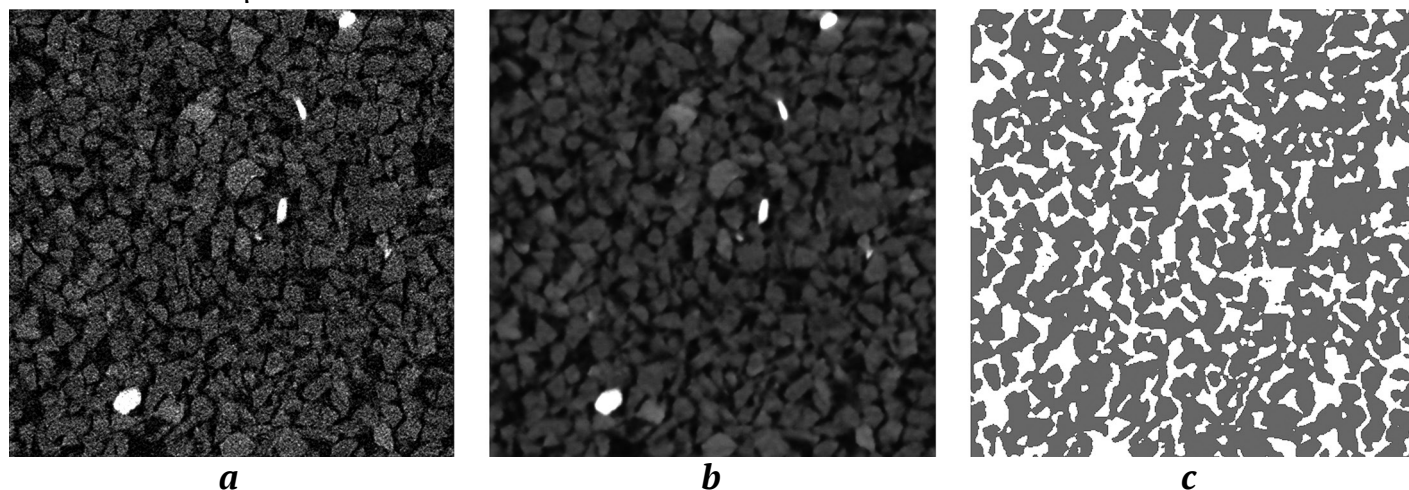


Fig. 1. The main stages of preprocessing and segmentation of tomographic data:

a – part of the projection of the reconstructed image; *b* – part of the projection of the image after preliminary processing and smoothing; *c* – the same area after segmentation into two phases: gray represents matrix grains, white represents pores



Geodesic tortuosity was assessed based on the construction of the shortest paths from one face of a sample to the opposite face in each direction. Tortuosity was determined as the ratio of the path length through the pore space to the geometric length of the sample.

Unlike tortuosity, which can take into account narrow areas inaccessible to real fluid, the percolation path search algorithm constructed physically realistic trajectories, taking into account the diameter of a passing particle. The algorithm excluded paths with bottlenecks (throats) smaller than the specified diameter and selected those channels through which a particle could pass without disrupting continuity. For each direction, the following were calculated: the length of the percolation path (the actual distance that a particle would travel); the maximum diameter (the minimum cross-sectional size along the path, the narrowest point) determining passability. As a result of visualization, a set of filtration channels corresponding to the physical conditions of fluid conductivity was obtained. Thus, the study applied a physically oriented approach to percolation, allowing the identification of effective filtration flow trajectories, taking into account geometric constraints.

Based on the binary model, fluid (air) flow through a pore space was simulated using the Navier–Stokes equations [31] in a steady laminar configuration:

$$-\mu\Delta\vec{u} + \rho(\vec{u} \cdot \nabla)\vec{u} + \nabla p = \vec{f},$$

where μ is fluid viscosity, Pa·s; \vec{u} is fluid velocity, m/s; ρ is fluid density, kg/m³; p is pressure, Pa; \vec{f} is body force, N/m³.

The mass conservation equation in this case takes the form:

$$\nabla \cdot \vec{u} = 0.$$

The permeability of a material can be calculated using Darcy's law:

$$Q = \frac{-kA}{\mu} \cdot \frac{P_b - P_a}{L},$$

where Q is fluid flow rate, m³/s; k is permeability of the medium, m²; A is cross-sectional area of the flow, m²; μ is viscosity of the fluid, Pa·s; P_b and P_a are pressures, Pa; L is the length over which this pressure drop occurs, m.

In this study, the LIR solver [32] was used for numerical simulation of filtration. The calculations were performed with a specified pressure drop of 100 Pa. The criterion for completing the calculations is an error bound of 0.1 [33]. Periodic boundary conditions with 10-voxel layers at the inlet and outlet were set in the calculation direction to ensure flow uniformity. Symmetric boundary conditions were set in the

tangential direction [33]. The following were calculated at the output: velocity and pressure fields; integral permeability value for each direction (according to Darcy's generalized law); visualization of velocity channels reflecting active filtration paths. Unlike traditional permeability assessment methods, such as laboratory filtration tests, ϕ – k correlations, and Carman-Kozeny models, the approach used is based on direct numerical simulation of filtration using 3D microtomography data. It allows not only to take into account the actual geometry of the pore space and anisotropy, but also to conduct a detailed analysis of the structure of filtration channels.

To accurately assess the heterogeneity of the pore space structure, layer-by-layer porosity cartograms were constructed [34]. The model was averaged across layers perpendicular to the selected axis, and then the porosity was displayed as a two-dimensional color map. This made it possible to identify vertical or horizontal fluctuations in the structure and visually assess the homogeneity of a sample.

In addition to numerical simulation, laboratory measurements of permeability along Z axis of core and in XY bedding plane were carried out at the TILTS installation of IPMech RAS [9]. The laboratory values obtained were used to validate the digital model and compare it with the results of direct numerical calculations.

2. The Findings and Discussion

Table 1 shows the summary results of the digital analysis for three characteristic samples. The final digital samples were cubes measuring 500 voxels, which were used to perform filtration calculations in three mutually perpendicular directions, X , Y , and Z (Z axis coincided with the longitudinal axis of a core). The table includes the values of geodesic tortuosity (minimum, maximum, and average), length calculated during the assessment of trajectory tortuosity (minimum, maximum, and average), percolation path parameters (average maximum particle diameter and average physical path length across all channels in a given direction), as well as open and closed porosity values and calculated permeability. The table is structured by sample: rows are grouped by sample number, each row corresponds to one simulation direction.

The obtained porosity data demonstrate high uniformity of the pore space both in quantitative terms and in spatial distribution. The open porosity in all three orthogonal directions is practically identical and amounts to about 26% (see Table 1), with differences between the directions not exceeding hundredths of a percent. The maximum open porosity value is observed along X -axis ($\approx 26.007\%$),



the minimum one is along Y -axis ($\approx 25.995\%$), and along Z -axis the value is $\approx 26.008\%$. Thus, the difference in open porosity between X , Y , and Z is negligible (no more than 0.013 percentage points) that indicates the absence of directional anisotropy of open porosity and confirms the textural homogeneity of the samples. The standard deviation of the open porosity values between the samples for each direction does not exceed 0.005%, and the coefficient of variation is less than 0.02% that indicates high reproducibility of the results obtained. Closed porosity also demonstrates very low values (in the order of tenths of a percent) and varies insignificantly between directions. It is unusual that in Y direction it turned out to be slightly higher ($\approx 0.413\%$) compared to Z ($\approx 0.204\%$) and X ($\approx 0.176\%$). At first glance, this result contradicts the expected effect: normally, a higher proportion of isolated pores (closed porosity) should impair filtration properties. In this case, however, the difference is so small in absolute terms that its effect is not noticeable – Y direction remains the most permeable even with increased closed porosity. Low Dead-end porosity values confirm the high degree of connectivity of the void space and correlate with the proportion of closed pores that may indicate their occurrence mainly due to the intersection of isolated pores by the boundaries of the structures under consideration. On the whole, such a small variation in porosity values (less than 0.5% relative) allows the pore framework to be considered practically isotropic in terms of porosity.

The geodesic tortuosity of the pore space shows limited, albeit stable, fluctuations from ~ 1.03 to 1.26. These values indicate that the actual filtration paths

are only slightly longer than the direct (geometric) size of a sample. The variation in average tortuosity between different samples is insignificant (at standard deviation of ~ 0.01 , coefficient of variation of $\sim 1\%$) that emphasizes the reproducibility of this parameter. An atypical difference is observed in the bedding plane (X and Y axes): the average tortuosity along Y axis is slightly less than that along X axis (by $\sim 3\text{--}4\%$), despite the location of both directions in the rock bedding plane. At the same time, Z axis (core axis) predictably shows higher tortuosity reflecting the influence of bedding. Nevertheless, all τ values obtained remain low (~ 1.1), confirming the high connectivity of the pore channels.

Analysis of percolation paths provided additional information about the geometry of the pore space that goes beyond purely geodesic characteristics. For each direction (X , Y , Z), 100 percolation paths were determined, representing physically realizable trajectories along which a particle could pass through the pore system. Unlike tortuosity, which reflects only the length of a geometric curve, the percolation algorithm takes into account the minimum sizes of pore bottlenecks capable of passing a particle of a certain diameter. Fig. 2 shows, using one of the samples as an example, the percolation paths in three orthogonal directions ($a - X$, $b - Y$, $c - Z$) with a color gradient superimposed, representing the length of each trajectory from the input to the output surface. In all three directions, the percolation channels form an organized, well-connected network structure with long continuous flow zones, without sharp local distortions or spots that could indicate the presence of areas requiring bypassing or indicating local barriers.

Table 1

Summary Results of the Digital Analysis

Sample No.	Axis	Min. tortuosity	Max. tortuosity	Average tortuosity	Min. trajectory length, μm	Max. trajectory length, μm	Average trajectory length, μm	Average max. particle diameter, μm	Average physical path length, μm	Calculated permeability, Darcy	Open porosity, %	Closed porosity, %	Dead-end porosity, %
1	X	1.045	1.244	1.117	2,590	3,081	2,767	22.64	4,290	3.334	26.011	0.176	0.036
	Y	1.036	1.161	1.081	2,568	2,875	2,678	22.88	4,456	4.296	25.998	0.413	0.081
	Z	1.061	1.201	1.106	2,628	2,976	2,740	22.58	4,133	3.583	26.010	0.204	0.044
2	X	1.051	1.262	1.134	2,604	3,088	2,751	22.43	4,280	3.316	26.007	0.180	0.031
	Y	1.035	1.158	1.089	2,556	2,820	2,651	22.56	4,459	4.301	25.995	0.407	0.087
	Z	1.067	1.198	1.101	2,615	2,925	2,749	22.91	4,074	3.572	26.008	0.206	0.039
3	X	1.049	1.236	1.105	2,596	3,087	2,763	22.48	4,304	3.340	26.014	0.175	0.040
	Y	1.030	1.182	1.090	2,517	2,897	2,670	22.77	4,377	4.308	25.999	0.414	0.086
	Z	1.057	1.201	1.092	2,593	2,981	2,700	22.82	4,146	3.590	26.012	0.205	0.062

Fig. 3 shows the distribution of filtration flow velocities; in all cases, similar elongated areas of high velocities corresponding to the “main” flow channels are visible. This indicates that the samples contain directed filtration pathways with minimal geometric obstacles and confirms that the degree of connectivity of the pore space is high in any direction. Thus, despite the weak anisotropy of filtration properties (see below), the geometry of the pore framework itself is close to isotropic, in terms of both integral indicators (porosity, tortuosity) and the structural arrangement of percolation paths.

Unlike porosity, filtration properties exhibit weak but distinct anisotropy. The calculated permeability values (see Table 1) differ between the three axes.

A weak manifestation of an atypical type of anisotropy is observed: one of the horizontal directions X turned out to be less permeable than the vertical direction Z , and the preferred filtration flow is oriented along Y axis. Quantitatively, this anisotropy is small (ratios $k_Y : k_X \approx 1.3$, $k_Y : k_Z \approx 1.2$), but it is consistently reproduced in all samples. The spread of permeability values between different samples for each axis does not exceed 0.01 D (relative coefficient of variation $< 0.5\%$), thanks to which the difference identified between X , Y , and Z is statistically significant and is due to the microstructure of the rock. This is confirmed by independent physical tests: the laboratory measurements on core material showed permeability of ~ 5.6 D along the core axis and ~ 6.1 D in the XY bedding plane.

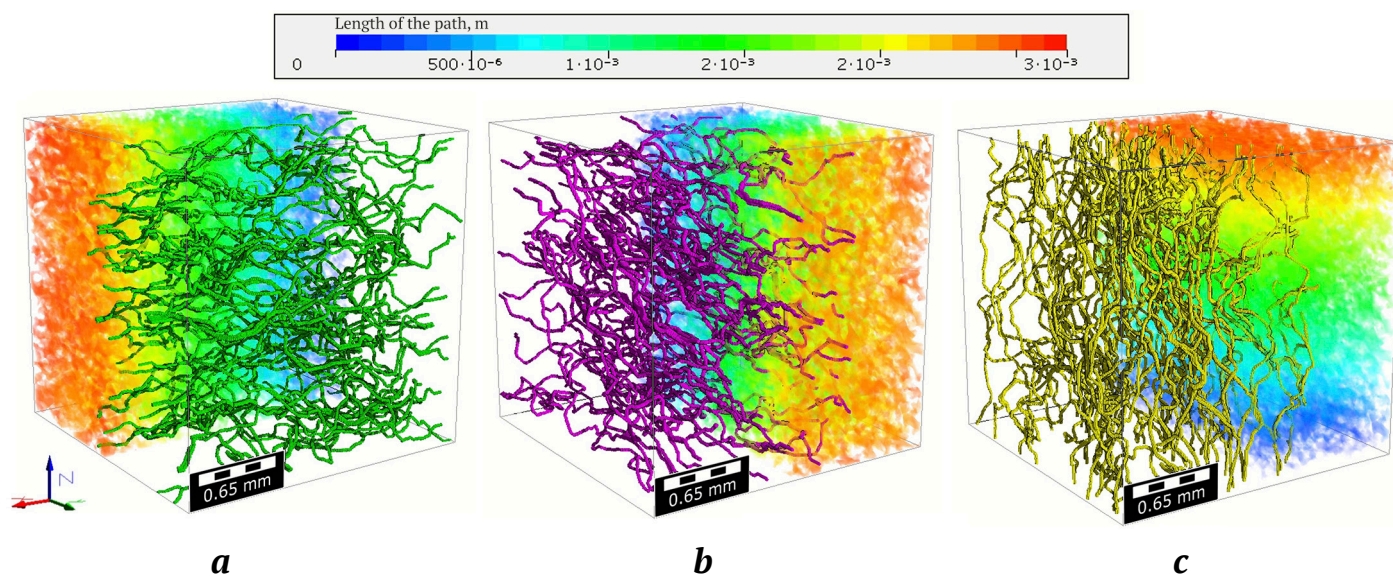


Fig. 2. Visualization of the spatial distribution of some percolation paths and integral gradient mapping of path lengths along X , Y , and Z Axes

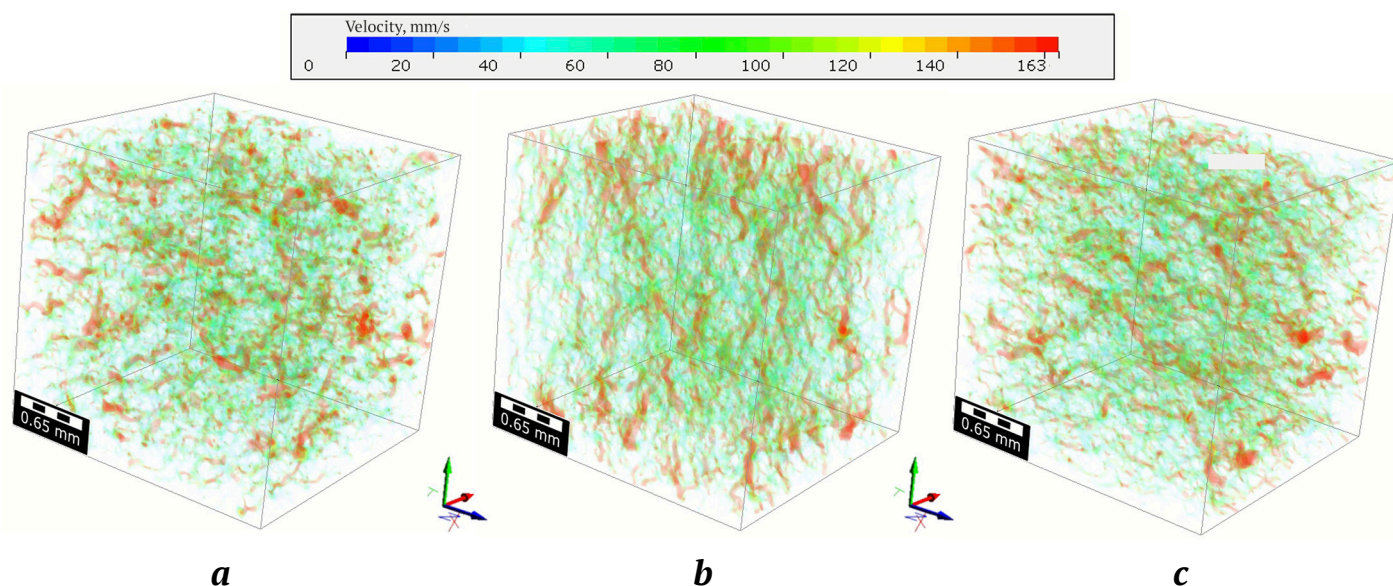


Fig. 3. Visualization of spatial distribution of filtration flow velocities along X , Y , and Z Axes

Although the absolute values in the laboratory proved slightly higher, the ratio between the directions is similar to the model data, indicating the presence of weak but stable transverse anisotropy of the filtration properties of the rock. The good agreement between the numerical simulation and the tests results confirms the correctness of the digital approach used and the adequacy of the model for simulating the actual filtration behavior of the samples.

Porosity cartograms obtained by layer-by-layer averaging in each direction are shown in Fig. 4. The color scale reflects local porosity values, where blue corresponds to minimum values, red to maximum values. In all three projections ($a - YZ$, $b - XZ$, $c - XY$), the distribution of the values demonstrates a similar structure: the images are dominated by areas with a uniform transition from blue to green-yellow shades, which corresponds to porosity values close to the average value. Local deviations occur, but do not form clusters or pronounced directional anomalies. This indicates that the structure of the pore space retains a near-isotropic character not only in terms of integral values, but also in terms of pore distribution in volume. This suggests that the observed differences in filtration properties are not related to porosity as such, but to the geometry of the pore connections – their tortuosity, throat width, and degree of connectivity.

The results show that, with the same porosity, differences in pore space geometry (tortuosity, channel size, connectivity) significantly affect permeability. Y direction demonstrates the highest permeability, combining minimal average tortuosity and a slightly larger average pore channel diameter (see Table 1). According to the Carman-Kozeny equation (as modified by Becker) for a homogeneous porous medium:

$$k = \frac{\phi^3}{(1-\phi)^2} \frac{1}{C\tau^2 S_0^2},$$

where ϕ is porosity; C is a structure constant; τ is tortuosity coefficient; S_0 is specific surface area of grains.

The ratio is a qualitative illustration of known relationships, but is often used for a preliminary assessment of the properties of porous media. The porosity in the samples under consideration is almost constant ($\phi \approx 26\%$), and differences in specific surface area can be estimated based on the characteristic size of the pore channel. Assuming that S_0 is inversely proportional to average pore diameter d , the formula can be simplified to: $k \propto d^2/\tau^2$. This reflects the intuitively expected relationship: an increase in the cross-sectional area of a flow (larger d) and a decrease in tortuosity (smaller τ) increase permeability. Indeed, the observed anisotropy is consistent with this model: Y direction has the largest average pore diameter ($\sim 22.8 \mu\text{m}$) and the lowest tortuosity (~ 1.08), thus demonstrating the maximum k .

However, quantitatively, the classical model underestimates the effect. Calculations show that with a decrease in τ of only $\sim 3\%$ and an increase in d of $\sim 1\%$ (in Y direction relative to X), the relative increase in k should be only about 10%, whereas according to the simulation, it reaches $\sim 30\%$. Similarly, the Katz-Thompson percolation model (which links permeability to the square of the critical pore channel radius) predicts nearly equal values of k for X and Y due to the virtually identical size of the “bottlenecks” (in the case under consideration, the average maximum diameter of the limiting holes differs by less than 1%). Thus, the standard models do not fully explain the observed anisotropy that indicates the presence of additional factors. The higher permeability along Y -axis is probably due to the fine-scale arrangement of the pore channels, which is not directly reflected in the averaged parameters d and τ (e.g., pore network configuration, radius distribution, etc.). In Y direction, more direct and through flows are realized due to the lithological orderliness of the structure, while in X direction, some of the channels are blocked or deflected. In other words, the permeability of poorly consolidated sandstones is extremely sensitive to the changes in the tortuosity

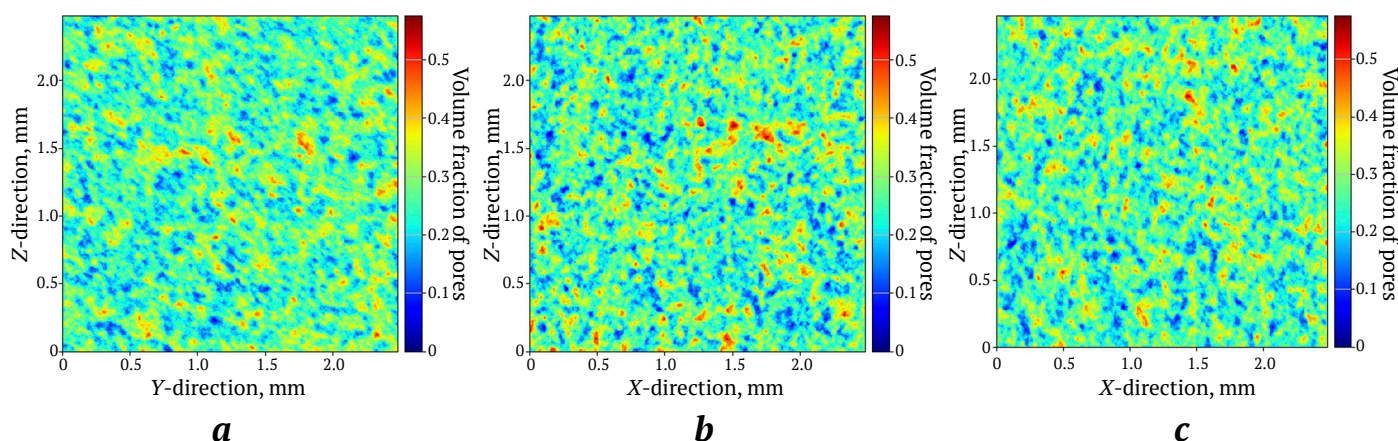


Fig. 4. Distribution of average porosity values along X , Y , and Z Axes

and connectivity of pores: even a slight “straightening” of the channels results in a disproportionately large increase in k . Similar conclusions are made in [35], which shows that in sandstone and carbonate, the logarithmic relationship between permeability and porosity has a large spread and strongly depends on sorting and diagenesis. This observation is confirmed in the present study, which highlights the limitations of using porosity alone as a prognostic parameter. Similarly, in a later work [36], based on statistical simulation of 13,000 porous structures, it was concluded that the correlation between permeability and porosity may be insufficient, especially at porosities below 0.7, and that geometric parameters such as tortuosity and conductivity, when correctly formalized, provide a more accurate description of the filtration characteristics of a pore space. A similar relationship between porosity and permeability is emphasized for oil-bearing sandstones in [37]. It is particularly important that, despite its minimal open porosity, Y direction proved to be the most permeable that is consistent with the hypotheses [38] about the role of lithological orderliness and textural orientation in the formation of effective filtration channels. This highlights the need for a comprehensive approach to assessing reservoir properties,

including not only classic petrophysical parameters, but also topological analysis of the pore network, direct hydrodynamic simulation, and morphological characterization of the pore framework.

To correctly evaluate the parameters of the pore space of a digital model, it is necessary to determine the representative elementary volume (REV) – the minimum volume of a porous medium for which the values of the characteristics under study (in this case, porosity) become statistically stable and cease to depend on a sample set size. Knowledge of this parameter ensures the reliability and reproducibility of further calculations, in particular, the simulation of filtration processes and permeability assessment.

To numerically determine REV, a method was used involving the step-by-step division of the digital model into smaller domains, followed by analysis of the porosity distribution in each of them. Within this approach, the three-dimensional binary model (obtained after reconstruction and segmentation) was sequentially divided into cubic domains of various sizes: from large (300 voxels per edge) to smaller (10 voxels per edge). At each stage of the division, the porosity of each selected domain was determined, after which a cumulative curve of porosity values was constructed.

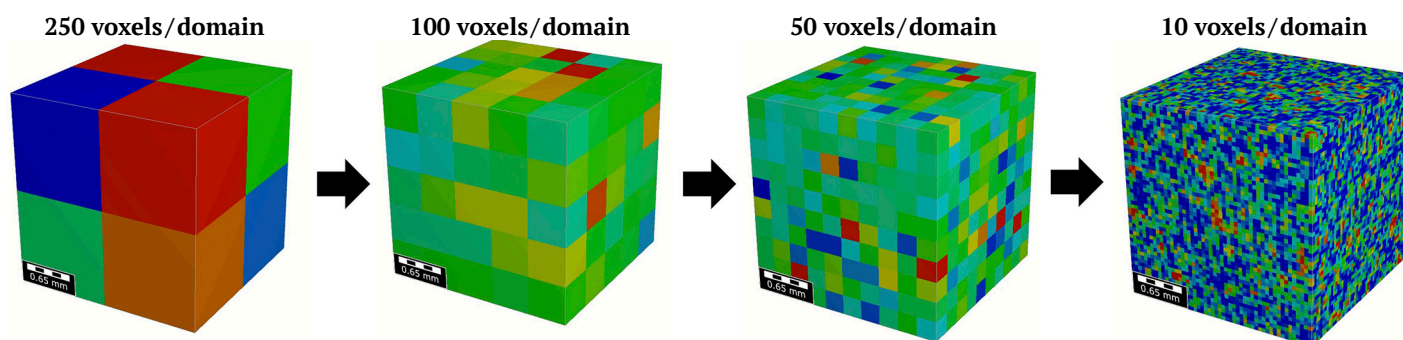


Fig. 5. Visualization of the process of determining the representative elementary volume (REV) by the method of sequential reduction of domain size

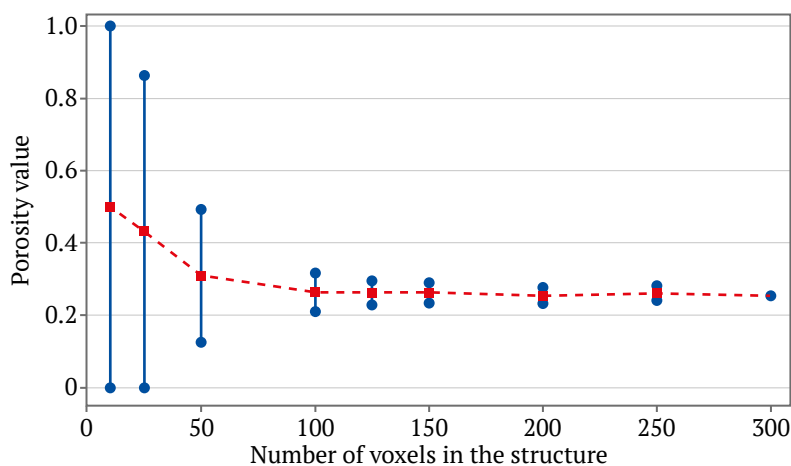


Fig. 6. Dependence of porosity value on domain size (number of voxels per edge) when determining representative elementary volume (REV)



Figure 5 shows the general process of dividing the initial models into smaller domains. Figure 6 shows the results of quantitative analysis of domain porosity: the horizontal axis shows the linear dimensions of the domains (in voxels), and the vertical axis shows the calculated porosity value for each domain. Each blue dot corresponds to the porosity of a single domain of a given size, and the red dotted line corresponds to the average porosity value for the corresponding scale. A decrease in the spread of values as the domain size increases indicates that the parameter has reached statistical stability. As can be seen from the graph, for large domain sizes (more than 150 voxels), the spread of porosity values between different domains becomes minimal, and the average value stabilizes. When calculations fall below this threshold, the characteristics lose stability that can lead to incorrect generalizations based on the model. All calculations performed in this work were carried out on models with linear dimensions of 500 voxels. An assessment of REV was also carried out based on a sandstone model quality control algorithm, which confirmed the adequacy of the structure size used ($N(REV) > 25$). This approach takes into account the ratio of the minimum structure length to the effective grain diameter [40] and provides a reliable estimate of REV for single-phase fluid flow in sandstones.

3. Practical Conclusions and Recommendations

The identified permeability anisotropy is associated with the oriented structure of the pore space in the bedding plane. The identified profile confirms the feasibility of drilling horizontal wells along a formation – in the direction of the natural rock texture, where the most conductive filtration channels are formed. Special attention should be paid to the choice of well direction in the plane of bedding due to the manifestation of atypical anisotropy: correct orientation of wellbores will allow maximum utilization of highly permeable paths and maximize formation drainage.

The high degree of connectivity of the pore space and the absence of barrier anisotropy in throat opening indicate uniform filtration in all directions. This means that the displacement front (for example, when pumping or advancing a gas/water front) will be stable and uniform, without premature breakthrough in certain directions. The uniform internal architecture is also conducive to complete drainage of a formation and efficient involving condensate into the flow. The minimal proportion of isolated pores (closed porosity $< 0.5\%$) and large pore throats reduce the risk of capillary isolation of condensate – the liquid phase does not get stuck in micropores, but continues to participate in filtration. This ensures more stable exploita-

tion of a gas condensate reservoir without a sharp drop in productivity due to the formation of stagnant condensate zones.

Knowledge of the morphometric characteristics of pore networks allows for more accurate selection of the optimal proppant size for hydraulic fracturing and the degree of filtration of the injected water. This prevents pore blockage by particles and the removal of rock material that preserves the permeability of a formation. The digital analysis methods used allow for reliable assessment of filtration and storage properties in conditions of limited core material and can provide rapid assessment of a reservoir at the exploration stage: prompt receipt of data on porosity, permeability, and anisotropy speeds up decision-making, reducing dependence on lengthy laboratory studies.

A detailed analysis of microstructure made it possible to assess the rock's vulnerabilities in terms of particle removal. The visualization of the flows revealed the presence of continuous high-speed filtration channels. In poorly consolidated sandstones, such flow concentration zones can cause increased stress on the matrix and contribute to grain removal. However, the uniform distribution of pores and high total connected pore space mean that there are no pronounced "bottlenecks" where the velocity would increase extremely locally. This reduces the risk of sudden sand production. The results obtained should be taken into account when designing well operating modes: preventing excessive depressions and ensuring uniform distribution of withdrawal across the formation will contribute to the stability of the well walls. Integrating the obtained data into geotechnical models will enable quantitative prediction of critical pressure gradients at which rock failure is possible, thereby minimizing the risk of sand production.

4. Research Prospects

Further development of research areas is planned by substantiating models of pore space tortuosity in poorly consolidated sandstones and identifying its impact on the filtration properties of these rocks. It is planned to clarify the boundary conditions for the applicability of the Carman-Kozeny equation and percolation models for the poorly consolidated reservoirs under consideration. A separate task is to ensure the scalability of parameters from the micro level to core and formation scales so that digital models better reflect the properties at a formation level. An important area of focus is the development of digital models of pore space for the use in simulation of multiphase or thermo-hydromechanical processes that will allow for the consideration of actual conditions in a reservoir. In addition, the development of machine lear-



ning methods for automatic prediction of filtration and capacity properties based on microstructural analysis data is equally relevant.

From an applied perspective, one of the key areas for further research is the development of procedures for rapid assessment of permeability using digital models. An important task is to integrate the results of digital simulation into geological and hydrodynamic models of fields, especially when the amount of source data is limited. The practical significance lies in adapting the methodology to rocks with complex and heterogeneous pore structures (e.g., carbonates and fractured sandstones) that will allow the approach to be extended to a wider class of reservoirs.

Conclusion

A study of the anisotropy of the filtration and storage properties of poorly consolidated sandstones in a gas condensate field based on digital core analysis has provided new data on the relationship between the microstructure of a pore space and filtration characteristics. A comprehensive approach involving microtomography, 3D simulation, and numerical calculations confirmed the high accuracy of digital methods in assessing reservoir properties, especially in conditions of limited core material, and also allowed a number of conclusions to be drawn that are important for assessing reservoir properties and optimizing reservoir development.

1. The open porosity values are practically identical in all directions (~26%), but the permeability shows a weak but stable atypical anisotropy. The highest permeability values are observed along one of the directions in the bedding plane that was associated with reduced tortuosity and pore size in this direction.

2. It has been shown that, with the same porosity, permeability significantly depends on the tortuosity of the channels, the width of the throats, and the con-

nectivity of the pores. Classic Carman-Kozeny models underestimate the influence of these factors that highlights the need for a comprehensive analysis of pore space morphology.

3. The optimal direction of horizontal wells should take into account the identified features of permeability anisotropy (up to 30% difference in different directions) to maximize drainage that will allow maximum utilization of the most permeable paths towards a well, contribute to a reduction in depression at the same withdrawal rates, and help improve formation coverage when injecting working agents.

4. The established uniformity of the pore space structure, including the diameter of the filtered particles, helps minimize the risk of sand production by reducing local filtration flow velocities. In addition, low closed porosity values reduce the likelihood of capillary lock-up of condensate.

5. Digital methods enable rapid assessment of reservoir properties during exploration and minimize uncertainty when core samples are scarce. This requires a minimal sample volume (starting from 5 mm³), which is critically important for offshore fields with a shortage of core material. The wide range of data obtained can be quickly integrated into hydrodynamic models, significantly improving their predictive capabilities. The results of numerical simulation are in good agreement with laboratory measurements, confirming the reliability of the approach for predicting filtration properties in complex geological conditions.

Thus, the work demonstrates the effectiveness of digital technologies for studying reservoir anisotropy and provides tools for optimizing field development, especially in offshore production conditions, where access to physical samples is limited and the requirements for forecast reliability are high. Further research may focus on refining tortuosity models and scaling the results to the scale of a formation.

References

1. Ponomarev A.A., Kadyrov M.A., Tugushev O.A., et al. Digital core reconstruction research: challenges and prospects. *Geology, Ecology, and Landscapes*. 2024;8(1):49–56. <https://doi.org/10.1080/24749508.2022.2086201>
2. Abdollahi-Mamoudan F., Savard S., Filleter T., et al. Numerical simulation and experimental study of capacitive imaging technique as a nondestructive testing method. *Applied Sciences*. 2021;11(9):3804. <https://doi.org/10.3390/app11093804>
3. Novikova E. V., Trimonova M. A., Dubinya N. V. et al. Estimation of breakdown pressure in laboratory experiments on hydraulic fracturing. *Materials Physics and Mechanics*. 2023;51(5):52–65. https://doi.org/10.18149/MPM.5152023_6
4. Hommel J., Coltman E., Class H. Porosity–permeability relations for evolving pore space: a review with a focus on (bio-)geochemically altered porous media. *Transport in Porous Media*. 2018;124(2):589–629. <https://doi.org/10.1007/s11242-018-1086-2>
5. Jing W., Zhang L., Li A., et al. Phase behaviors of gas condensate at pore scale: direct visualization via microfluidics and in-situ CT scanning. *SPE Journal*. 2024;29(5):2566–2577. <https://doi.org/10.2118/218421-PA>



6. Hosseinzadegan A., Mahdiyar H., Raoof A., et al. The pore-network modeling of gas-condensate flow: elucidating the effect of pore morphology, wettability, interfacial tension, and flow rate. *Geoenergy Science and Engineering*. 2023;229:211937. <https://doi.org/10.1016/j.geoen.2023.211937>
7. Wang S., Qu H., Yu S., Zhang S.X. Nondestructive investigation on close and open porosity of additively manufactured parts using an X-ray computed tomography. *Materials Today: Proceedings*. 2022;70:124–130. <https://doi.org/10.1016/j.matpr.2022.08.559>
8. Bushuev Y.G., Grosu Y., Chorążewski M.A., Meloni S. Subnanometer topological tuning of the liquid intrusion/extrusion characteristics of hydrophobic micropores. *Nano Letters*. 2022;22(6):2164–2169. <https://doi.org/10.1021/acs.nanolett.1c02140>
9. Khimulia V.V., Karev V.I. Pore-Scale Computational Study of Permeability and Pore Space Geometry in Gas Condensate Reservoir Rocks. In: Karev V. (ed.) *Proceedings of the 9th International Conference on Physical and Mathematical Modelling of Earth and Environmental Processes. PMMEEP 2023. Springer Proceedings in Earth and Environmental Sciences*. Cham: Springer; 2024. Pp. 243–256. https://doi.org/10.1007/978-3-031-54589-4_26
10. Panini F., Ghanbarian B., Borello E.S., Viberti D. Estimating geometric tortuosity of saturated rocks from micro-CT images using percolation theory. *Transport in Porous Media*. 2024;151(7):1579–1606. <https://doi.org/10.1007/s11242-024-02085-w>
11. Lian S., Meng T., Song H., et al. Relationship between percolation mechanism and pore characteristics of recycled permeable bricks based on X-ray computed tomography. *Reviews on Advanced Materials Science*. 2021;60(1):207–215. <https://doi.org/10.1515/rams-2021-0022>
12. Yang Y., Wang D., Yang J., Wang B., Liu T. Fractal analysis of CT images of tight sandstone with anisotropy and permeability prediction. *Journal of Petroleum Science and Engineering*. 2021;205:108919. <https://doi.org/10.1016/j.petrol.2021.108919>
13. Aljawad M.S. Permeability anisotropy impact on wormhole propagation in openhole and limited-entry completions: a 3D numerical study. *Gas Science and Engineering*. 2023;116:205050. <https://doi.org/10.1016/j.jgsce.2023.205050>
14. Lux M., Szanyi J. Effects of vertical anisotropy on optimization of multilateral well geometry. *Journal of Petroleum Science and Engineering*. 2022;208:109424. <https://doi.org/10.1016/j.petrol.2021.109424>
15. Wang N., Chang H., Zhang D., et al. Efficient well placement optimization based on theory-guided convolutional neural network. *Journal of Petroleum Science and Engineering*. 2022;208:109545. <https://doi.org/10.1016/j.petrol.2021.109545>
16. Muravyev A.V. Gas condensate wells: challenges of sampling, testing and production optimization. *Energies*. 2022;15(15):5419. <https://doi.org/10.3390/en15155419>
17. Poplygin V. V., Riabokon E. P., Turbakov M. S. et al. Changes in rock permeability near-wellbore due to operational loads. *Materials Physics and Mechanics*. 2022;48(2):175–183. https://doi.org/10.18149/MPM.4822022_3
18. Yusupov Y., Zaglyadin Y. Application of a 4D geomechanical model to reduce the risks of offshore field (Russian Federation) development throughout the entire life cycle. In: *ARMA/DGS/SEG International Geomechanics Symposium*. Kuala Lumpur, Malaysia, November 18–20, 2024. Paper IGS-2024-0194. <https://doi.org/10.56952/IGS-2024-0194>
19. Zhen W., Liu H., Chi M., et al. Investigation into the influence of stress conditions on the permeability characteristics of weakly cemented sandstone. *Applied Sciences*. 2023;13(22):12105. <https://doi.org/10.3390/app132212105>
20. Deng X., Zhou X., Patil S., et al. Multiphase flow dynamics with micro-CT imaging: review of applications in oil and gas industry. *Energy & Fuels*. 2023;37(21):16311–16332. <https://doi.org/10.1021/acs.energyfuels.3c02446>
21. Razavifar M., Mukhametdinova A., Nikoos E., et al. Rock porous structure characterization: a critical assessment of various state-of-the-art techniques. *Transport in Porous Media*. 2021;136:431–456. <https://doi.org/10.1007/s11242-020-01518-6>
22. Ye Z.L., Lu H.W., Gao X., et al. Research progress of micro-CT in the field of petroleum engineering. In: *International Field Exploration and Development Conference*. Singapore: Springer; 2023. Pp. 726–738. https://doi.org/10.1007/978-981-97-0468-2_55
23. Revina A.V., Konnov D.A., Revina N.S., Kolesnikova V.A. Analysis of the dependence of permeability on the open porosity of carbonate reservoir rocks in the areas of the Astrakhan gas condensate field. *Oil and Gas Technologies and Environmental Safety*. 2023;(3):48–56. <https://doi.org/10.24143/1812-9498-2023-3-48-56>
24. Manzoor S., Zeidani K., Syed A. et al. Unified near wellbore modelling and impact of velocity-dependent relative permeability on performance of gas condensate fields. In: *ECMOR 2024 – 21st Europe-*



- an Conference on the Mathematics of Oil Recovery. Naples, Italy, 3–6 June 2024. Houten: EAGE; 2024. Pp. 1–17. <https://doi.org/10.3997/2214-4609.202437069>
25. Bera A., Shukla B., Jogani D. A perspective review of applications of the computed tomography (CT) scan imaging technique for microscopic reservoir rock characterization. *Deep Underground Science and Engineering*. 2025. (In press) <https://doi.org/10.1002/dug2.12138>
 26. Khimulia V.V. Digital examination of pore space characteristics and structural properties of a gas condensate field reservoir on the basis of μ CT images. In: *Conference on Physical and Mathematical Modeling of Earth and Environment Processes*. Cham: Springer Nature Switzerland; 2023. Pp. 23–34. https://doi.org/10.1007/978-3-031-54589-4_3
 27. Kong H., Wu J., Liang W., et al. An improved non-local means algorithm for CT image denoising. *Multimedia Systems*. 2024;30(2):79. <https://doi.org/10.1007/s00530-024-01283-2>
 28. Withers P.J., Bouman C., Carmignato S., et al. X-ray computed tomography. *Nature Reviews Methods Primers*. 2021;1(1):18. <https://doi.org/10.1038/s43586-021-00015-4>
 29. Cayron C., Lowe T., Thompson A., MacDonald E. Comparison of dimensional measurements from images acquired by synchrotron tomography with VGSTUDIO MAX and ImageJ. In: *Proceedings of the Special Interest Group Meeting on Advancing Precision in Additive Manufacturing*. Bedford, UK, 2021. Bedford: European Society for Precision Engineering and Nanotechnology; 2021. Pp. 98–101.
 30. Lu X., Huang J., Xu J., Lu J., et al. Comparison between two numerical methods for the computation of thermal conductivities of particulate composites: FEM and GeoDict. In: *Proceedings of the 22nd International Conference on Electronic Packaging Technology (ICEPT)*. Xiamen, China, 2021. Pp. 1–5. <https://doi.org/10.1109/ICEPT52650.2021.9568014>
 31. Soulaire C. Micro-continuum modeling: an hybrid-scale approach for solving coupled processes in porous media. *Water Resources Research*. 2024;60(2):e2023WR035908. <https://doi.org/10.1029/2023WR035908>
 32. Linden S., Wiegmann A., Hagen H. The LIR space partitioning system applied to the Stokes equations. *Graphical Models*. 2015;82:58–66. <https://doi.org/10.1016/j.gmod.2015.06.003>
 33. Hilden J., Cheng L., Linden S., Planas B. *FlowDict User Guide. GeoDict release 2022*. Published: November 9, 2021. <https://doi.org/10.30423/userguide.geodict2022-flowdict>
 34. Khimulia V.V. Digital analysis of changes in hydrocarbon reservoir pore space characteristics after filtration tests. *Russian Journal of Earth Sciences*. 2025;1:1–13. <https://doi.org/10.2205/2025ES000988>
 35. Nelson P.H. Permeability–porosity relationships in sedimentary rocks. *The Log Analyst*. 1994;35(3):SPWLA-1994-v35n3a4. <https://doi.org/10.2118/SPWLA-1994-v35n3a4>
 36. Rezaei Niya S.M., Selvadurai A.P.S. A statistical correlation between permeability, porosity, tortuosity and conductance. *Transport in Porous Media*. 2018;121(3):741–752. <https://doi.org/10.1007/s11242-017-0983-0>
 37. Zakirov T.R., Galeev A.A., Korolev E.A., et al. Estimation of sandstone reservoir properties using X-ray CT studies in Ashalchinskoye oil field. *Oil Industry*. 2015;(8):96–99. (In Russ.)
 38. Yang Y., Aplin A.C. A permeability–porosity relationship for mudstones. *Marine and Petroleum Geology*. 2010;27(8):1692–1697. <https://doi.org/10.1016/j.marpetgeo.2009.07.001>
 39. Liu W., Han D., Wang G., Chu X. Representative elementary volume evaluation of coal microstructure based on CT 3D reconstruction. *Fuel*. 2023;336:126965. <https://doi.org/10.1016/j.fuel.2022.126965>
 40. Saxena N., Hows A., Hofmann R., et al. Imaging and computational considerations for image computed permeability: Operating envelope of Digital Rock Physics. *Advances in Water Resources*. 2018;(116):127–144. <https://doi.org/10.1016/j.advwatres.2018.04.001>

Information about the author

Valerii V. Khimulia – Cand. Sci. (Phys. & Math.), Researcher at the Laboratory of Geomechanics, Ishlinsky Institute for Problems in Mechanics of the Russian Academy of Sciences, Moscow, Russian Federation; ORCID [0000-0003-2116-6483](https://orcid.org/0000-0003-2116-6483), Scopus ID [57224741664](https://orcid.org/57224741664), ResearcherID [ACJ-7411-2022](https://orcid.org/ACJ-7411-2022); e-mail khim@ipmnet.ru

Received 27.05.2025

Revised 31.07.2025

Accepted 17.10.2025



ENVIRONMENTAL PROTECTION

Research paper

<https://doi.org/10.17073/2500-0632-2025-04-392>

UDC 630*181:581.5



Impact of tin ore mining on the streamflow of small rivers in mining regions

N.K. Rastanina¹ , D.A. Golubev^{1,2} , N.A. Kayumov^{1,2} , P.L. Rastanin¹ , I.A. Popadyev¹ ¹ Pacific National University, Khabarovsk, Russian Federation² Primorsky State Agrarian-Technological University, Khabarovsk, Russian Federation

n.rastanina@yandex.ru

Abstract

Mineral extraction exerts a significant impact on the environment, particularly on the hydrological regime of rivers. The placement of tailings storage facilities in river valleys is a common practice in ore processing. Forest stands and river networks in such areas undergo intensive transformation involving large-scale deforestation with removal of the root-inhabited soil layer and alteration of river channels. As a result, the streamflow in the affected sections becomes less abundant. Since the 1970s, active tin ore mining and processing have been carried out in the Silinka River basin of the Khabarovsk Territory. Mining activities have produced technogenic landforms such as tailings storage facilities, open pits, and waste dumps, which pose both ecological and technogenic hazards and act as sources of pollution for groundwater, surface water, soil, vegetation, and the atmosphere. Forest cover is one of the key indicators determining river runoff and can be used to estimate the capitalized value of 1 km² of the study area. Using the Normalized Difference Vegetation Index (NDVI), this study assessed the impact of tin ore mining on the Silinka River basin. The results indicate a 25% decrease in the average capitalized value of 1 km² of the study area.

Keywords

mining system, tailings storage facility, environmental damage, river runoff, river basin, Normalized Difference Vegetation Index (NDVI), capitalized value

Funding

This research was supported by the Russian Science Foundation, project No. 24-27-20085 (<https://rscf.ru/project/24-27-20085/>), and by the Ministry of Education and Science of the Khabarovsk Territory (Agreement No. 121C/2024).

For citation

Rastanina N.K., Golubev D.A., Kayumov N.A., Rastanin P.L., Popadyev I.A. Impact of tin ore mining on the streamflow of small rivers in mining regions. *Mining Science and Technology (Russia)*. 2025;10(4):369–378. <https://doi.org/10.17073/2500-0632-2025-04-392>

ОХРАНА ОКРУЖАЮЩЕЙ СРЕДЫ

Научная статья

Влияние добычи оловорудного сырья на речной сток малых рек горнопромышленных районов

Н.К. Растанина¹ , Д.А. Голубев^{1,2} , Н.А. Каюмов^{1,2} , П.Л. Растанин¹ , И.А. Попадьеv¹ ¹ Тихоокеанский государственный университет, г. Хабаровск, Российская Федерация² Приморский государственный аграрно-технологический университет, г. Хабаровск, Российская Федерация

n.rastanina@yandex.ru

Аннотация

Добыча полезных ископаемых оказывает значительное воздействие на окружающую среду, особенно на гидрологический режим рек. Формирование отходов переработки горнорудного сырья в виде хвостохранилищ в долинах рек является общепринятой практикой. Лесной массив, как и речная сеть в данном случае, подвергаются активной трансформации. Происходит сплошная вырубка со снятием корнеобитаемого слоя и изменяется русло реки. При этом речной сток, формирующийся на участке, становится менее водоносным. С 70-х годов XX в. в бассейне р. Силинки Хабаровского края активно развивается деятельность по извлечению и переработке оловорудного сырья. Вследствие деятельности горнопромышленных предприятий формируются техногенные объекты в виде хвостохранилищ,



карьеров, отвалов и т.д., которые являются объектами экологической и техногенной опасности, источниками загрязнения грунтовых и поверхностных вод, почвы, растительности и атмосферы. Лесистость территории является одним из основных показателей формирования речного стока, позволяющих рассчитать капитализированную стоимость 1 км² исследуемой территории. В работе с помощью расчёта лесистости через нормализованный разностный индекс вегетации дана оценка влияния процесса добычи оловорудного сырья в бассейне р. Силинки. Определено снижение средней стоимости 1 км² исследуемой территории на 25 %.

Ключевые слова

горнопромышленная система, хвостохранилище, экологический ущерб, речной сток, речной бассейн, нормализованный разностный индекс растительности, капитализированная стоимость

Финансирование

Исследование выполнено за счет гранта Российского научного фонда, проект № 24-27-20085 <https://rscf.ru/project/24-27-20085/> и Министерства образования и науки Хабаровского края (Соглашение № 121С/2024).

Для цитирования

Rastanina N.K., Golubev D.A., Kayumov N.A., Rastanin P.L., Popadyev I.A. Impact of tin ore mining on the streamflow of small rivers in mining regions. *Mining Science and Technology (Russia)*. 2025;10(4):369–378 <https://doi.org/10.17073/2500-0632-2025-04-392>

Introduction

Mineral extraction is one of the key sources of revenue for the Russian Federation but also results in significant negative environmental impacts. More than 80 billion tons of mining waste have already accumulated in Russia, occupying a total area of 1.1 million hectares disturbed by mining activities. Each year, this number continues to increase, leading to the degradation of essential forest functions in areas located at or near mining and mineral processing sites. The establishment of such facilities is accompanied by extensive deforestation, removal of the fertile soil layer, and alterations to river channels and runoff patterns¹ [1].

The condition of forest ecosystems plays a crucial role in the formation of river basins through surface runoff, particularly in mining regions [2]. M.E. Tkachenko (1952) considered the water protection role of forests in a broader context, not limiting it to the quantitative assessment of runoff. In his view, the beneficial effects of forests extend not only to surface waters (rivers, lakes, reservoirs) but also to groundwater, which often serves as the main source of water supply for both communities and industrial enterprises [3].

According to the concept of the general moisture-retaining function of forests, these ecosystems contribute to moisture accumulation within catchment areas, thereby increasing the total annual runoff [4]. However, an opposing view exists that considers forests as strong evaporators of moisture,

suggesting that an increase in forest cover reduces river runoff [5]. O. I. Krestovsky, based on studies in the southern taiga, established that after clear cutting, the evaporation component decreases by 20–40%. As a result, the runoff regime deteriorates: during the high-water period, liquid runoff increases, whereas during low-water periods, rivers become shallower [6]. Anthropogenic impacts not only modify the conditions of various runoff types [7–9] but also transform the characteristics of diffuse pollution, affecting the quality of surface water bodies [10]. This is particularly significant when toxic elements such as heavy metals and arsenic are present, leading to suppression and die-off of forest vegetation due to their spread across natural and technogenic environmental components [11].

Thus, the formation of river runoff may depend on the following factors:

1. Natural and climatic conditions, which influence the total annual river runoff and its distribution through the amount and type of precipitation, its spatial and temporal distribution, air temperature and humidity, and wind speed, all of which determine runoff losses due to evaporation [4, 12].

2. Topography, including the steepness of slopes and channel gradients, which shape the conditions for infiltration of melt and rainwater into the soil, slope and subsurface flow, and recharge of groundwater horizons [13].

3. Soil and hydrological conditions, where higher rock permeability and thicker deposits provide greater underground storage capacity and regulatory ability, ensuring more stable runoff throughout the year [14].

4. Vegetation cover, which affects the rate of snowmelt and surface water flow, thereby influencing the overall hydrological regime [13].

¹ State (National) Report on the Status and Use of Lands. URL: <https://rosreestr.gov.ru/activity/gosudarstvennoe-upravlenie-v-sfere-ispolzovaniya-i-okhrany-zemel/gosudarstvennyy-natsionalnyy-doklad-o-sostoyanii-i-ispolzovanii-zemel-rossiyskoy-federatsii> (Accessed: 7 November 2024).

5. Catchment size and shape, which correlate directly with the uniformity of runoff through variations in the share of subsurface (groundwater) recharge [15].

6. Lake and wetland coverage within the catchment, which tends to reduce river runoff because highly saturated lake-bog systems or lowland wetlands regulate flow and decrease the amplitude of discharge fluctuations [16].

7. Anthropogenic influences, including regulation and redistribution of river flow, water abstraction and discharge in industry and agriculture, land reclamation, and other activities that fundamentally alter the natural runoff regime [17].

8. Forest cover, which is one of the key factors regulating the water balance, as forest stands promote infiltration and maintain base flow. Deforestation reduces moisture retention, thereby amplifying seasonal fluctuations in river discharge [18].

9. Soil disturbance, particularly the removal of the root-inhabited layer, which decreases the soil's water-retaining capacity [19];

10. Mining facilities, such as tailings storage facilities and waste rock dumps, which modify the filtration properties of catchments, while pollutants can alter the chemical composition of water [20, 21].

The tailings storage facilities of the Solnechny Mining and Processing Plant (Solnechny MPP) represent sites of ecological and technogenic hazard, acting

as sources of contamination for groundwater, surface water, soils, vegetation, and the atmosphere due to dust emissions from their surfaces [14, 22, 23]. The purpose of this study is to assess the impact of mining operations on river runoff formation and the reduction of streamflow in small rivers within the Silinka River basin. The study addressed the following objectives: 1 – to analyze literature data on factors affecting the formation of river runoff in small rivers; 2 – to describe the disturbed area occupied by the tin mining enterprise; 3 – to assess the forest cover and water-protective function of forests within the influence zone of the Solnechny Mining and Processing Plant.

Study area and methods

The study area comprises the disturbed lands of the former Solnechny MPP, located within the Silinka River catchment, Solnechny District, Khabarovsk Territory [13, 24]. Solnechny MPP was the district's principal enterprise and the main economic driver of the area. Since 1969, large volumes of toxic waste have accumulated and been stored in three tailings storage facilities (TSFs).

As a result of open-pit and underground mining of cassiterite and cassiterite-sulfide deposits, large open pits and dumps of substandard ores and host rocks remain on the surface, along with numerous adits from which waste rock and mine water are discharged onto the slopes (Fig. 1).

SILINKA RIVER BASIN, Khabarovsk Territory

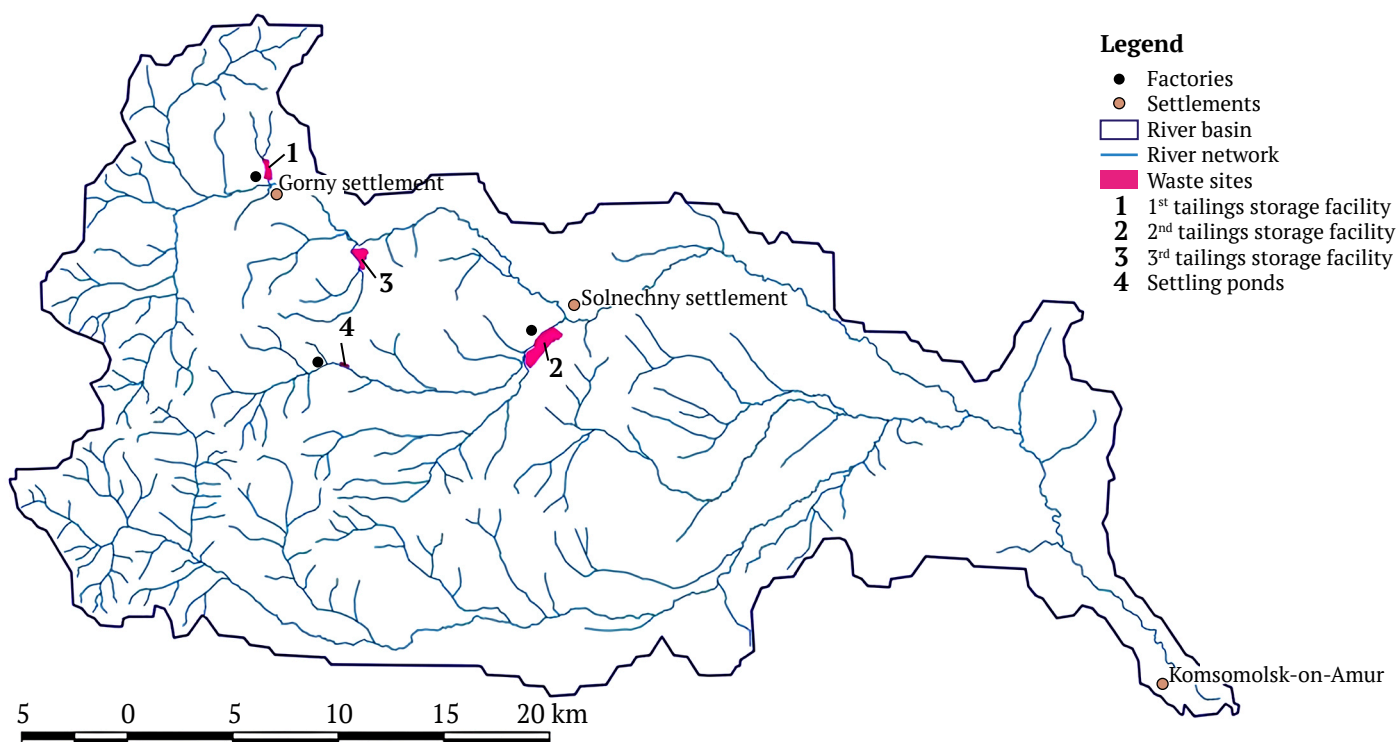


Fig. 1. Schematic map of technogenic facilities within the Silinka River basin

The mining–technogenic system that developed in the Komsomolsk tin-ore district has intensified supergene processes due to the expanded contact area between weathering agents and exposed surfaces of sulfide ores, as well as finely ground sulfides in the tailings. These processes have progressed to a more advanced technogenic stage.

The tailings storage facilities of the Solnechny MPP are composed of gray hydraulic-fill sands, sometimes stained brownish by iron hydroxides formed through oxidation of sulfides. The grain size of the sands is predominantly less than 0.5 mm. Coarse fractions greater than 2 mm account for about 1% of the total volume (up to 3% in certain layers), while 70–83% of the material consists of particles in the 0.1–0.5 mm range, and 13–14% are finer than 0.1 mm (up to 28% in individual horizons). The vertical grain-size distribution is heterogeneous. According to previous assessments of

waste hazard classes, the dried tailings belong to the highly hazardous toxicity class [25]. No land reclamation was undertaken in the disturbed area, despite the requirements of the Russian Federation's Law on Subsoil [26].

The first tailings storage facility lies opposite the settlement of Gornyy, approximately 100–500 m from the concentration plant. Its area is 44 hectares, with a total volume of 10.4 million tons (Fig. 2, *a*).

The waste material from the second tailings storage facility is currently being reprocessed by LLC Geoprominvest to produce tin and copper concentrates (Fig. 2, *b*).

At present, the assets of the former Solnechny MPP, including the Festivalnoye and Perevalnoye deposits, are managed by JSC Tin Ore Company, which has restarted tin and tungsten mining operations and continues to fill the third tailings storage facility (Fig. 2 *c, d*).



a



b



b



d

Fig. 2. Mining-disturbed areas of the former Solnechny Mining and Processing Plant:

- a* – operating processing plant of JSC Tin Ore Company;
- b* – surface of the second tailings storage facility; *c* – surface of the third tailings storage facility;
- d* – surface of the settling pond at the Festivalnoye deposit

The forest cover of the Silinka River basin was assessed using the Normalized Difference Vegetation Index (NDVI) calculated from Landsat 8 satellite data processed in QGIS. According to previous research [27], NDVI values below 0.3 correspond to non-forested areas, while values above 0.3 indicate forested land.

The ecological and economic assessment of the impact of mineral exploration and mining activities is not standardized and lacks a unified methodological framework. In this study, cartographic modeling was performed using the open-source software QGIS 3.10, along with the recommended method for estimating the economic damage to river runoff based on forest cover [28]:

$$M = -1.02 + 0.068 \times F, \quad (1)$$

where M is the runoff modulus per 1 km² of the catchment area, and F is the forest cover percentage.

Results and discussion

The catchment area of the Silinka River is 1,016 km² [29]. The river basin belongs to the Far Eastern taiga forest region and lies within the boundaries of two forestry districts – Komsomolsk and Solnechny. In the northwest, it borders the protected area of the regional natural monument “Amut Landslide Lake”, while the rest of the forested land is located within the green zone or classified as production forests.

Between 2012 and 2024, the total area of mining-disturbed lands within the Silinka River basin increased from 341.5 ha to 430.8 ha (Fig. 3).

According to GIS-based analysis using the Normalized Difference Vegetation Index (NDVI) calculated in QGIS from Landsat satellite data, the maximum NDVI value in the Silinka River basin does not exceed 0.494, which corresponds to a moderate level of forest biomass development (Fig. 4).

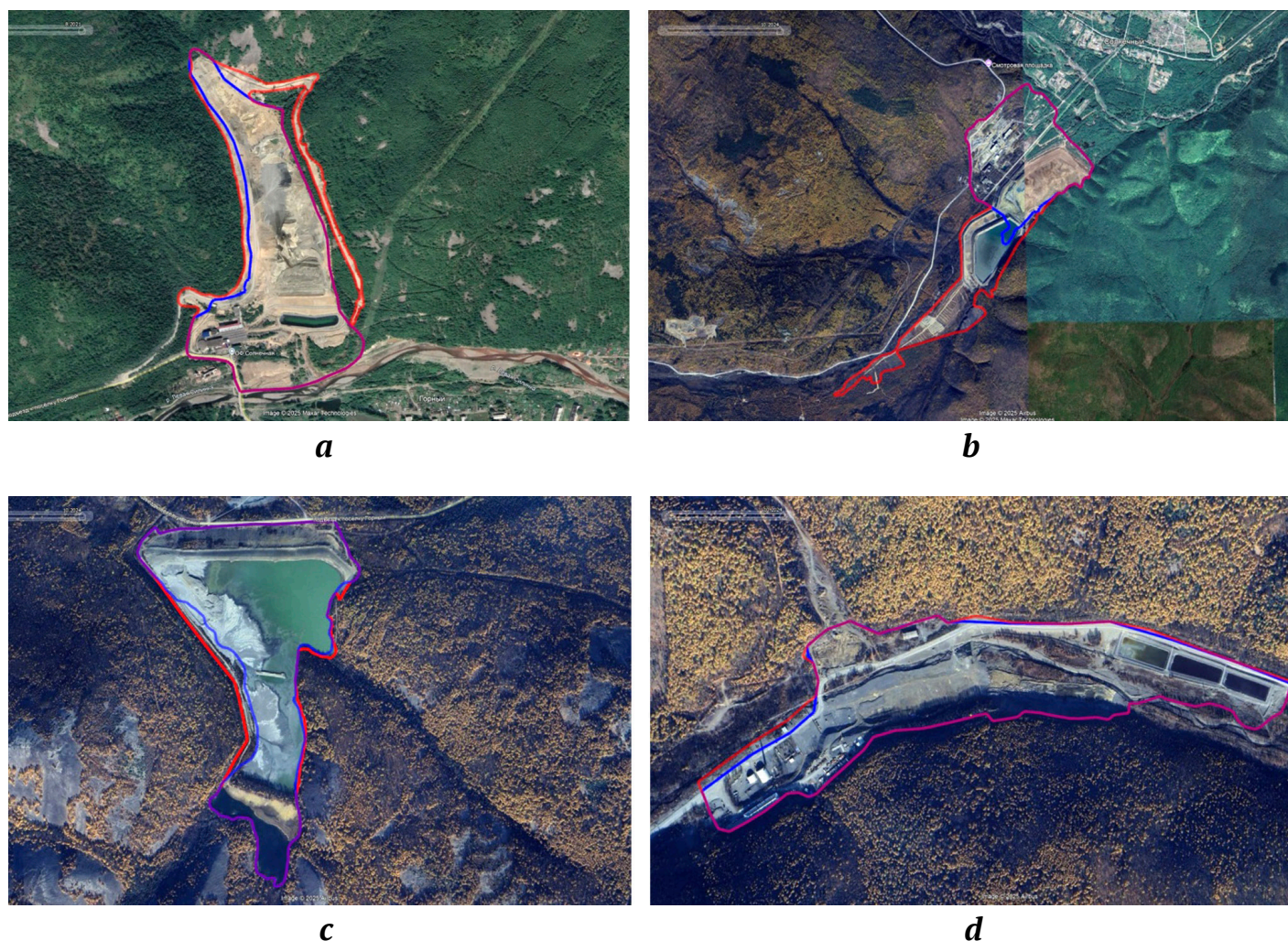


Fig. 3. Schematic map of mining-disturbed areas: *a* – first tailings storage facility; *b* – second tailings storage facility; *c* – third tailings storage facility; *d* – settling pond at the Festivalnoye deposit.

Note: blue – extent of the disturbed area in 2012; red – extent of the disturbed areas in 2024; purple – combined outline for 2012 and 2024.

Analysis of the resulting raster images (Table 1, Fig. 5) showed that forest cover in the Silinka River basin within the areas affected by the Solnechny MPP has changed in response to the expansion of mining-disturbed land (Fig. 6). NDVI-based estimation of forest cover indicated a decrease of 14.8%.

Based on the recommendations for estimating economic losses associated with changes in river runoff as a function of forest cover (Eq. 1), the specific runoff from 1 km² of the catchment area was 3.978×10^3 m³ in 2012 and decreased to 2.9726×10^3 m³ by 2024.

The statutory charge for withdrawing 103 m³ of surface water from water bodies within the Amur

River basin (Far Eastern region) within the approved quarterly abstraction limits is 264 rubles. For withdrawals exceeding these limits, the rate is applied at five times the standard level. In addition, a coefficient of 1.1 is applied to the water-use tax rate in 2024.

As a result, the charge for 103 m³ of water in 2012 and 2024 amounted to 5,776.05 rubles and 4,314.76 rubles, respectively.

The capitalized value of the study area² amounted to 57,760.5 rubles in 2012 and 43,147.6 rubles in 2024.

² Order No. 81 of February 11, 1998 "On Approval of the Methodology for Calculating the Damage from Groundwater Pollution". State Committee of the Russian Federation for Environmental Protection. 1998.

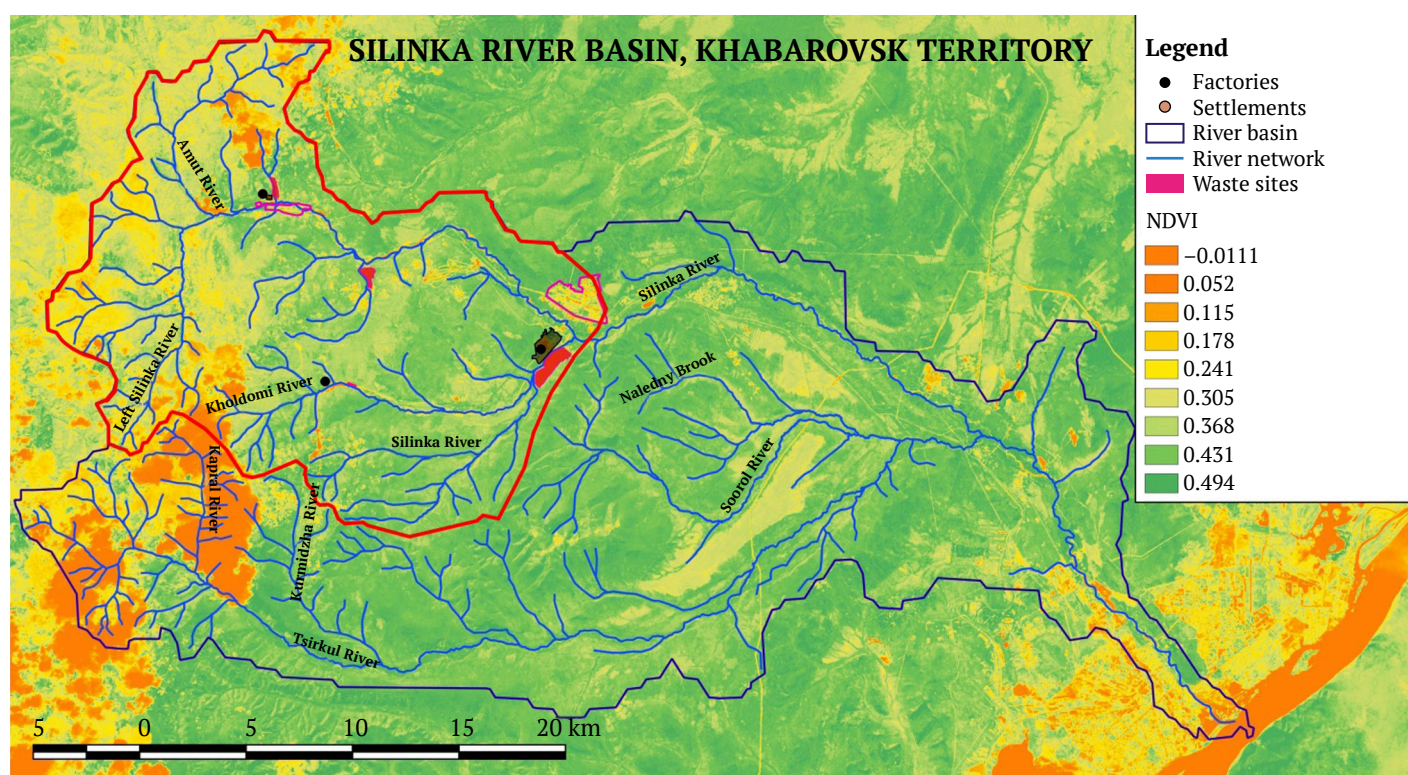


Fig. 4. Schematic map of the Silinka River basin with Normalized Difference Vegetation Index (NDVI).

Note: boundary of the analysed river network section

Table 1

Forest cover parameters derived from NDVI for river basins hosting technogenic facilities of the studied mining enterprises

Year	2013	2014	2015	2016	2017	2018	2019	2020	2021	2022	2023	2024
Forest cover, %	73.5	69.6	73.8	68.5	76.5	71.3	72.6	63.2	66.3	58.7	62.6	61.4
Area of the 1 st tailings storage facility, ha	40.5	40.5	40.5	40.5	40.5	40.5	40.5	44	44	44	44	44
Area of the 2 nd tailings storage facility, ha	195	195	233	233	233	233	233	256	256	312	312	312
Area of the 3 rd tailings storage facility, ha	40.1	40.1	40.8	40.8	40.8	40.9	40.9	40.9	44	44	44	44
Area of the settling pond, ha	30.8	30.8	30.8	30.8	30.8	30.8	30.8	30.8	30.8	30.8	30.8	30.8

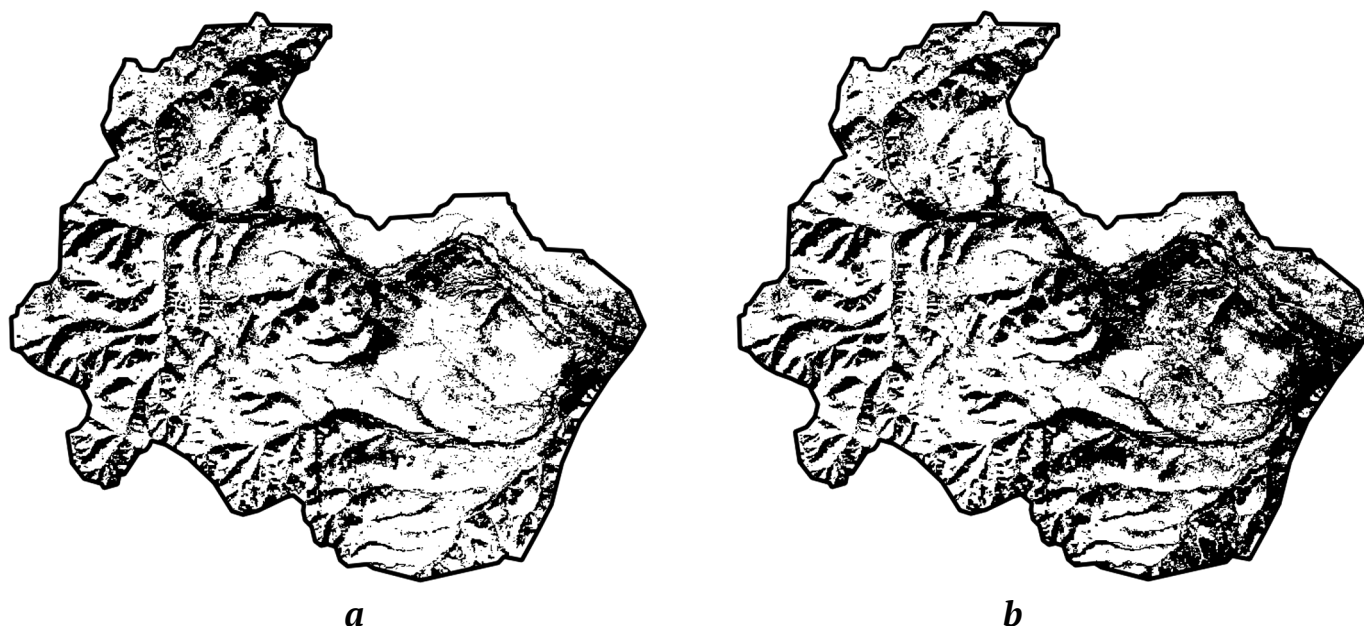


Fig. 5. NDVI-based forest cover in river basins hosting mining facilities, 2012 (a) and 2024 (b)

Note: black pixels represent non-forested areas

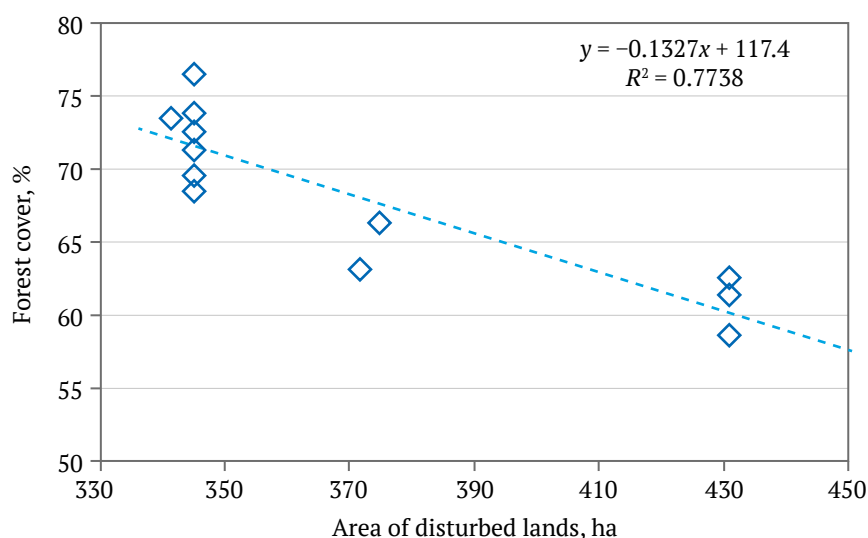


Fig. 6. Relationship between forest cover and the extent of disturbed land in the Silinka River basin

The reduction in the value of 1 km² of territory performing water-protection functions within the Silinka River basin can therefore be expressed as the difference between the capitalized values calculated for 2012 and 2024.

According to the calculations, the average value per 1 km² of the study area decreased by 14,612.9 rubles, which corresponds to a reduction of about 25% as a result of mining activity.

Conclusion

Geoinformation analysis based on the Normalized Difference Vegetation Index (NDVI) revealed a 14.8% decrease in forest cover within the section

of the Silinka River basin affected by the former Solnechny Mining and Processing Plant, relative to the 2012 baseline. This confirms the degradation of the water-regulating function of the vegetation cover. The reduction in forest cover is accompanied by a decrease in specific runoff of 1.0064×10^3 m³ per km², which is equivalent to a 25% decline in streamflow.

The calculated average value per 1 km² of the study area in 2024 decreased by 14,612.9 rubles due to mining operations. Thus, the extraction of tin ore within the Silinka River basin (Solnechny District, Khabarovsk Territory) leads to a reduction in forest cover, which in turn causes a directly proportional decrease in the streamflow of small rivers.



References

1. Boltryov V.B., Degtyarev S.A., Seleznev S.G., Storozhenko L.A. Ecological damages in territories of mining waste formation and accumulation. In: Osipov V.I., Maksimovich N.G., Baryakh A.A., et al. (Eds.) *Sergeevskie Chteniya: Proceedings of the Annual Session of the RAS Scientific Council on Geoecology, Engineering Geology, and Hydrogeology*. April 2–4, 2019. Perm: State National Research University. Vol. 21. Pp. 151–156. (In Russ.)
2. Rybnikova L.S. Technogenic impact of the Urals mining works upon the hydrosphere status. *Water Sector of Russia: Problems, Technologies, Management*. 2012;(1):74–91. (In Russ.)
3. Tkachenko M.E. *General forestry*. 2nd ed. Moscow: Goslesbumizdat; 1952. 598 p. (In Russ.)
4. Pobedinskiy A.V. *Water protection and soil conservation role of forests*. 2nd ed. Pushkino: VNIILM; 2013. 208 p. (In Russ.)
5. Kasimov D.V., Kasimov V.D. *Some approaches to assessing ecosystem functions of forest stands in environmental management practice*. Moscow: Mir Nauki; 2015. 91 p. (In Russ.)
6. Gaparov K.K. *The influence of forestry practices on hydrological and protective functions of spruce forests in Issyk-Kul region*. Bishkek: Institute of Forest and Nut Farming named after Prof. P.A. Gan of the National Academy of Sciences of the Kyrgyz Republic; 2007. 103 p. (In Russ.)
7. Krestovskiy O.I. *The influence of forest cutting and restoration on river water content*. Saint Petersburg: Gidrometeoizdat; 1986. 118 p. (In Russ.)
8. Alekseevskiy N.I. River runoff: geographical role and indicative properties. *Problems of Geography*. 2012;133:48–71. (In Russ.)
9. Koronkevich N.I., Melnik K.S. Impact of urbanized landscapes on the river flow in Europe. *Izvestiya Rossiiskoi Akademii Nauk. Seriya Geograficheskaya*. 2019;(3):78–87. (In Russ.) <https://doi.org/10.31857/S2587-55662019378-87>
10. Yasinskiy S.V., Venitsianov E.V., Vishnevskaya I.A. Diffuse pollution of waterbodies and assessment of nutrient removal under different land-use scenarios in a catchment area. *Vodnye Resursy*. 2019;46(2):232–244. (In Russ.) <https://doi.org/10.31857/S0321-0596462232-244>
11. Buzmakov S.A., Nazarov A.V., Sannikov P.Yu. Influence of mining on vegetation. *Izvestia of Samara Scientific Center of the Russian Academy of Sciences*. 2012;(5):261–263. (In Russ.)
12. Lebedev Yu. V., Neklyudov I. A. *Assessment of water conservation and water regulation functions of forests: methodological guidelines*. Yekaterinburg: Ural State Forest Engineering University; 2012. 36 p. (In Russ.)
13. Kireeva M.B., Ilich V.P., Sazonov A.A., Mikhaylyukova P.G. An assessment of changes in land usage and their impact on Don River basin runoff using satellite imagery. *Sovremennyye Problemy Distantionnogo Zondirovaniya Zemli iz Kosmosa*. 2018;15(2):191–200. (In Russ.) <https://doi.org/10.21046/2070-7401-2018-15-2-191-200>
14. Makarov V.N. Geochemical assessment of tailings of mining and processing plants in Yakutia. *Nedropolzovanie XXI Vek*. 2023;(3–4):34–41. (In Russ.)
15. Abakumova V.Y. Research of relief impact on river network structure (Zabaikalsky Krai). In: *Environmental cooperation in transboundary ecological regions: Russia – China – Mongolia*. Chita: Poisk; 2012. Vol. 3. Pt. 1. Pp. 199–203. (In Russ.)
16. Inishev N.G., Voronova A.A. The influence of landscape features of wetland watersheds on the hydrographs of spring flood. In: Inisheva L.I. (Ed.) *Swamps and the Biosphere*. Proceedings of the IX All-Russian School-Conference of Young Scientists with international participation. Vyatkin, Vladimir Oblast, September 14–18, 2015. Vyatkin: PresSto; 2015. Pp. 199–203. (In Russ.)
17. Georgiadi A.G., Koronkevich N.I., Zaitseva I.S., et al. Climatic and anthropogenic factors in long-term alterations of the Volga river runoff. *Water Sector of Russia: Problems, Technologies, Management*. 2013;(4):4–19. (In Russ.)



18. Zemlyanukhin I.P., Radceвич G.A. Influence of morphology and woodiness of reservoirs on formation of the drain. *Modeli i Tekhnologii Prirodoustroistva (Regional'nyi Aspekt)*. 2016;(2):41–46. (In Russ.)
19. Konokova B.A. The problem of preservation of fresh water quality in the mountains. *New Technologies*. 2012;(2):1–6. (In Russ.)
20. Denmukhametov R.R., Sharifullin A.N. Antropogenic components of the river flow dissolved substances. *Ekologicheskii Konsalting*. 2011;(1):34–41. (In Russ.)
21. Krupskaya L.T., Melkonyan R.G., Zvereva V.P., et al. Ecological hazard of accumulated mining waste and recommendations on risk reduction in the Far Eastern Federal District. *Mining Informational and Analytical Bulletin*. 2018;(12):102–112. (In Russ.)
22. Krupskaya L.T., Golubev D.A., Rastanina N.K., Filatova M.Yu. Reclamation of tailings storage surface at a closed mine in the Primorsky Krai by bio remediation. *Mining Informational and Analytical Bulletin*. 2019;(9):138–148. (In Russ.) <https://doi.org/10.25018/0236-1493-2019-09-0-138-148>
23. Nazarkina A.V. Physical properties and hydraulic regime of alluvial soils in floodplains of rivers in the Sikhote-Alin mountains. *Eurasian Soil Science*. 2008;41(5):509–518. <https://doi.org/10.1134/S1064229308050062> (Orig. ver.: Nazarkina A. V. Physical properties and hydraulic regime of alluvial soils in floodplains of rivers in the Sikhote-Alin mountains. *Pochvovedenie*. 2008;(5):576–586. (In Russ.))
24. Rastanina N.K., Kolobanov K.A. Impact of technogenic dust pollution from the closed mining enterprise in the Amur Region on the ecosphere and human health. *Mining Science and Technology (Russia)*. 2021;6(1):16–22. <https://doi.org/10.17073/2500-0632-2021-1-16-22>
25. Rastanina N.K., Galanina I.A., Popadyev I.A. Mining and environmental monitoring of soil changes within the boundaries of the influence of tin ore mining in the Amur Region. *Modern Science: Actual Problems of Theory & Practice. Series Natural & Technical Sciences*. 2024;(5):22–26. (In Russ.) <https://doi.org/10.37882/2223-2966.2024.05.28>
26. Krupskaya L.T., Ionkin K.V., Krupskiy A.V., et al. On the issue of assessing tailing dumps as a source of environmental pollution. *Mining Informational and Analytical Bulletin*. 2009;(5):234–241. (In Russ.)
27. Komarov A.A. Assessment of grass stand condition using NDVI vegetation index. *Izvestiya Saint Petersburg State Agrarian University*. 2018;(2):124–129. (In Russ.)
28. Tishkov A.A., Bobylev S.N., Medvedeva O.E., et al. *Economics of biodiversity*. Moscow: Institut Ekonomiki Prirodopol'zovaniya; 2002. 604 p. (In Russ.)
29. Belov D.V., Brovko P.F. Recreational potential of the Silinka River basin (Khabarovsk region). *The Pacific Geography*. 2020;(4):65–73. (In Russ.) <https://doi.org/10.35735/tig.2020.4.4.007>

Information about the authors

Natalia K. Rastanina – Cand. Sci. (Biol.), Associate Professor of the Higher School of Industrial Engineering, Pacific State University, Khabarovsk, Russian Federation; ORCID [0000-0002-0252-6220](https://orcid.org/0000-0002-0252-6220); e-mail n.rastanina@yandex.ru

Dmitry A. Golubev – Cand. Sci. (Eng.), Associate Professor of the Higher School of Management, Pacific State University, Khabarovsk; Leading Researcher of the Department of Forest Protection and Forest Ecology, Far East Forestry Research Institute, Khabarovsk, Russian Federation; ORCID [0000-0001-9416-2913](https://orcid.org/0000-0001-9416-2913); e-mail poet.golubev@mail.ru



Nikita A. Kayumov – Student, Pacific State University, Khabarovsk, Russian Federation; Far East Forestry Research Institute, Khabarovsk, Russian Federation; ORCID [0009-0001-6875-3290](https://orcid.org/0009-0001-6875-3290); e-mail nik.kayumov@mail.ru

Pavel L. Rastanin – Student, Pacific State University, Khabarovsk, Russian Federation; ORCID [0009-0008-6693-2747](https://orcid.org/0009-0008-6693-2747)

Ilya A. Popadyev – Student, Pacific State University, Khabarovsk, Russian Federation; ORCID [0009-0009-7054-3856](https://orcid.org/0009-0009-7054-3856)

Received 15.04.2025

Revised 20.06.2025

Accepted 21.06.2025



BENEFICIATION AND PROCESSING OF NATURAL AND TECHNOGENIC RAW MATERIALS

Research paper

<https://doi.org/10.17073/2500-0632-2025-09-454>

UDC 622.775.4:549.211.2:661.183



Regulation of the oil receptivity of the surface of diamonds and kimberlite minerals using various classes of regulating agents

V.A. Chanturiya , V.V. Morozov , E.L. Chanturiya , A.L. Samusev

Research Institute of Comprehensive Exploitation of Mineral Resources of the Russian Academy of Sciences, Moscow, Russian Federation dchmggu@mail.ru

Abstract

The purpose of the research is to select appropriate agents for regulating the oil receptivity of diamond and kimberlite mineral surfaces in the conditioning of diamond-kimberlite products prior to their beneficiation by froth flotation and X-ray luminescence separation using phosphor-containing modifying agents and collecting agents, the basis of which is apolar collecting agents. The paper presents the results of comprehensive physicochemical studies of the influence of various classes of regulating agents on the attachment of apolar collecting agents on the surface of diamonds and kimberlite minerals (visiometric analysis, measurement of limiting wetting angles in a mineral–organic collecting agent–aqueous phase system, measurement of surface tension at the organic collecting agent–aqueous phase–frothless flotation phase boundary). Based on the analysis of the data obtained, effective regulating agents have been identified and selected to ensure the selectivity of diamond beneficiation. Regulating agents belonging to the classes of alkylarylphosphonates (NTPA, OEDPA), aminopolycarboxylic acids (EDTA), cationic polymers (PEG-1500, Neonol AF-9-6), polyphosphates (STPP), bifunctionally modified carboxymethylcellulose derivatives (CMC 75-V and Kamcel-600), mixtures of alkyl phosphates, alkyl phosphonates, and anionic polymers (IS-3), ionogenic and non-ionogenic nitrogen-containing polymers (Emulsifier OP-4, Oxypav A1218.30), amino alcohols (TEA), hydroxy acids (lactic acid), and quaternary ammonium bases (ammonium sulfate) were tested. Talc, pyrite, calcite, muscovite, phlogopite, serpentine, and dolomite were selected as the main minerals of kimberlite prone to adhesion of apolar collecting agents. It has been established that the limiting wetting angle is reduced most significantly by the agents Neonol AF-9-6, Emulsifier OP-4, and Oxypav A1218.30 that is associated with a significant decrease in the surface tension of the interface between an organic collecting agent and the aqueous phase. A thermodynamic assessment of the oil receptivity of kimberlite minerals conducted using the Dupré–Young equation and based on measurements of limiting wetting angles and surface tension showed that the energy of adhesion of an organic collecting agent on kimberlite minerals with the addition of regulating agents decreases by 2–6 times and reaches values of 6–17 J/m², approaching the adhesion energy of water (5 J/m²). On diamonds, the energy of adhesion of an apolar collecting agent at maximum concentrations decreases only to 17–27.5 J/m² that determines its stable attachment. The results of flotation tests confirmed the depressing ability of the studied regulating agents in relation to the flotation-responding minerals of kimberlite. Based on the analysis of the data obtained, effective regulating agents have been selected and recommended for testing in industrial froth separation modes, ensuring increased selectivity of apolar collecting agent attachment on the surface of diamonds and kimberlite minerals: NTPA, OEDPA, IS-3, OP-4.

Keywords

diamonds, kimberlite, minerals, collecting agent, oil receptivity, agents, surfactants, work of adhesion, flotation, selectivity

Financing

This research was funded by a grant No. 25–17–00009 from the Russian Science Foundation, <https://rscf.ru/project/25-17-00009/>

For citation

Chanturiya V.A., Morozov V.V., Chanturiya E.L., Samusev A.L. Regulation of the oil receptivity of the surface of diamonds and kimberlite minerals using various classes of regulating agents. *Mining Science and Technology (Russia)*. 2025;10(4):379–392. <https://doi.org/10.17073/2500-0632-2025-09-454>



ОБОГАЩЕНИЕ, ПЕРЕРАБОТКА МИНЕРАЛЬНОГО И ТЕХНОГЕННОГО СЫРЬЯ

Научная статья

Регулирование олеофильности поверхности алмазов и минералов кимберлита добавками реагентов-регуляторов различных классов**В.А. Чантурия**  , **В.В. Морозов**   , **Е.Л. Чантурия**  , **А.Л. Самусев**  *Институт проблем комплексного освоения недр им. академика Н.В. Мельникова Российской академии наук, г. Москва, Российская Федерация* dchmggu@mail.ru**Аннотация**

Цель проведенных исследований – обоснованный выбор реагентов для регулирования олеофильности поверхности алмазов и минералов кимберлита в процессах кондиционирования алмазо-кимберлитовых продуктов перед их обогащением пенной сепарацией, флотацией и рентгенолюминесцентной сепарацией с применением люминофорсодержащих реагентов-модификаторов и собирателей, основой состава которых являются аполярные коллекторы. В работе представлены результаты комплексных физико-химических исследований влияния реагентов-регуляторов различных классов на закрепление аполярных коллекторов на поверхности алмазов и минералов кимберлита (визиометрический анализ, измерение краевых углов смачивания в системе минерал – органический коллектор – водная фаза, измерение поверхностного натяжения на границе раздела фаз органический коллектор – водная фаза – беспенная флотация). На основе анализа полученных данных обоснованы и выбраны эффективные реагенты-регуляторы, обеспечивающие селективность обогащения алмазов. Исследованы реагенты-регуляторы, принадлежащие к классам алкиларилфосфонатов (НТФК, ОЭДФ), аминополикарбоновых кислот (ЭДТА), катионоактивных полимеров (ПЭГ-1500, Неонол АФ-9-6), полифосфатов (ТПФ), бифункционально модифицированных производных карбоксиметилцеллюлозы (КМЦ 75-В и Камцел-600), смеси алкилфосфатов, алкилфосфонатов и анионных полимеров (ИС-3), ионогенных и неионогенных азотсодержащих полимеров (Эмульгатор ОП-4, Оксипав А1218.30), аминокспиртов (ТЭА), гидроксикислот (молочная кислота), четвертичных аммониевых оснований (сульфат аммония). В качестве основных минералов кимберлита, склонных к адгезии аполярных коллекторов, выбраны тальк, пирит, кальцит, мусковит, флогопит, серпентин, доломит. Установлено, что в наибольшей мере краевой угол смачивания снижают реагенты Неонол АФ-9-6, Эмульгатор ОП-4, Оксипав А1218.30, что связано с существенным снижением поверхностного натяжения границы раздела фаз органический коллектор – водная фаза. Термодинамическая оценка олеофильности минералов кимберлита, проведенная по уравнению Дюпре–Юнга с использованием результатов измерения краевых углов смачивания и поверхностного натяжения, показала, что энергия адгезии органического коллектора на минералах кимберлита при добавках реагентов-регуляторов снижается в 2–6 раз и достигает значений 6–17 Дж/м², приближающихся к энергии воды (5 Дж/м²). На алмазах энергия адгезии аполярного коллектора при максимальных концентрациях снижается только до 17–27,5 Дж/м², что и обуславливает его устойчивое закрепление. Результаты флотационных опытов подтвердили депрессирующую способность исследованных реагентов-регуляторов по отношению к флотоактивным минералам кимберлита. На основе анализа полученных данных выбраны и рекомендованы для апробации в промышленных режимах пенной сепарации эффективные реагенты-регуляторы, обеспечивающие повышение селективности закрепления аполярного коллектора на поверхности алмазов и минералов кимберлита: НТФК, ОЭДФ, ИС-3, ОП-4.

Ключевые слова

алмазы, кимберлит, минералы, коллектор, олеофильность, реагенты, поверхностно-активные вещества, работа адгезии, флотация, селективность

ФинансированиеИсследование выполнено за счет гранта Российского научного фонда №25–17–00009, <https://rscf.ru/project/25-17-00009/>**Для цитирования**Chanturiya V.A., Morozov V.V., Chanturiya E.L., Samusev A.L. Regulation of the oil receptivity of the surface of diamonds and kimberlite minerals using various classes of regulating agents. *Mining Science and Technology (Russia)*. 2025;10(4):379–392. <https://doi.org/10.17073/2500-0632-2025-09-454>



Introduction

The current task in developing a process for extracting weakly and abnormally luminescent diamonds in X-ray luminescence separation processes is to increase the selectivity of attachment of phosphor-containing modifying agents on the surface of diamonds and the rational selection of regulating agents preventing the attachment of apolar collecting agents, which are part of the modifying agents used, on the hydrophobic minerals of kimberlite [1, 2]. A similar objective, increasing the selectivity of attachment of apolar collecting agents on the surface of diamonds, is a prerequisite for improving the efficiency of flotation and froth separation processes [3, 4]. In both cases, in order to select effective agent modes, it is necessary to establish the regularities of attachment of organic collecting agents and regulating agents that regulate hydrophobicity and oil receptivity on diamonds and kimberlite minerals [1, 5].

The purpose of the research is to select appropriate agents for regulating the oil receptivity of diamond and kimberlite mineral surfaces in the conditioning of diamond-kimberlite products prior to their beneficiation by froth flotation and X-ray luminescence separation using phosphor-containing modifying agents and collecting agents, the basis of which is apolar collecting agents.

The objectives of the research were:

- identification of kimberlite minerals most prone to adhesion of organic collecting agent drops;
- determining the influence of regulating agents on the adhesion energy of apolar collecting agents on the surface of diamonds and oleophilic kimberlite minerals;
- selection of regulating agents that maximally increase the contrast in the flotation response of diamonds and kimberlite minerals.

The basis for selecting research methods and approaches to solving the task at hand is an analysis of current scientific and technical developments and research in the field of regulating surface processes in water-mineral disperse systems [6, 7].

A significant number of studies in this area have been conducted in relation to the processes of froth flotation and separation of diamonds from kimberlites¹ [8, 9]. Along with the selection of collecting agents, the presented works recommended a specific set of regulating agents designed to suppress the floatability of kimberlite.

The results of research in related fields were also used to make an informed choice of regulating agents.

The studies related to the use of layered aluminosilicate minerals as sorbents for heavy metals and petroleum products from wastewater [10] are similar in nature to the task at hand. However, due to the inverse final objective (increasing the sorption of pollutants), most of the theoretical and experimental provisions of these works only partially describe hydrophilization processes.

Research into the methods of increasing oil recovery from oil reservoirs is also of interest, particularly with regard to the use of regulating agents that help reduce the hydrophobicity of reservoir minerals, including layered aluminosilicate minerals [11]. However, due to the different mineral composition of the host rocks, the characteristics of the organic phase (oil), temperature, and pressure, most of the theoretical principles and experimental data are only of limited applicability for describing the hydrophilization processes of kimberlite minerals.

Another area in which a similar task of reducing the fouling of working surfaces with hardness salts is being addressed is the process of agent conditioning of aqueous media in thermal units and reverse osmosis plants [12].

Despite the differences between the processes considered and those occurring during processing of diamond-containing products prior to X-ray luminescence and froth separation processes, the similarity of the tasks to be solved – increasing the hydrophilicity of rock minerals and cleaning the surface of working elements from hydrophilic coatings – is the basis for selecting the range of regulating agents for the research being conducted.

To make an informed choice of agents that regulate the selectivity of attachment of agents modifying X-ray spectral characteristics and collecting agents on the surface of diamonds in the processes of X-ray luminescence and froth separation, a complex of physical and chemical research methods and thermodynamic modeling of the action of regulating agents on the attachment of organic collecting agents on hydrophobic kimberlite minerals in high-salt waters was used.

Research Techniques

The following objects were selected for the research: diamond crystals with polished surfaces, kimberlites of different degrees of metamorphism, as well as polished sections and plates of the most significant kimberlite minerals. CCHGO (cat cracking heavy gas oil) with additives of bunker fuel (BF) and luminol was used as a collecting agent. The studies were conducted using solutions of twelve regulating agents of different classes in model high-salt water, similar in composition to reclaim waters of beneficiation plants processing diamond-bearing kimberlites.

¹ Yun R.-Kh., Kuznetsov D. Method for Extracting Diamonds from Vein Minerals. RF Patent No. 2412901, C2, publ. on 27.02.2011, Bul. No. 6 (In Russ.)

To preliminarily assess the intensity of organic collecting agent attachment on kimberlite minerals, a vision-based method [2] was used, which included treating a sample with an emulsion of a phosphor-containing organic collecting agent and obtaining and analyzing images of the mineral surface under ultraviolet light. The intensity of an organic collecting agent attachment to the surface of diamonds, individual minerals, and kimberlite grains was determined by analyzing images of the surface area occupied by the organic collecting agent after treatment of mineral samples. To measure the proportion of the surface occupied by the collecting agent (the degree of coverage), the areas with characteristic luminescence ($\lambda = 500$ nm) corresponding to the radiation of a mixture of CCHGO with BF and luminol were recorded.

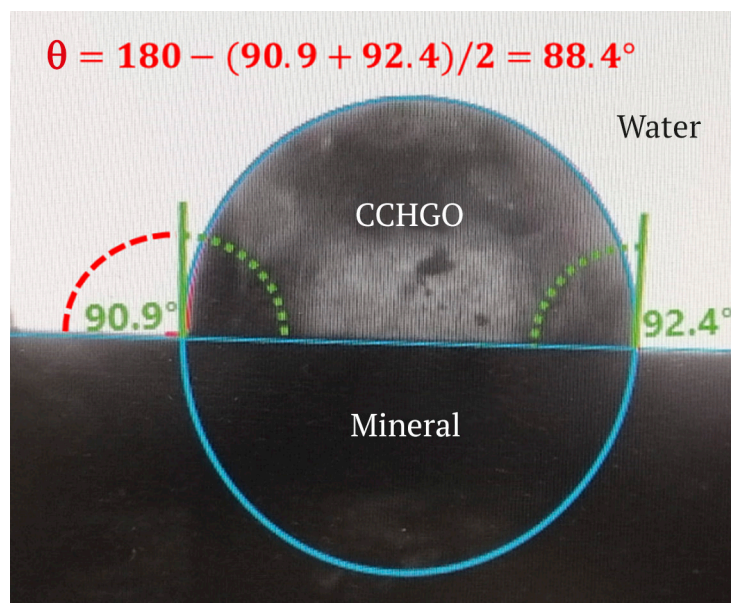
To evaluate the influence of regulating agents on the oil receptivity of kimberlite minerals, wetting contact angles were measured in the mineral–organic collecting agent–aqueous phase system [13]. Methods for measuring wetting contact angle have previously been used to evaluate the restoration of hydrophobicity in natural diamonds through various types of physical and physicochemical treatment [14]. A DSA25 instrument equipped with image processing software² was used to measure the wetting contact angle.

The built-in program determined the wetting contact angle at the moment of stabilization of the mineral – organic collecting agent drop – aqueous phase system (Fig. 1, *a*).

After each measurement, the surface of a diamond was cleaned using toluene and a 1N hydrochloric acid solution. To measure the wetting contact angle on kimberlite minerals, polished sections or plates of a mineral obtained by splitting natural samples were used.

The wetting contact angle in the apolar liquid–mineral–aqueous phase system is an informative quantitative characteristic of oil receptivity and is widely used to describe the wetting process of various surfaces in technological processes [15]. To study the attachment of a collecting agent on minerals in an aqueous phase, a dynamic method for measuring three-phase wetting contact angle was used [4, 16]. According to the method used, the surface of a mineral sample was first held in an aqueous phase of a specified composition, then the level of the aqueous phase in the cuvette was lowered to the level of the sample surface, and a drop of an organic collecting agent of a specified volume was applied. After applying a drop of a collecting agent to the surface of a sample in the cuvette, the liquid level was increased. At the same time, part of the drop detached from the surface of the sample and settled at the interface between the aqueous phase and the air. The wetting contact angle on the three-phase wetting perimeter was measured after equilibrium was established without removing the aqueous phase. The method used simulates the process of attachment of an apolar collecting agent on a mineral in a turbulent environment typical for the conditioning of diamond–kimberlite products prior to X-ray luminescence and froth separation processes.

² Drop Shape Analyzer DSA25 Specifications. URL: <https://www.kruss-scientific.com/files/kruss-techdata-dsa25-en.pdf/>



a



b

Fig. 1. Image of a drop of organic collecting agent, CCHGO (cat cracking heavy gas oil):
a – on the surface of a mineral polished section with the results of measuring the wetting contact angle on the DSA25 instrument; *b* – on the curved capillary of the ST-1 stalagmometer

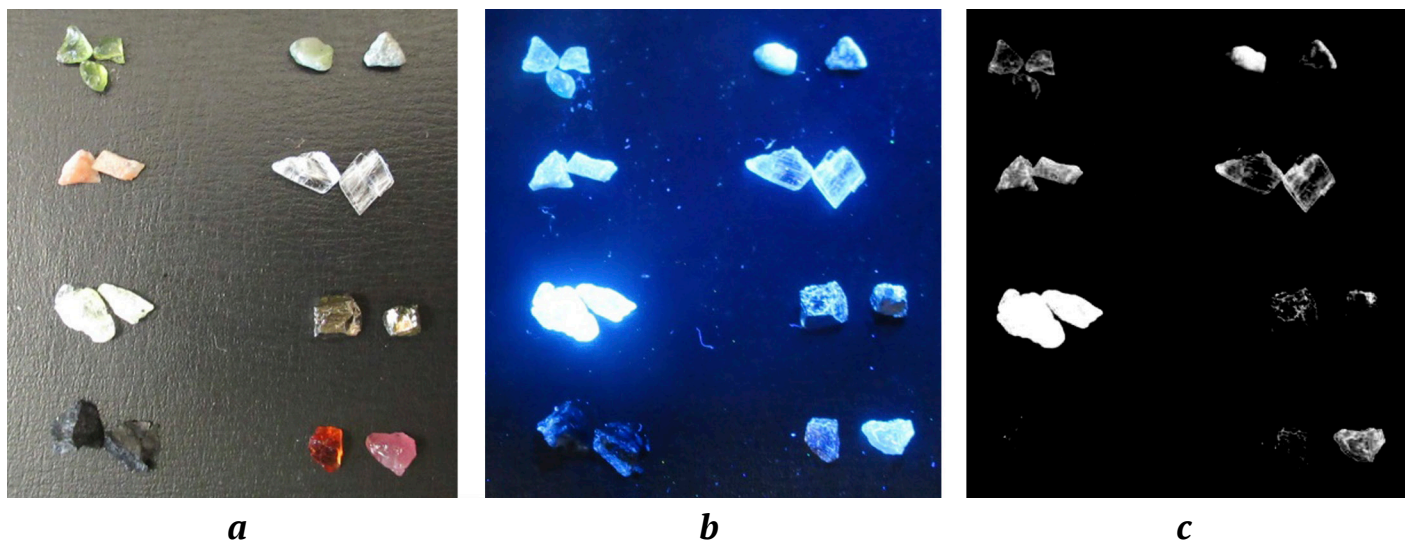


Fig. 2. Images and results of visiometric analysis of the attachment of an organic collecting agent with dissolved phosphor on the surface of kimberlite minerals and associated minerals: *a* – in daylight; *b* – in UV light after treatment with a collecting agent; *c* – distribution of an organic collecting agent across mineral samples. Here (from right to left, top to bottom): olivine, calcite, celestine, muscovite, talc, pyrite, chromite, pyrope

To calculate the adhesion energy of an apolar collecting agent on the surface of minerals using the Dupré–Young equation, the surface tension of the interface between the organic collecting agent and the aqueous phase was determined. The measurements were performed using a ST-1 stalagmometer by determining the volume of floating drops of the collecting agent that detached from the curved capillary (Fig. 1, *b*), in accordance with the standard method³. The surface tension at the interface between the aqueous phase and air was measured by determining the volume of falling drops from a straight capillary in accordance with the method.

The flotation of diamonds, minerals, and kimberlite grains was carried out using the frothless flotation method in a Hallimond tube. The experimental method included preparing a mineral sample, preparing a liquid phase (high-salt water), water conditioning with a regulating agent, mineral sample conditioning with a collecting agent in water containing an oil receptivity regulating agent, flotation of diamonds, kimberlite, or kimberlite minerals, dewatering, drying, and weighing of the flotation products [4].

Visiometric analysis of organic collecting agent attachment on samples of kimberlite mineral components

At the initial stage of the research, kimberlite minerals were selected that are characterized by significant adhesion of the apolar collecting agent (CCHGO with BF and luminol) from aqueous emul-

sions. Minerals most commonly found in kimberlites of different degree of metamorphism were selected for the research. Model high-salt water was used to obtain the collecting agent emulsion. The concentration of the phosphor-containing collecting agent in the emulsion was 200 mg/L. The treatment time was 1 min. After the treatment and removing excess emulsion, the mineral sample was rinsed with reclaim water for 30 seconds.

The analysis of the images of mineral samples under ultraviolet light revealed significant differences in the intensity of organic collecting agent attachment on their surfaces: from almost complete coverage (talc, see Fig. 1) to complete absence of attachment (chromite, Fig. 2).

Table 1
Results of visiometric analysis of apolar collecting agent attachment on kimberlite minerals

No.	Mineral	Prevalence in kimberlite, %	Percentage of surface area covered by organic collecting agent, %
1	Diamond	2–10 carats/t	56–95
Kimberlite minerals			
2	Calcite	1–40	22–65
3	Muscovite	0.1–5	25–50
4	Talc	0.1–5	80–93
5	Pyrite	0.05–1	35–55
6	Phlogopite	0.1–5	15–25
7	Serpentine	1–10	7–10
8	Dolomite	0.5–15	7–12

³ GOST R 50097–92 “Surfactants. Determination of Interfacial Tension. Drop Volume Method”.



The results of the visiometric measurements allowed to select seven kimberlite minerals with high and medium degrees of coverage by the apolar collecting agent for further research (Table 1).

Minerals associated with diamonds that have a relatively high tendency to adhesion with organic collecting agents (celestine, pyrope, etc.) were not studied, as their contents in kimberlite are very insignificant.

Selection of agents for regulating the oil receptivity of kimberlite minerals

When selecting the initial range of agents for regulating the oil receptivity of kimberlite minerals, both traditional and new classes of organic compounds used to regulate the properties of minerals during flotation were considered: phosphorus-containing chelates, bifunctional cationic and anionic polymers, hydroxy acids, amino alcohols, bifunctionally modified carboxymethylcellulose derivatives, cationic nitrogen-containing olefins, aliphatic amines, quaternary ammonium compounds, and cationic polymers⁴ [8]. Initially, the list for the research included the agents used in related industries. For instance, the agents of

the alkylarylphosphonate, nitrogen-containing olefin, and aliphatic amine classes are effectively used in oil production to increase oil recovery by reducing the hydrophobicity of reservoir minerals [17, 18]. The selection criteria were the requirements of commercial production of the agents of the listed classes and validation in flotation processes and related industries. In accordance with these requirements, 14 agents presented in Table 2 were selected for the studies.

A preliminary assessment of the effectiveness of the regulating agents under consideration was carried out by determining the “critical” concentration at which the attachment of an organic collecting agent ceases. The criterion for the effectiveness of regulating agents was their ability to minimize the wetting contact angle to the point of removing an organic collecting agent drop from the surface of a mineral sample when treated with regulating agent solutions in the concentration range from 10 to 1000 mg/L. Phlogopite was selected as an indicator mineral.

The results of the studies showed that a significant decrease in the wetting contact angle and detachment of an organic collecting agent drop from the surface of phlogopite in the specified concentration range is achieved when using 13 regulating agents (with the exception of ammonium sulfate). Therefore, all these agents were selected for subsequent tests (Table 2).

Table 2

Critical concentrations of regulating agents for attachment of organic collecting agent on phlogopite

No.	Regulating agent (of technical grade)	Class of organic compounds	Critical concentration of regulating agent, mg/L	
			with partial detachment of a collecting agent drop	with complete detachment of a collecting agent drop
1	Zinc complexonate of nitrilotrimethylphosphonic acid (NTPA)	Nitrilalkyl triphosphonate	130	166
2	Oxyethylidenediphosphonic acid (OEDPA)	Alkyl diphosphonate	90	130
3	Ethylendiaminetetraacetic acid (EDTA)	Aminopolycarbonic acid	130	166
4	Polyethylene glycol (PEG-1500)	Cationic polymer	90	130
5	Sodium tripolyphosphate (STPP)	Polyphosphate	90	130
6	Polyethylene glycol ether of monoalkyl phenols (Neonol AF-9-6)	Cationic nitrogen-containing polymer	50	70
7	Modified carboxymethylcellulose (CMC 75-V)	Bifunctionally modified CMC derivatives	70	90
8	Compound action antiscalant (AKVA-IS3)	A mixture of alkyl phosphates, alkyl phosphonates, and anionic polymers	130	170
9	Technical glyoxylic sodium carboxymethylcellulose (Kamcel-600)	Bifunctionally modified CMC derivatives	50	70
10	Alkyl C8-12-phenol ethoxylated (Emulsifier OP-4)	Short-chain aliphatic amine	50	70
11	Alkyldimethylamine oxide C12–C18 (Oxipav A1218.30)	Nonionic nitrogen-containing polymer	70	90
12	Triethanolamine (TEA)	Amino alcohol	500	1000
13	2-hydroxypropanoic acid (Lactic acid)	Hydroxy acid	330	500
14	Ammonium sulfate	Quaternary ammonium compound	–	–

⁴ Yun R.-Kh., Kuznetsov D. Method for Extracting Diamonds from Vein Minerals. RF Patent No. 2412901, C2, published on 27.02.2011, Bul. No. 6 (In Russ.).



Research and thermodynamic analysis of the influence of regulating agents on the oil receptivity of kimberlite minerals

The thermodynamically justified parameter of the wetting ability of an organic collecting agent and, at the same time, the oil receptivity of a mineral surface is the work (energy) of adhesion. The work of adhesion of an apolar collecting agent on a mineral surface can be calculated using the Dupré–Young equation [19]:

$$W_{oc-m} = \sigma_{oc-w} (1 - \cos \theta), \quad (1)$$

where W_{oc-m} is the work of adhesion of a collecting agent on a mineral, J/m²; σ_{oc-w} is the interfacial tension at the interface between an organic collecting agent and an aqueous phase, N/m; θ is the three-phase wetting contact angle for a drop of organic collecting agent on a mineral surface in an aqueous phase, degrees.

To calculate the adhesion of an apolar collecting agent on a mineral surface, the wetting contact angles on diamond and kimberlite minerals (see Table 1) were measured using a DSA25 instrument in the aqueous phase (model high-salt water) with regulating agents dissolved in it in the concentration range of 0–500 mg/L. A mixture of CCHGO and BF (85 and 15%) was used as an organic collecting agent. During preliminary wetting of the polished sections, high-salt model water with additives of regulating agents was also used. A drop of an organic collecting agent was applied to the surface of a moistened mineral sample using a DSA25 dispenser syringe, after which the aqueous phase level in the cuvette was raised and images of a collecting agent drop attached to the surface of the mineral sample were obtained (see Fig. 1, a).

Next, using a ST-1 stalagmometer according to the method described in GOST R 50097–92⁵, the mass and volume of ten drops of an organic collecting agent, which detached themselves from a curved capillary in an aqueous medium were measured. Based on the data obtained, the cell constant K (measured using kerosene) was found and the surface tension at the interface between an organic collecting agent and the aqueous phase (σ_{oc-w}) was determined for different agents in the concentration range of 0–500 mg/L:

$$K = \frac{47.5}{V(\rho_{water} - \rho_{kerosene})}; \quad (2)$$

$$\sigma_{oc-w} = KV(\rho_w - \rho_{oc}), \quad (3)$$

where V is the volume of a droplet, m³; ρ_{water} is density of water, kg/m³; $\rho_{kerosene}$ is density of kerosene, kg/m³; 47.5 is the surface tension of kerosene–water inter-

face, mN/m; ρ_w is density of aqueous phase, kg/m³; ρ_{oc} is density of organic collecting agent, kg/m³.

The results of measuring the wetting contact angle showed that the selected agents affect the wettability of the surface of diamond, talc, calcite, and muscovite (Fig. 3, a, b) with an apolar collecting agent to different extent. It has been established that the agent Neonol AF-9-6 reduces the wetting contact angle of kimberlite minerals to the greatest extent. However, when using this agent, the wetting contact angle decreases on the surface of diamonds too. An effect on a diamond that differs from other agents is observed when emulsifier OP-4 is added: after an initial decrease in the wetting contact angle in the concentration range of 0–130 mg/L, a noticeable increase in the measured value is observed at higher concentrations (see Fig. 3, a).

The minimal decrease in the wetting contact angle on kimberlite minerals is observed with the addition of alkylarylphosphonates (using NTPA as an example) and aliphatic alcohols (using PEG-1500 as an example). However, it should be noted that the decrease in the wetting contact angle when using these agents is significantly greater than on diamonds that indicates the potential benefit from their application. Organic polymers based on carboxymethylcellulose have the property of effectively reducing the oil receptivity of kimberlite minerals, but they also have a similar effect (to a lesser extent) on the attachment of apolar collecting agents on diamonds (see Fig. 3), which allows them to be used at very low concentrations.

The results of surface tension measurements at the collecting agent–aqueous phase interface, partially presented in Table 3, indicate differences in the action of the studied regulating agents. The agents representing the classes of ionogenic and non-ionogenic nitrogen-containing polymers (Neonol AF 9-6 and Oxypav A1218.30) and short-chain aliphatic amine (OP-4) exhibit surfactant properties, reducing the surface tension at the interface between an organic collecting agent and aqueous phase by 2.8–3 times (see Table 3).

Agents of other classes exhibit significantly lower surfactant properties, reducing surface tension by 10–25% at a concentration of 300–500 mg/L. The results of the surface tension measurements at the interface between an organic collecting agent and the aqueous phase in the presence of regulating agents were used to calculate the adhesion energy using equation (1).

The results of the calculations of adhesion energy on diamond, talc, calcite, and muscovite presented in Fig. 4 show that the agents studied reduce the adhesion energy of the apolar collecting agent on kimberlite minerals to different extent.

⁵ GOST R 50097–92 (ISO 9101–87) “Surfactants. Determination of Interfacial Tension. Drop Volume Method”.

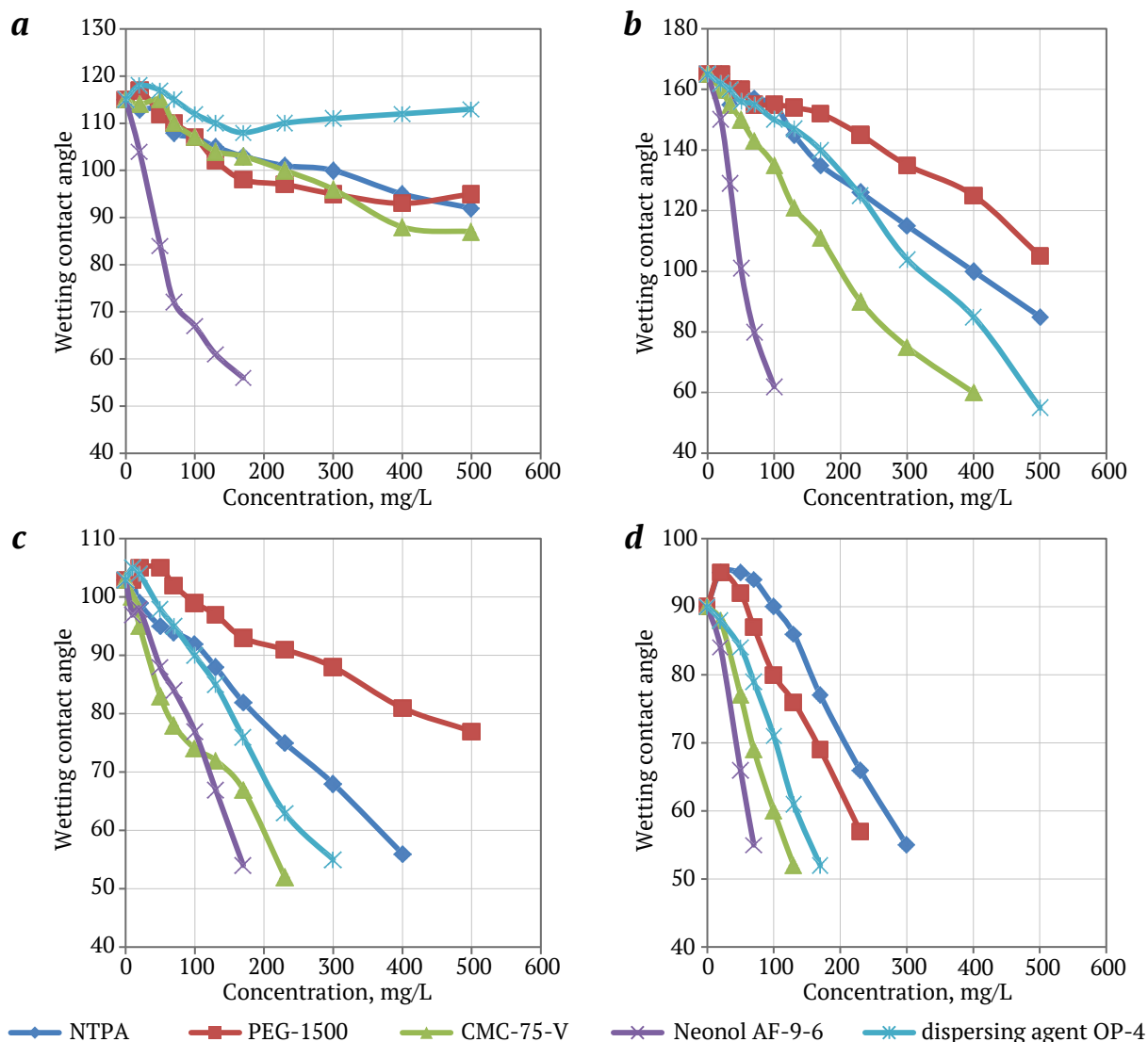


Fig. 3. The effect of regulating agents on wetting contact angle for the three-phase wetting perimeter of mineral – organic collecting agent – aqueous phase for diamond (a), talc (b), calcite (c), and muscovite (d)

Table 3

Results of measuring and calculating surface tension at the interface between organic collecting agent and aqueous phase (model high-salt water)

Regulating agents	Concentration, mg/l						
	0	50	100	170	230	300	500
	Surface tension, mN/m						
NTPA	30.43	30.08	28.04	27.44	27.04	26.56	26.08
OEDPA	30.43	27.43	25.34	22.99	21.65	20.34	20.17
EDTA	30.43	30.13	30.01	29.60	29.14	26.33	22.08
PEG-1500	30.43	28.45	27.05	24.83	24.00	24.45	24.60
STPP	30.43	26.20	25.24	25.01	24.78	25.12	22.50
Neonol AF 9-6	30.43	24.21	20.14	16.32	15.91	14.23	12.33
CMC 75-V	30.43	28.34	27.77	27.22	26.95	25.45	23.47
IS-3	30.43	30.01	29.07	28.56	28.34	27.77	27.40
KAMCEL-600	30.43	28.56	28.13	27.89	27.73	27.10	27.30
OP-4	30.43	23.11	19.10	16.24	15.22	13.56	11.65
OXYPAV A1218.30	30.43	20.66	14.34	11.01	9.52	9.45	9.04
Triethanolamine	30.43	28.33	27.40	26.22	26.00	26.04	25.91
Lactic acid	30.43	28.00	27.25	27.02	26.86	25.34	23.30

The adhesion energy of the organic collecting agent on diamond with the addition of regulating agents (except for Neonol AF-9-6) decreases by 1.5–2 times to values of 17–27.5 J/m² (see Fig. 4, *a*). On kimberlite minerals, the adhesion energy of the organic collecting agent decreases by 2.5–6 times and reaches values of 6–17 J/m² (see Fig. 4, *b, c, d*). Neonol AF-9-6 has the unusual ability to sharply reduce the adhesion energy of organic collecting agents on all samples, including diamonds.

To justify the hydrophilization of minerals under the influence of regulating agents, it seems appropriate to compare the adhesion energy of the organic collecting agent at “pre-critical” (before a collecting agent drop detaches) concentrations of regulating agents and the adhesion energy of the aqueous phase.

The measurement results showed that for muscovite, the measured value of the wetting contact angle of a model water drop in air was 38 degrees and, accordingly, the calculated adhesion energy of the aqueous phase was 5.7 J/m². The value obtained is close to the adhesion energy at “pre-critical” concentrations of regulating agents, ranging from 7 to 10.5 J/m² (see Fig. 4, *d*). Extrapolating the dependence of the adhesion energy on concentration to the “critical” concentration gives an adhesion energy value at the moment of a drop detachment of 5–7.5 J/m². This result allows to conclude that the detachment of a drop of the organic collecting agent from the mineral surface, i.e., its hydrophilization, occurs when the adhesion energies of water and the apolar collecting agent on the mineral are equal or close in value.

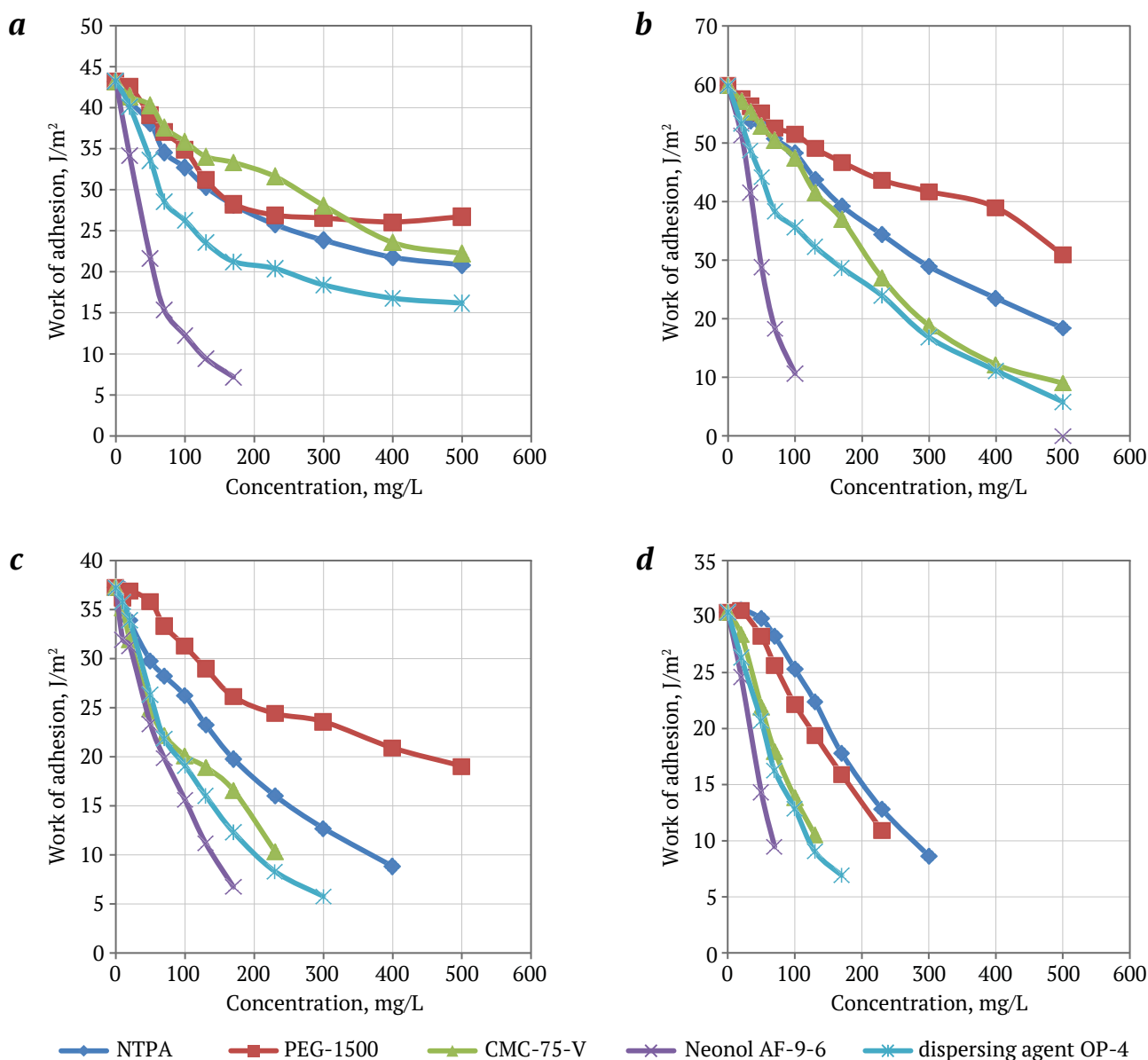


Fig. 4. The effect of regulating agents on the energy (work) of adhesion of an apolar collecting agent on diamond (*a*), talc (*b*), calcite (*c*), and muscovite (*d*)

Studies of the influence of regulating agents on the floatability of kimberlite minerals using an apolar collecting agent

The general regularities described above regarding the influence of regulating agents on the attachment of an organic collecting agent have been confirmed by the results of the studies on the floatability of kimberlite minerals and diamonds.

Flotation in laboratory conditions can be used to simulate the industrial process of froth separation. When studying the interaction of apolar collecting agents with the surface of floatable minerals, a close correlation is observed between the extent of collecting agent attachment on minerals and their floatability [20]. The monomineral flotation method in a Hallimond tube is a widely recognized method for assessing the hydrophobicity of mineral surfaces and evaluating the potential for using collecting agents in industrial processes [21].

For flotation tests, a fraction of a size of $-250 + 75 \mu\text{m}$ was separated from the crushed mo-

nominal material by screening, from which a mineral sample weighing 150 mg was taken. The sample was kept in a 35 ml of aqueous phase for 60 minutes. Then, a regulating agent was added to the aqueous phase, the sample was kept for 5 minutes, and a collecting agent, F-5 bunker fuel, was added. The conditioning stage with the collecting agent lasted 1 minute. The collecting agent consumption was 2 μl (about 1.86 mg) per 35 ml of the aqueous phase, and the collecting agent concentration during conditioning was 52 mg/l. After conditioning, the sample with the aqueous phase was loaded into a flotation unit, topped up with the aqueous phase, and floated for 4 minutes at a total air flow rate of 50 ml. The temperature of the aqueous phase in the conditioning and flotation stages was 24 °C.

The results of the flotation tests showed that the addition of different classes of regulating agents has different effects on the floatability of diamonds and kimberlite minerals (Fig. 5).

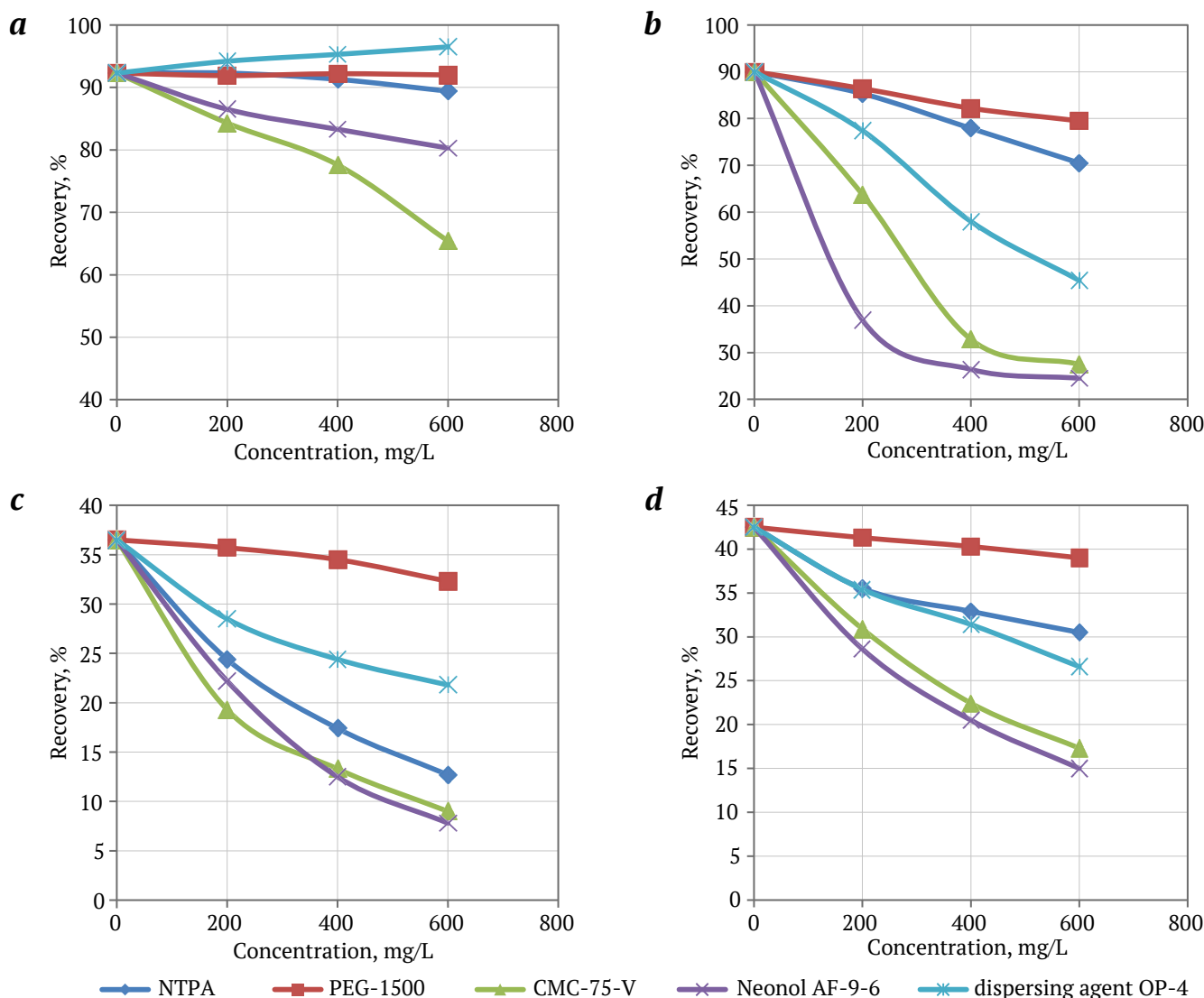


Fig. 5. The effect of regulating agents on floatability of diamond (a), talc (b), calcite (c), and muscovite (d)



A noticeable decrease in the recovery of diamonds and kimberlite minerals with the addition of a regulating agent is observed with CMC-75-V and Neonol AF-9-6. The character of the dependencies of diamond and kimberlite mineral recovery on the consumption of other regulating agents differs significantly. For instance, with NTPA addition, diamond recovery remains virtually unchanged, while the floatability of kimberlite minerals significantly decreases. PEG-1500 agent does not reduce the floatability of diamonds and has a relatively weak effect on the floatability of kimberlite minerals. OP-4 dispersing agent increases the floatability of diamonds and reduces the floatability of kimberlite minerals.

Further studies were conducted on kimberlites differing in the degree of metamorphism and mineral composition: kimberlite sample 1 was represented mainly by primary minerals: olivine (55%), phlogopite and muscovite (8%), pyroxene (7%), calcite (aragonite) (6%), dolomite (2.2%), chromite (2%), iron sulfides (1.2%), titanomagnetite (1.0%), pyrope (0.3%), etc.; kimberlite sample 2 was represented by calcite (aragonite) (34%), olivine (22%), phlogopite and muscovite (6.5%), dolomite (6.4%), pyroxene (4.4%), chromite (2%), talc (2%), iron sulfides (1.1%), titanomagnetite (1.0%), pyrope (0.25%), etc.

Before flotation, a kimberlite sample was deslimed and a material with a particle size of $-400 + 180$ μm went to flotation. The method of prepara-

tion and flotation of kimberlite corresponded to the method of flotation of diamonds and individual kimberlite minerals.

Based on the analysis of the data obtained during the flotation of diamonds and individual kimberlite minerals, a concentration of 200 mg/L of regulating agents was selected for kimberlite flotation tests (with an additional 50 mg/L for Neonol AF-9-6 and Oxypav A1218.30).

The results of the studies showed that it is feasible to suppress the floatability of kimberlites when using the tested regulating agents. The agents Neolon AF-9-6, Oxypav A1218.30, IS-3, and Kamcel 600 most intensively reduce the floatability (yield) of kimberlites (Table 4).

However, since applying certain agents resulted in a decrease in diamond recovery, specialized criteria, such as selectivity criteria, must be applied to assess their effectiveness and suitability for use. The selectivity was evaluated using the equation proposed in [1] for the froth separation process:

$$S = \varepsilon - 1.3\gamma, \quad (4)$$

where S is selectivity criterion; ε is diamond recovery; γ is yield (recovery) of kimberlite into concentrate.

The analysis of the calculated selectivity criterion showed that the highest selectivity of diamond flotation was achieved when using NTPA, OEDPA, IS-3, and OP-4 regulating agents (see Table 4).

Table 4

Influence of regulating agents on the flotation selectivity of diamonds and kimberlite

Regulating agent	Diamond recovery, %	Kimberlite yield into froth product, %		Selectivity criterion S , %	
		Sample 1	Sample 2	Sample 1	Sample 2
No additives	92.3	3.77	4.94	87.40	85.88
NTPA	92.5	2.04	2.51	89.85	89.24
OEDPA	92.3	2.57	2.56	88.96	88.97
EDTA	90.5	2.44	2.82	87.33	86.83
PEG-1500	91.9	5.65	4.86	84.56	85.58
STPP	88.3	2.31	3.69	85.30	83.50
Neonol AF 9-6	86.3	0.67	1.92	85.43	83.80
Neonol AF 9-6 (50 mg/L)	90.5	2.12	2.66	87.74	87.04
CMC 75-V	88.5	2.16	1.79	85.69	86.17
IS-3	90.4	1.36	2.44	88.63	87.23
KAMCEL-600	88.8	1.97	2.43	86.24	85.64
OP-4	94.2	2.44	5.12	91.03	87.54
Oxypav A1218.30	84.3	1.33	1.48	82.57	82.38
Oxipav A1218.30 (50 mg/L)	88.3	1.15	1.22	86.81	86.71
Triethanolamine	88.3	3.4	3.87	83.88	83.27
Lactic acid	89.2	3.2	3.99	85.04	84.01



Nevertheless, the feasibility of using some other studied regulating agents to increase the selectivity of flotation extraction of diamonds from kimberlites of various origins has been confirmed.

Thus, the studies conducted have established the feasibility of reducing the floatability of kimberlite minerals and kimberlite rock particles and improving the performance indicators of diamond-bearing kimberlite flotation using regulating agents of classes of alkylarylphosphonates, short-chain aliphatic amines, and complex agents. The use of agents with strong surfactant properties (ionic and nonionic nitrogen-containing short-chain polymers) will yield positive results when varying their consumption based on the data from the tests with reduced consumption of Neonol AF-9-8 and Oxypav A1218.30 agents.

Key findings

Based on the analysis of comprehensive physico-chemical studies of the interaction of apolar collecting agents and regulating agents of various classes with the surface of diamond-bearing kimberlite minerals and the results of flotation studies, regulating agents have been justified and selected that ensure increased selectivity of the processes of diamond-bearing kimberlite beneficiation by froth and X-ray luminescence separation.

Visiometric analysis has determined that, among kimberlite minerals, talc, calcite, muscovite, pyrite, and phlogopite possess the highest adhesive activity in relation to apolar collecting agents (oil receptivity) and flotation response.

According to the measurements of the wetting contact angle, a clear trend has been identified towards a decrease in the adhesive activity of flotation-active

kimberlite minerals in relation to the apolar collecting agent when using alkylarylphosphonates (NTPA, OEDPA), aliphatic alcohols (PEG-1500); bifunctionally modified CMC derivatives (CMC-75-V; Kamcel 600), ionogenic and non-ionogenic nitrogen-containing polymers (Neonol AF-9-6, Oxypav A1218.30), short-chain aliphatic amines (OP-4 dispersing agent), complex agents (IS-3 agent).

The calculations using the Dupré–Young equation (based on the experimentally obtained values of the wetting contact angle and surface tension at the interface between the organic collecting agent and the aqueous phase) showed that when regulating agents were added, the adhesion energy of the apolar collecting agent on kimberlite minerals, with the exception of talc, decreased by 2.5–6 times and reached values of 6–15 J/m², comparable to the adhesion energy of the aqueous phase (5.7 J/m²). At the same time, under similar conditions, the adhesion energy of the collecting agent on diamonds decreased to the values of 17–27.5 J/m² that caused the apolar collecting agent to adhere to diamonds stably. This fact predetermines the enhancement of the contrast in the flotation response of kimberlite minerals and diamonds due to applying the regulating agents and justifies the feasibility of increasing the selectivity of diamond flotation from kimberlites.

The results of the flotation studies on diamonds and kimberlites of different degrees of metamorphism confirmed the feasibility of increasing the selectivity of diamond flotation when using NTPA, OEDPA, IS-3, and OP-4 regulating agents. The listed regulating agents are recommended for testing in industrial froth separation processes in diamond-bearing kimberlite processing flowsheets.

References

1. Chanturiya V.A., Morozov V.V., Dvoichenkova G.P., et al. Optimizing composition and application conditions of agents for modifying spectral characteristics of diamonds in X-ray luminescence separation. *Mining Science and Technology (Russia)*. 2023;8(4):313–326. <https://doi.org/10.17073/2500-0632-2023-09-154>
2. Morozov V.V., Chanturia V.A., Dvoichenkova G.P., Chanturia E.L. Hydrophobic interactions in the diamond–organic liquid–inorganic luminophore system in modification of spectral and kinetic characteristics of diamonds. *Journal of Mining Science*. 2022;58(2):257–266. <https://doi.org/10.1134/S1062739122020090>
3. Kovalenko E.G., Babushkina A.L., Chut-Dy V.A. Application of multi-component collectors and selection of temperature modes for frother separation of diamond-bearing kimberlites. *Gornyi Zhurnal*. 2023;(12):51–62. (In Russ.) <https://doi.org/10.17580/gzh.2023.12.12>
4. Morozov V.V., Kovalenko E.G., Dvoichenkova G.P., et al. Current trends of improving the efficiency of froth separation of diamond-bearing kimberlites. *Mining Science and Technology (Russia)*. 2024;9(2):134–145. <https://doi.org/10.17073/2500-0632-2023-07-136>
5. Morozov V.V., Chanturia V.A., Dvoichenkova G.P., et al. Selecting organic collectors for luminophore-bearing modifying agents to extract weakly fluorescent diamonds. *Journal of Mining Science*. 2023;59(2):292–301. <https://doi.org/10.1134/S1062739123020126>



6. Nguyen A. V., Schulze H. J. *Colloidal science of flotation*. New York: Marcel Dekker; 92004. 850 p.
7. Kondratyev S. A. Thermodynamic conditions for the presence of physically sorbed collectors on a mineral surface in an elementary act of flotation. *Tsvetnye Metally*. 2024;(7):118–136. <https://doi.org/10.17580/tsm.2024.07.02>
8. Zhang J., Kouznetsov D. L., Yu M., et al. Improving the separation of diamond from gangue minerals. *Minerals Engineering*. 2012;36–38:168–171. <https://doi.org/10.1016/j.mineng.2012.03.015>
9. Verkhoturov M. V., Amelin S. A., Konnova N. I. Diamond beneficiation. *Mezhdunarodnyi Zhurnal Eksperimental'nogo Obrazovaniya*. 2012;(2):61. (In Russ.)
10. Sergienko V. I., Perfilov A. V., Ksenik T. V., Yudakov A. A. Obtaining and application of hydrophobic adsorbents on the basis of aluminosilicates. *Proceedings of the Kola Science Centre of the Russian Academy of Sciences*. 2015;(5):108–112. (In Russ.)
11. Zemtsov Yu. V., Mazaev V. V. *Current state of physicochemical enhanced oil recovery methods: a literature and patent review*. Yekaterinburg: LLC «Izdatel'skie resheniya»; 2021. 239 p. (In Russ.)
12. Popov K. I., Kovaleva N. E., Rudakova G. Y., et al. Recent state-of-the-art of biodegradable scale inhibitors for cooling-water treatment applications (review). *Thermal Engineering*. 2016;63(2):122–129. <https://doi.org/10.1134/S0040601516010092> (Orig. ver.: Popov K. I., Kovaleva N. E., Rudakova G. Y., et al. Recent state-of-the-art of biodegradable scale inhibitors for cooling-water treatment applications (review). *Teploenergetika*. 2016;(2):46–53. (In Russ.) <https://doi.org/10.1134/S0040363616010094>)
13. Siddiqui M. A. Q., et al. Current understanding of shale wettability: A review on contact angle measurements. *Earth-Science Reviews*. 2018;181:1–11. <https://doi.org/10.1016/j.earscirev.2018.04.002>
14. Dvoichenkova G. P., Kovalenko E. G., Timofeev A. S., Podkamennyi Yu. A. Enhanced efficiency of diamond foam separation after complex removal of hydrophilic slime coats from diamond surface. *Mining Informational and Analytical Bulletin*. 2022;(10):20–38. (In Russ.) https://doi.org/10.25018/0236_1493_2022_10_0_20
15. Bogatov M. V., Yudin P. E., Verevkin A. G., Berkov D. V. Effect of hydrophilicity, oleficity on formation of asphalt resin paraffin deposits. *Petroleum Engineering*. 2022;20(6):117–126. (In Russ.) <https://doi.org/10.17122/ngdelo-2022-6-114-123>
16. Samara H., Jaeger P. Experimental determination of wetting behavior under non-atmospheric conditions relevant to reservoirs: a practical guide. *SN Applied Sciences*. 2022;4:85. <https://doi.org/10.1007/s42452-022-04963-8>
17. Belhaj A. F., Elraies K. A., Mahmood S. M., et al. The effect of surfactant concentration, salinity, temperature, and pH on surfactant adsorption for chemical enhanced oil recovery: a review. *Journal of Petroleum Exploration and Production Technology*. 2020;10(1):125–137. <https://doi.org/10.1007/s13202-019-0685-y9>
18. Tret'yakov N. Yu., Panicheva L. P., Turnaeva E. A., et al. Synthesis of alkyl phosphates and investigation of their surface-active properties in an alkaline surfactant polymer system for enhanced oil recovery. *Proceedings of Universities. Applied Chemistry and Biotechnology*. 2021;11(1):147–158. (In Russ.) <https://doi.org/10.21285/2227-2925-2021-11-1-147-158>
19. Deryabin V. A., Farafontova E. P. *Physical chemistry of disperse systems*. Moscow: Yurayt; 2018. 86 p. (In Russ.)
20. Kondrat'ev S. A. Action of physisorbed collector in particle–bubble attachment. *Journal of Mining Science*. 2021;57(1):106–122. <https://doi.org/10.1134/S1062739121010129> (Orig. ver.: Kondrat'ev S. A. Action of physisorbed collector in particle–bubble attachment. *Fiziko-Tekhnicheskiye Problemy Razrabotki Poleznykh Iskopaemykh*. 2021;(1):118–136. (In Russ.) <https://doi.org/10.15372/FTPRI20210112>)
21. Błaszczów A., Ratajczak T., Szyszka D. Flotation of hydrophobic minerals in Hallimond tube. *Mining Science*. 2024;31:219–227. <https://doi.org/10.37190/msc243112>

Information about the authors

Valentin A. Chanturiya – Dr. Sci. (Eng.), Professor, Academician of the Russian Academy of Sciences, Research Institute of Comprehensive Exploitation of Mineral Resources of the Russian Academy of Sciences, Moscow, Russian Federation; ORCID [0000-0002-4410-8182](https://orcid.org/0000-0002-4410-8182), Scopus ID [7004497128](https://orcid.org/7004497128), ResearcherID [J-9712-2014](https://orcid.org/J-9712-2014); e-mail vchan@mail.ru

Valeriy V. Morozov – Dr. Sci. (Eng.), Professor of the Department of General and Inorganic Chemistry, Research Institute of Comprehensive Exploitation of Mineral Resources of the Russian Academy



of Sciences, Moscow, Russian Federation; ORCID [0000-0003-4105-944X](#), Scopus ID [7402759618](#); e-mail dchmggu@mail.ru

Elena L. Chanturiya – Dr. Sci. (Eng.), Professor, Professor of the Department of Enrichment and Processing of Mineral Resources and Technogenic Raw Materials, Research Institute of Comprehensive Exploitation of Mineral Resources of the Russian Academy of Sciences, Moscow, Russian Federation; ORCID [0000-0002-5757-4799](#), Scopus ID [57196009376](#), ResearcherID [J-4214-2014](#); e-mail elenachan@mail.ru

Andrey L. Samusev – Cand. Sci. (Eng.), Head of the Laboratory of Theory of Mineral Components Separation, Research Institute of Comprehensive Exploitation of Mineral Resources of the Russian Academy of Sciences, Moscow, Russian Federation; ORCID [0000-0001-7324-0353](#), Scopus ID [54894913500](#); e-mail samusev_a@ipkonran.ru

Received 01.09.2025

Revised 30.09.2025

Accepted 01.10.2025




POWER ENGINEERING, AUTOMATION, AND ENERGY PERFORMANCE

Research paper

<https://doi.org/10.17073/2500-0632-2025-09-461>

UDC 622:621.311

**Integration of digital technologies into the design process of power supply systems for mining enterprises**V.L. Petrov¹  , E.K. Burmatova², A.V. Pichuev¹   ¹ University of Science and Technology MISIS, Moscow Russian Federation² Promstroy Engineering LLC, Moscow, Russian Federation allexstone@mail.ru**Abstract**

The study focuses on the development of an integrated software solution for the automation of power supply system (PSS) design for industrial enterprises. The relevance of this work arises from systemic issues observed in existing software packages, such as fragmented design processes, the need for repeated manual data transfer between different platforms, dependence on specific manufacturers' equipment, and the lack of universal component selection tools. The research included a comprehensive analysis of current approaches to PSS design, the development of new automation methods, and the creation of algorithms for calculating electrical loads and selecting equipment. The methodological framework was based on regulatory standards and the principles of modular architecture, implemented in C# with integration into BIM platforms (nanoCAD) and spreadsheet processors (Excel). The key result is the creation of digital software that automates data collection from BIM models, calculation of electrical loads and short-circuit currents, and selection of PSS components. Practical testing on the power supply project of the Kumroch gold processing plant demonstrated an 80% reduction in manual operations, improved calculation accuracy, and independence from specific equipment manufacturers. The developed software solution effectively eliminates the main shortcomings of existing analogues by providing an end-to-end automated design process, which significantly enhances the efficiency, accuracy, and flexibility of design activities in the context of power sector digitalization.

Keywords


mining enterprises, digital technologies, electrical systems, power supply systems, design, digitalization, software, digital transformation, design automation

For citation

Petrov V.L., Burmatova E.K., Pichuev A.V. Integration of digital technologies into the design process of power supply systems for mining enterprises. *Mining Science and Technology (Russia)*. 2025;10(4):393–403. <https://doi.org/10.17073/2500-0632-2025-09-461>

ЭНЕРГЕТИКА, АВТОМАТИЗАЦИЯ И ЭНЕРГОЭФФЕКТИВНОСТЬ

Научная статья

Интеграция цифровых технологий в процесс проектирования систем электроснабжения горнопромышленных предприятийВ.Л. Петров¹  , Е.К. Бурматова², А.В. Пичуев¹   ¹ Университет науки и технологий МИСИС, г. Москва, Российская Федерация² ООО «Промстрой Инжиниринг», г. Москва, Российская Федерация allexstone@mail.ru**Аннотация**

Исследование направлено на разработку интегрированного программного решения для автоматизации проектирования систем электроснабжения (СЭС) промышленных предприятий. Актуальность работы обусловлена наличием системных проблем в существующих программных комплексах, таких как: фрагментированность процессов проектирования, необходимость многократного ручного переноса данных между различными платформами, зависимость от оборудования конкретных производителей и отсутствие универсальных решений для подбора компонентов. В ходе исследования выполнен ком-



плексный анализ современных подходов к проектированию СЭС, разработаны новые методики автоматизации, созданы алгоритмы расчета электрических нагрузок и подбора оборудования. Методологическую основу составили положения нормативных документов и принципы модульной архитектуры, реализованные на языке C# с обеспечением интеграции с BIM-платформами (*nanoCAD*) и табличными процессорами (*Excel*). Ключевым результатом стало создание цифрового программного обеспечения, автоматизирующего сбор исходных данных из BIM-моделей, расчет электрических нагрузок, токов короткого замыкания и подбор элементов СЭС. Практическая апробация на проекте электроснабжения золотоизвлекающей фабрики «Кумроч» продемонстрировала сокращение ручных операций до 80 %, повышение точности расчетов и обеспечение независимости от производителей оборудования. Разработанное программное решение эффективно устраняет основные недостатки существующих аналогов, обеспечивая сквозной автоматизированный процесс проектирования, что позволяет существенно повысить производительность, качество и гибкость проектных работ в контексте реализации стратегии цифровизации энергетики.

Ключевые слова

горнопромышленные предприятия, цифровые технологии, электротехнические системы, системы электроснабжения, проектирование, цифровизация, программное обеспечение, цифровая трансформация, автоматизация проектирования

Для цитирования

Petrov V.L., Burmatova E.K., Pichuev A.V. Integration of digital technologies into the design process of power supply systems for mining enterprises. *Mining Science and Technology (Russia)*. 2025;10(4):393–403 <https://doi.org/10.17073/2500-0632-2025-09-461>

Introduction

The electrical systems of mining enterprises are subject to specific requirements determined not only by the need to ensure efficiency and safety but also by the complexity of technological processes involved in the extraction and processing of mineral resources [1]. The key requirements include reliability, stability, safety, electric power quality, cost efficiency, ease of operation, and flexibility for modernization. However, the design of power supply systems (PSS) that meet these criteria involves addressing a set of unique challenges that have no universal solutions. This is primarily due to a combination of factors such as the diversity of mining technologies, variability of technological chains, as well as the geological and geographical uniqueness of deposits, which collectively preclude the possibility of creating invariant design approaches [2–4]. Therefore, the formalization of new design methodologies that can adapt to the specifics of a particular facility while integrating modern digital tools represents a relevant scientific and practical task.

Modern digital technologies for designing power supply systems of industrial facilities comprise a set of specialized programs within software packages that employ computer-based methods for creating, modifying, analyzing, and optimizing design solutions. This enables the development of more accurate PSS models, improves collaboration between design participants, and provides the possibility of visualizing projects.

Digital design technologies employ specialized programs, including BIM platforms (*Revit*, *nanoCAD* *BIM*, *ArchiCAD*), computer-aided design (CAD) sys-

tems (*AutoCAD*, *nanoCAD*, *SketchUp*), and visualization tools (*Lumion*, *V-Ray*), among others¹.

To identify the key features, strengths, and weaknesses of power supply system design processes at industrial enterprises, to substantiate the relevance of this topic, and to assess the degree of its development, an analysis of current research [5–7] was conducted. These studies reflect the main approaches to the automation of engineering calculations in PSS design [7–9] and were evaluated according to the following criteria:

- relevance to the project topic (load calculation, equipment selection, CAD integration) [7];
- practical orientation (tools used, architecture, programming languages) [8–10];
- regulatory compliance (adherence to GOST, PUE, and SP standards);
- application of modern technologies (*BIM*, integration with *Excel* and *nanoCAD*) [11–13].

The analyzed publications cover a wide range of solutions—from highly specialized calculation programs for 6–10 kV networks to *BIM*-integrated general design platforms. Most of them focus on improving the accuracy and speed of engineering calculations through the automation and formalization of methods regulated by industry standards [14–16].

The main directions of development in digitalization, improvement, and practical implementation of software integrating digital technologies into the

¹ Electrical design: digital technologies and their role in modern construction. Energy-Systems. Energy-systems; Russian BIM technologies: designing power supply systems in Model Studio CS. Habr. URL: <https://habr.com/ru/companies/nanosoft/articles/581434/>



design of electrical systems for industrial enterprises include the following [17–19]:

1. Automation of electrical load and short-circuit current calculations. This functionality is fundamental to almost all analyzed systems. In many cases, it is implemented in environments that allow straightforward integration with Excel or other tabular formats² [18, 19].

2. Equipment selection (cables, circuit breakers, transformers). Approaches vary from manual selection using tabulated data to semi-automated modules tied to specific manufacturers' product lines. Universal and vendor-independent solutions remain scarce.

3. Development of interfaces and interoperability assurance. Significant attention is paid to ensuring compatibility with alternative environments, particularly *nanoCAD*. Some projects implement data exchange through *Excel* (as a universal format), while others use *BIM* platform *APIs*. Ease of use and accessibility of the interface are crucial factors determining practical applicability.

4. Modular architecture and scalability. The most advanced systems are built on the principle of expandable modules, allowing new functions to be introduced gradually and adapted to client-specific requirements.

5. Software development considering the evolution of programming languages. Both outdated environments (e.g., C++ with *Access*) and modern C#-based approaches are found. A noticeable gap exists between academic developments and commercial solutions: the former are often cumbersome and difficult to implement, whereas the latter tend to be proprietary and brand-dependent.

Studies consistently demonstrate growing interest in automating design processes; however, most existing solutions exhibit several limitations:

- Many systems are tailored for use with components from specific brands (*Schneider*, *Siemens*, *ABB*, etc.), thus restricting their applicability in design organizations using products from multiple suppliers.

- Complex or overloaded interfaces. Some software packages, such as *EPLAN*, feature excessively intricate architectures requiring user training, whereas most engineers need to perform standard calculations quickly and without deep customization.

- Lack of an independent equipment selection module. In many cases, the selection of cables and equipment remains a manual or semi-automated process relying on limited databases. The project developed within this research aims to implement automated selection based on generalized parameters, improving flexibility and accuracy.

- Weak integration with *BIM* environments. Despite the widespread adoption of *BIM* modeling tools in engineering practice, only a few solutions support direct integration. The proposed software enables Excel-based data export from *nanoCAD*, simplifying linkage between calculations and *BIM* models.

- Limited dissemination of open solutions. Academic developments often do not progress to a fully functional prototype, lack documentation, and cannot be scaled.

Despite recent technological advances, current PSS design workflows at industrial and mining enterprises still include processes that require extensive, repetitive manual work. This issue primarily arises from the need to repeatedly transfer identical data between different software environments, often multiple times, since design inherently involves numerous revisions and iterations. These stages not only increase labor intensity and time consumption but also introduce a high probability of human error due to monotony and data volume.

Most existing software packages are produced by electrical equipment manufacturers, which compromises calculation objectivity and ties users to specific brands. Meanwhile, client companies typically maintain approved brand lists, requiring designers to use components from particular suppliers.

Analogous programs often have complex structures and unintuitive interfaces, demanding excessive time and effort to master.

Digitalization offers broad opportunities for implementing innovative solutions and optimizing the design process itself. This enables more accurate calculations, reduces the number of errors, and enhances overall project efficiency—particularly important under conditions where construction speed and resource optimization are critical.

Digital design technologies for PSS not only improve project quality but also significantly influence overall project budgets. The implementation of automated systems and software can reduce the time required for design development by up to 30%.

Moreover, the reduction in errors and rework achieved through precise calculations and modeling decreases the risk of additional costs, leaving more flexibility within the approved budget and creating room for the adoption of even more effective technological solutions.

A promising direction for introducing digital technologies into PSS design for industrial enterprises involves combining artificial intelligence and big data to enable real-time project adjustments and integration with renewable energy sources—such as solar panels and wind turbines—for more efficient use of sustainable energy.

² RTM 36.18.32.4–92 Guidelines for Electrical Load Calculation. VNIPI Tyazhelektroproekt; 1992.

Research objectives and tasks

The objective of this study is to develop architectural and methodological solutions for integrating digital technologies into the design process of electrical systems at mining enterprises by adapting software for calculating electrical loads and selecting power supply system components.

The main research methods include: comparative analysis, used to assess the functionality and limitations of modern software packages (*BIM* platforms, *CAD* systems, and calculation tools); mathematical modeling, applied for developing algorithms to calculate loads and short-circuit currents according to regulatory methodologies; algorithm design and programming, involving the creation of modular software in *C#* to automate calculations, equipment selection, and two-way integration with *Excel* and *nanoCAD* platforms; experimental testing, based on validating the software using real data from the power supply project of the Kumroch gold processing plant; systems approach, aimed at optimizing the design workflow as a unified cycle that eliminates manual operations and integrates all stages.

During the software development process, the following tasks must be accomplished.

1. Identify systemic problems, limitations, and evaluate the functionality of existing software packages.

2. Formalize and algorithmize the methodology for calculating electrical loads and short-circuit currents in accordance with regulatory standards, and develop algorithms for selecting PSS components.

3. Implement an integrated software package in *C#* that automates calculations, equipment selection,

and two-way data exchange with *nanoCAD* and *Excel* platforms to eliminate manual data transfer.

4. Test software modules using real data from a mining enterprise power supply project.

The expected outcome is a software package capable of performing load calculations and automatically selecting optimal equipment parameters based on *Excel* input data, taking into account electrical loads, short-circuit currents, and the overall configuration of the power supply system.

The product is intended for use by mining companies during the design or technical upgrading stages. Potential users include design organizations involved in developing PSSs for mining enterprises.

Architecture of the PSS design framework

The design process can be illustrated using the schematic shown in Fig. 1.

Input data are typically provided as a list of electrical loads, specifying their type, rated electrical (or mechanical) power, rated supply voltage, efficiency, power factor, operating mode, control location, power supply reliability category as defined by the Electrical Installation Code (PUE), annual operating hours, and location.

At Stage 1, the technical characteristics are used to calculate electrical loads. The calculation is performed in Microsoft Excel using the method of maximum demand and utilization factors. Although the use of software automates the computational part, human input is still required: first, to manually assign electrical loads to distribution boards; and second, to select the maximum demand factor from reference tables based on the utilization factor and the effective number of electrical loads.

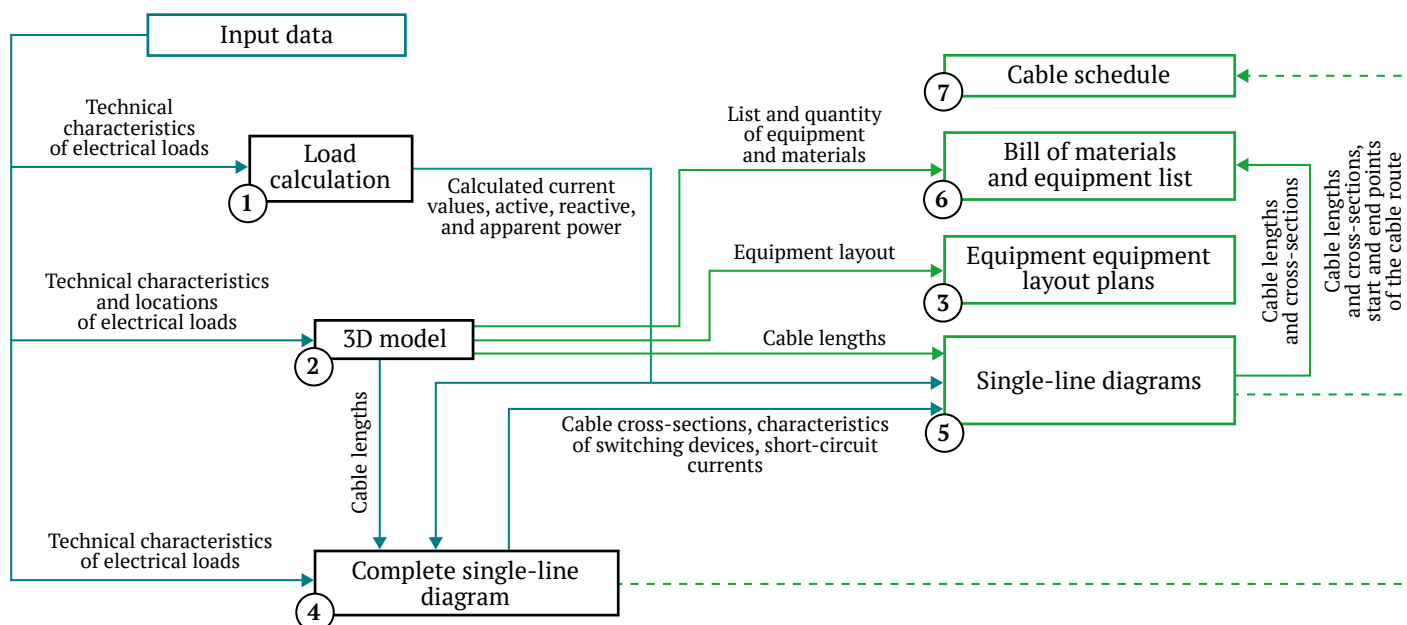


Fig. 1. Structural diagram of the current PSS design workflow

At Stage 2, using the initial data, electrical loads are manually added to the 3D model of the production facility created in the BIM platform. Each electrical load is then manually assigned to its power source in the model. Cable routes are generated automatically, but in some cases they require manual adjustment.

At Stage 3, equipment layout plans are prepared. This step is semi-automated: the designer defines section ranges to display each part of the production facility on separate drawings.

At Stage 4, the input data are used to create the complete single-line diagram of the power supply system. The diagram is manually assembled from individual elements (electrical loads, cable lines, bus sections, switching devices, etc.). The technical parameters of the loads and the cable lengths calculated at Stage 2 are entered manually, while the coefficients are adjusted so that the calculated values correspond to those obtained during the load calculation at Stage 1.

At Stage 5, single-line diagrams are prepared for each distribution board. Cable lengths from the board to each electrical load are automatically inserted into the diagrams based on the equipment arrangement in the model. The software also automatically selects cable cross-sections and the rated currents of circuit breakers. Unfortunately, many software packages do not display short-circuit current calculation results to the user, which forces designers either to use alternative tools for cable and switchgear selection or to perform these calculations manually. In the current workflow, this is done at Stage 4. The parameters of the devices and the cable cross-sections are then entered into the diagrams manually. For

each distribution board, the parameters calculated at Stage 1-active, reactive, and apparent power, design current, power factor, and utilization factor-are added.

At Stage 6, a bill of materials and equipment list are generated using built-in *BIM*-platform functions.

At Stage 7, a cable schedule is compiled within the *BIM* platform.

Thus, the existing design workflow requires repeatedly performing identical, monotonous operations to transfer information between different software environments and reconcile data between them. This not only complicates the designer's work and increases labor and time costs, but also introduces numerous errors caused by the human factor.

This workflow clearly requires optimization. The analysis shows that one of the most effective simplifications is to combine Stages 1 and 4 using an external software module. The corresponding design workflow is shown schematically in Fig. 2.

Key changes:

- stages 1 and 4 of the original workflow are eliminated through automation;
- data are exchanged between *Excel* and the *BIM* platform automatically, without manual intervention;
- load calculation, short-circuit current analysis, and equipment selection are integrated into a single computational algorithm.

Such optimization significantly reduces manual work, streamlines the design workflow, and minimizes the risk of data transfer errors when processing large volumes of project information.

The technological process implemented in the software is illustrated in Fig. 3.

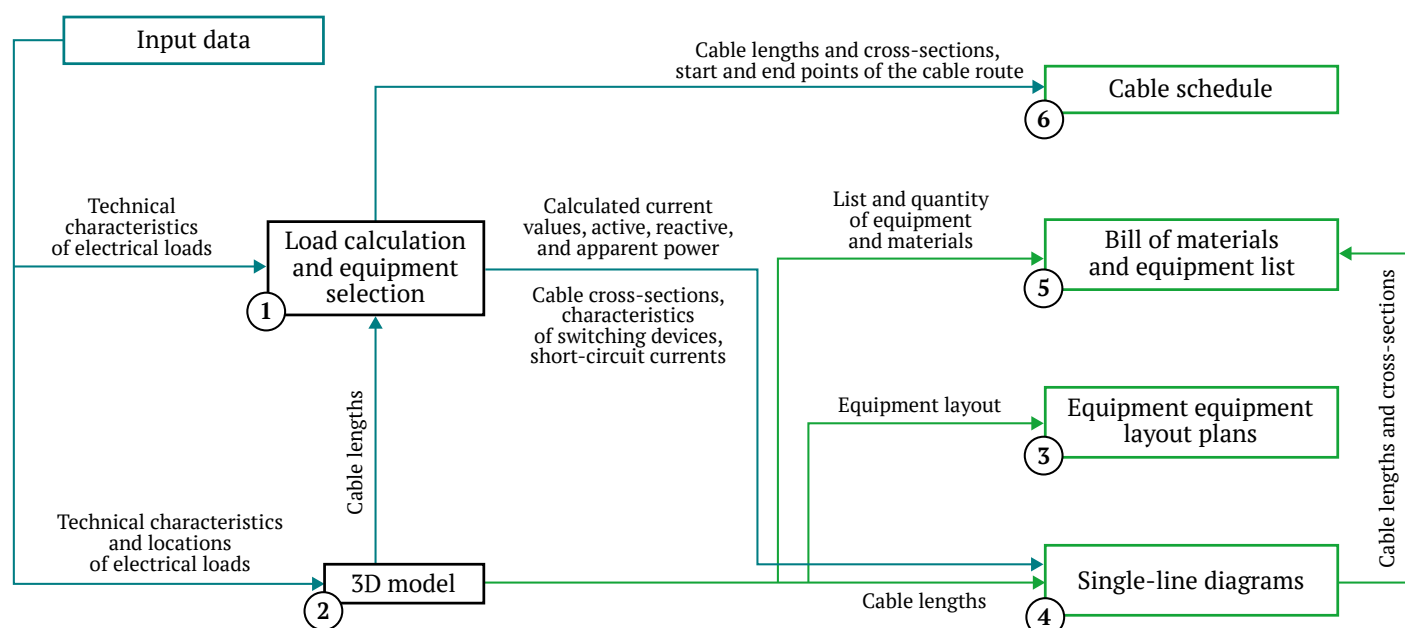


Fig. 2. Structural diagram of the optimized PSS design workflow



The block diagram represents the program structure designed to automate electrical load calculation and equipment selection in accordance with regulatory requirements. It integrates the stages of data input, parameter calculation, equipment selection, and report generation, meeting the research objective of reducing manual operations, improving accuracy, and ensuring interoperability with existing engineering tools.

The input data for the program are stored in an *Excel* spreadsheet that includes the electrical parameters of the loads, the power source, and the length

of the supply cable. These data are automatically imported from the *BIM* platform.

The electrical load calculation module performs computations in accordance with the regulatory methodology RTM 36.18.32.4-92, taking into account load grouping (individual consumers, low-voltage switchboards, and distribution panels), calculation coefficients, power types (active, reactive, apparent), and current values. At this stage, the program also determines the required capacity of reactive power compensation devices and selects transformer ratings.

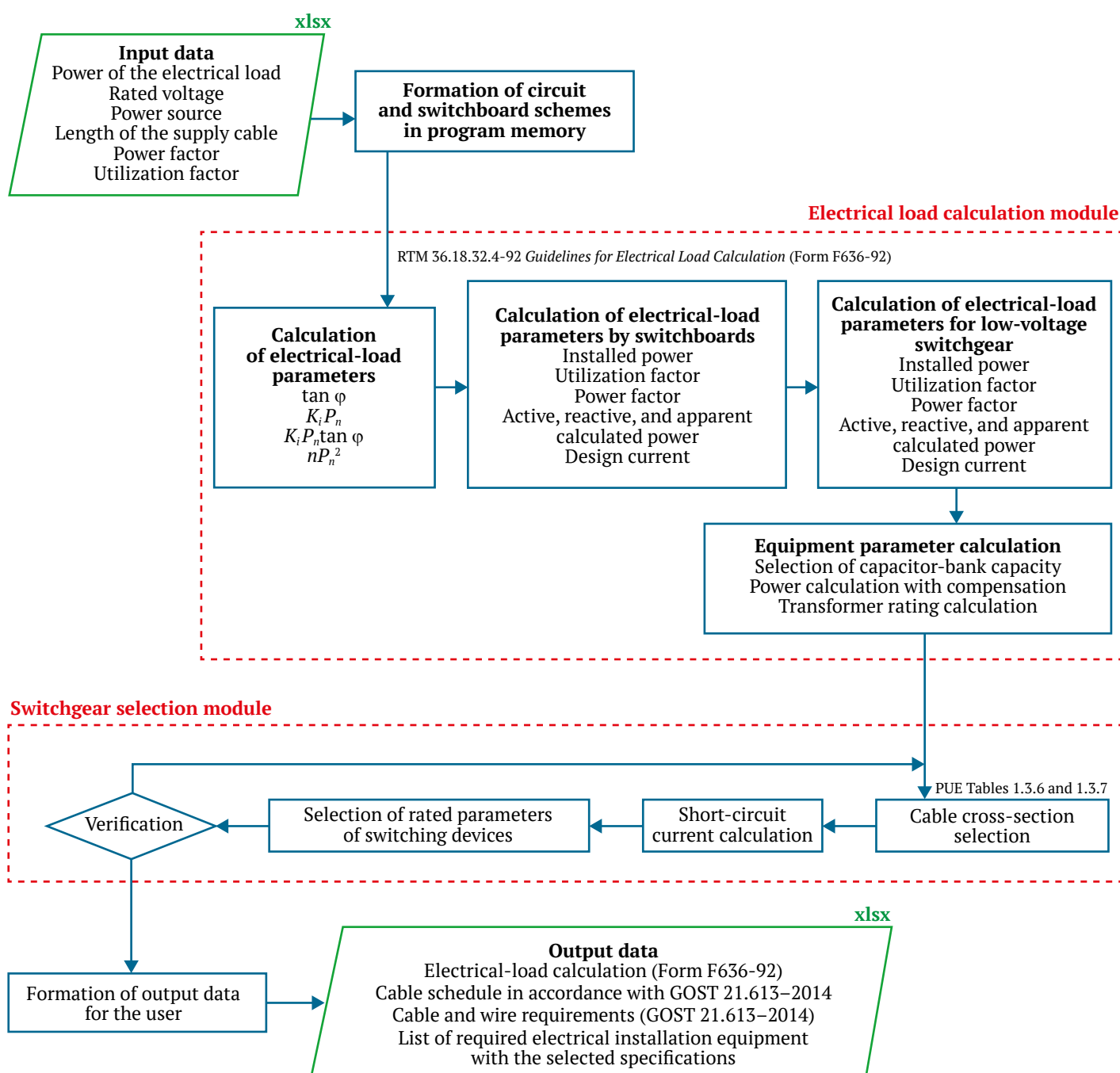


Fig. 3. General block diagram of the calculation algorithm



The next module is responsible for equipment selection. Based on the calculated data and short-circuit current values, the program determines cable cross-sections according to the PUE tables and selects the rated parameters of protective and switching devices. All results are automatically verified for compliance with specified parameters, after which the output data are generated.

The output data, presented in Excel format, include: electrical load calculations in accordance with Form F636-92; cable schedule compliant with GOST 21.613-2014; cable and wire specifications as per GOST 21.613-2014; a bill of materials and equipment list with the selected specifications.

The software is developed in C#, a programming language offering broad capabilities for engineering applications, including efficient tabular data processing (particularly *Excel*), convenient interface design tools, and native integration with the Windows environment, which is standard in engineering practice. C# provides high calculation reliability through strict typing and compile-time verification, while supporting modular architecture suitable for scalable functional expansion. These advantages make it an optimal choice for developing digital software (DS) for PSS design automation and equipment selection.

The choice of *Excel* and *nanoCAD* is driven by both technological and practical considerations related to the requirements of modern engineering and CAD environments. *Excel* serves as the primary tool for data entry, storage, and structuring, providing a universal, flexible, and widely accepted tabular format that easily adapts to various design stages. Its built-in data processing functions enable two-way communication between the calculation module and the engineering model, eliminating manual data transfer and reducing the risk of errors.

The *nanoCAD* platform functions as a *BIM*-modeling environment, meeting the requirements of modern design organizations and supporting an end-to-end information model of a building or industrial facility. Its capacity to store geometric and parametric data on equipment, cable routing, and connection points makes it indispensable for the comprehensive design of electrical networks within an integrated construction model. Furthermore, the availability of an open *API* ensures integration with external calculation algorithms and enables the automation of processes such as cable routing, specification generation, and single-line diagram creation. Thus, the combination of *Excel* and *nanoCAD* ensures effective linkage between analytical and graphical design components, reduces routine operations, enhances the accuracy of

engineering solutions, and ensures compliance with regulatory documentation.

Accordingly, the presented DS provides a unified design algorithm that encompasses all key stages—from data input to the generation of calculated and technical characteristics of the equipment. It automates repetitive operations, minimizes the human factor, and ensures conformity with regulatory standards. Integrating this algorithm into the design workflow significantly simplifies the process of electrical network design, enhancing its accuracy, reliability, and efficiency.

Practical implementation: case study of a gold processing plant power supply project

Let us consider the practical implementation of the project using the example of the power supply system of the Kumroch gold processing plant (GPP). The main power source for the GPP facilities is an autonomous containerized diesel power plant (DPP) with a rated voltage of 6.3 kV and heat recovery systems.

The digital software receives data on the formed circuits from the 3D model and generates load calculation tables for each distribution point at every level. A fragment of the electrical load calculation table for one of the transformer substations is shown in Fig. 4.

The calculation is performed in accordance with the technical guideline *Guidelines for Electrical Load Calculation* RTM 36.18.32.4-92 [18], and its results are documented using the standard Form F636-92³.

After the load calculation has been generated, the DS simultaneously performs short-circuit current calculations at all levels of the power supply system and selects the parameters of cable lines and switching devices, taking into account selectivity. This approach ensures high accuracy and speed of computations. The DS summarizes the calculation results in a table convenient for further use by the designer. Using the parameters calculated by the DS, the user can easily select equipment from the chosen manufacturer. A fragment of the equipment selection results is shown in the single-line diagram (Fig. 5).

Since the calculation in the program is performed automatically and requires virtually no additional actions from the designer, it is possible, if necessary, to repeatedly update the results with minimal labor input when the input data are revised. This increases the flexibility of the design process and adapts the DS to the conditions of continuous changes in system components during the development of power supply solutions.

³ Table 4. Guiding Technical Material “Guidelines for the Calculation of Electrical Loads” of 30.07.1992 No. RTM 36.18.32.4-92. VNIPI TYAZHPROMELECTROPROJECT; 1992.



Input data								Calculated quantities			Effective number of electrical loads (n_e)	Calculated load factor (K_p)	Calculated power			Calculated current, A
According to process specifications					According to reference data			$K P_n$	$K P_n \tan \varphi$	$n P_n^2$			$n_e = (\sum P_n)^2 / \sum n P_n^2$	Active power, kW	Reactive power, kvar**	
Electrical load (EL) description	EL designation	Quantity of EL, pcs (n)	Rated (installed) power, kW*		Utilization factor (K_i)	Reactive power factor								$P_p = K_p \sum K P_n$	$Q_p = 1.1 \sum K P_n \tan \varphi$ (if $n_e \leq 10$); $Q_p = \sum K P_n \tan \varphi$ (if $n_e > 10$)	$S_p = \sqrt{P_p^2 + Q_p^2}$
			of one EL, P_n	total $P_n = n P_n$			$\cos \varphi$	$\tan \varphi$								
1	2	3	4	5	6	7	8	9	10	11	12	13	14	15	16	17
TP-1, Gold Processing Plant site																
Ore preparation section – coarse crushing complex (KKD)																
Mobile crushing unit equipment																
Jaw crusher installation on crawler chassis CMS96:	1110-TJC-001															
Grizzly feeder	1110-GFS-001	1	15	15.00	0.6	0.82	0.70	9.000	6.282	225			9.00	6.28	10.98	
Jaw crusher	1110-CRJ-001	1	90	90.00	0.6	0.87	0.57	54.000	30.603	8100			54.00	30.60	62.07	
Main conveyor	1110-CVR-001	1	11	11.00	0.6	0.84	0.65	6.600	4.263	121			6.60	4.26	7.86	
Exhaust fan	V1	1	0.07	0.07	0.7	0.8	0.75	0.049	0.037	0.0049			0.05	0.04	0.06	
Electric heater	O1	3	0.80	2.40	0.6	0.95	0.33	1.440	0.473	1.92			1.44	0.47	1.52	
Operator workstation	ARM	1	0.75	0.75	1	0.8	0.75	0.750	0.563	0.5625			0.75	0.56	0.94	
Security cabinet KKD-SHOS (SPS-12 ver.12)	KKD-SHOS	1	0.7	0.70	1	1	0.00	0.700	0.000	0.49			0.70	0.00	0.70	
Server cabinet KKD TS-SS	KKD TS-SS	1	3.5	3.50	1	1	0.00	3.500	0.000	12.25			3.50	0.00	3.50	
Ore preparation section – SKDR (Equipment of the crushed ore loading unit with underground crushing tunnel)																
Apron feeder	1120-FDA-001+002	2	15	30.00	0.6	0.82	0.70	18.000	12.564	450			18.00	12.56	21.95	
Iron separator	1120-MGT-001	1	4	4.00	0.6	0.82	0.70	2.400	1.675	16			2.40	1.68	2.93	
Metal detector	1120-MGT-002	1	0.2	0.20	0.6	0.85	0.62	0.120	0.074	0.04			0.12	0.07	0.14	
Vibratory feeder	1120-FDA-003	1	5	5.00	0.1	0.85	0.62	0.500	0.310	25			0.50	0.31	0.59	
Emergency shower		6	6.5	39.00	0.4	0.9	0.48	15.600	7.555	253.5			15.60	7.56	17.33	
...																
Lime milk preparation section																
Tank for preparation of 10% lime milk solution	1840-TNK-002 1840-AGI-002	1	22	22.00	0.75	0.83	0.67	16.500	11.088	484			16.50	11.09	19.88	
Chemical pump	1840-PUM-004	1	15	15.00	0.75	0.82	0.70	11.250	7.853	225			11.25	7.85	13.72	
Service tank for lime milk solution	1840-TNK-003 1840-AGI-003	1	32	32.00	0.75	0.85	0.62	24.000	14.874	1024			24.00	14.87	28.24	
Emergency tank, V = 50 m³	1840-TNK-001 1840-AGI-001	1	22	22.00	0.75	0.83	0.67	16.500	11.088	484			16.50	11.09	19.88	
Total for TP-1		755	2677	3137	0.68	0.91	0.46	2128	982	280790	35	0.85	1808.85	981.70	2058.08	2970.58
Total (including transformer losses)															2160.98	3119.10
Transformer load factor Kz (1T1, 1T2 2×2500 kVA)															Kz=	0.43
Loads not included in the calculation:																
Electric hoist, lifting capacity 2 t	1210-HST-002	1	8	8.00	0.3	0.5	1.73	2.400	4.157	64			2.40	4.16	4.80	
Electric hoist, lifting capacity 2 t	1120-HST-001+002	2	5	10.00	0.1	0.85	0.62	1.000	0.620	50			1.00	0.62	1.18	
Scrubber pump	1210-PUM-006	1	30	30.00	0.75	0.85	0.62	22.500	13.944	900			22.50	13.94	26.47	
...																
Air compressor	8000-CMP-006	1	315	315.00	0.7	0.95	0.33	220.500	72.475	99225			220.50	72.47	232.11	
Screen feed pump	1210-PUM-002	1	22	22.00	0.7	0.75	0.88	15.400	13.582	484			15.40	13.58	20.53	
Total for TP-1, loads not included in the calculation				1502.8												
Total installed power for TP-1				4639.6												

Notes:

* Standby EL, as well as loads operating for short periods, are not included in the calculation

**The guidelines do not apply to the determination of electrical loads with highly variable load profiles (such as electric drives of rolling mills, arc furnaces, contact welding units, etc.), industrial electric transport, residential and public buildings, or electrical loads with a known load schedule.

Fig. 4. Fragment of electrical load calculation for transformer substation 1 (TP-1)

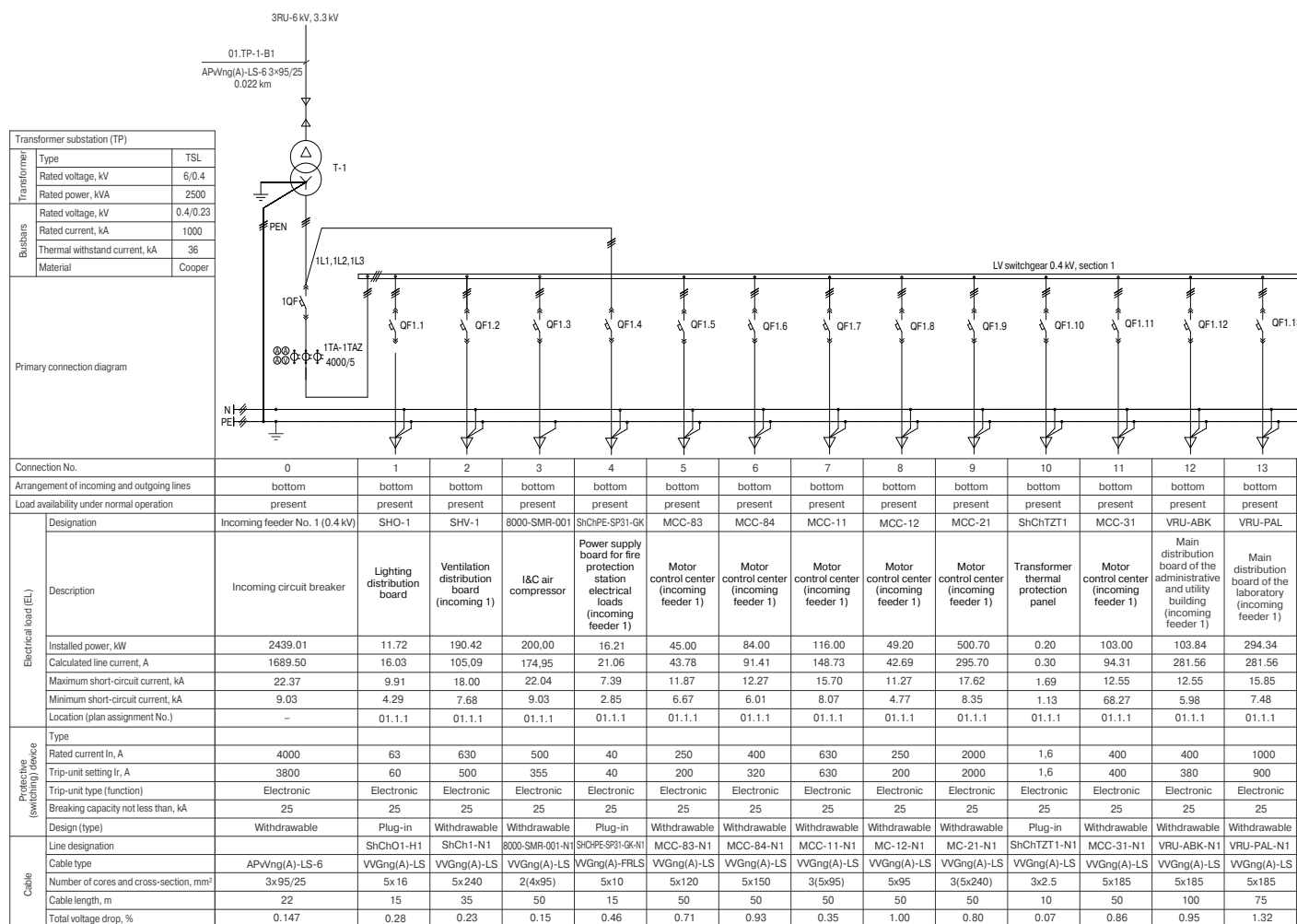


Fig. 5. Fragment of the single-line electrical diagram of TP-1

Based on the results of the power supply system calculation for the Kumroch GPP, the authors in [20] evaluated the effectiveness of potential use of alternative power sources in autonomous power supply systems [21].

Conclusions

The developed (DS significantly reduces the number of manual data transfer operations-by up to 80%-while remaining independent of equipment manufacturers' libraries. It requires minimal user involvement and does not demand specialized training to operate.

The DS automates the design process of power supply systems, simplifying and accelerating workflow operations, minimizing the likelihood of human error, and improving calculation accuracy. These features are essential for design organizations aiming to maintain client demand, remain competitive, and meet the current level of technological development.

Compared to existing software packages, the developed DS provides a more convenient format for in-

put and output data in Excel tables, which minimizes manual data transfer. This, in turn, simplifies and accelerates work and enhances the precision of calculations.

Unlike similar programs, data reading is fully automated, and the DS requires minimal human intervention, which eliminates the need for additional training, ongoing technical support, or consultations.

Another advantage is that the developed DS is not tied to any specific electrical equipment manufacturer, enabling users to perform equipment selection independently while retaining full freedom of choice for designers and customers.

The solution has considerable potential for implementation in design organizations, as it aligns with the digitalization strategy of the energy sector and meets the market demand for flexible, independent, and scalable design tools.

Future development prospects involve the integration of artificial intelligence for real-time automatic project adjustments and the addition of calculation modules for alternative energy sources.



References

1. Pichuev A. V., Peturov V. I., Suvorov I. F. *Impact of non-stationary modes on electrical safety during the operation of mining enterprises' electrical equipment*. Monograph. Moscow: Gornaya Kniga; 2011. 326 p. (In Russ.)
2. Klyuev R. V. Development of a methodology for calculating swings in an electrical system. *Sustainable Development of Mountain Territories*. 2024;16(3):1205–1213. <https://doi.org/10.21177/1998-4502-2024-16-3-1205-1213>
3. Petrov V. L., Pichuev A. V. Assessing the efficiency of measures to enhance electric power quality in variable-frequency drive for scraper conveyors. *Mining Science and Technology (Russia)*. 2024;9(1):60–69. <https://doi.org/10.17073/2500-0632-2024-01-198>
4. Klyuev R. V. Assessment of energy efficiency improvement strategies for ventilation and hoisting systems during the reconstruction of the Molibden mine. *Mining Science and Technology (Russia)*. 2025;10(1):84–94. <https://doi.org/10.17073/2500-0632-2024-10-362>
5. Shemetov A. N., Ilina E. A., Kondrashova Yu. N. Information processing in the automated power supply system of a residential microdistrict for determining electric loads. *Software of Systems in the Industrial and Social Fields*. 2021;9(2):29–37. (In Russ.) <https://doi.org/10.18503/2306-2053-2021-9-2-29-38>
6. Stepanov V. M., Kosyrikhin V. S. Application of the program-methodical complex for calculation and design of electrical supply. *Izvestiya Tula State University. Technical Sciences*. 2018;(12):180–186. (In Russ.)
7. Lyashan I. K., Parfenov Ya. A., Golovanova K. A. Design of internal power supply scheme. *Vestnik Nauki*. 2024;3(3):614–622. (In Russ.)
8. Dmitriev A. A., Gerasimov V. E., Ploskov A. N. Application of modern software capabilities in the design of power supply systems. *Electrical and Data Processing Facilities and Systems*. 2019;15(1):20–25. (In Russ.) <https://doi.org/10.17122/1999-5458-2019-15-1-20-25>
9. Klochkova N. N., Obukhova A. V. Automation of design of 6–10 kV power supply systems for industrial facilities. *Nauchnyi Almanakh*. 2024;(7–2):49–51. (In Russ.)
10. Bashirov M., Yusupova I., Bitkulov R. Comparative analysis of software and computing systems for the design of power supply systems. *Vestnik of Kazan State Power Engineering University*. 2021;13(1):37–51. (In Russ.)
11. Trunov S. S., Krupnov A. V. CAD with independent design of power supply systems, taking into account the criteria of reliability and efficiency. *Vestnik of Tver State Technical University. Series "Building, Electrical Engineering and Chemical Technology"*. 2024;(1):57–74. (In Russ.) <https://doi.org/10.46573/2658-7459-2024-1-57-74>
12. Anishchenko V. A., Kirspu A. Yu. Accounting for the uncertainty of initial information in the design of power supply systems. *Vestnik Gomel'skogo Gosudarstvennogo Tekhnicheskogo Universiteta imeni P. O. Sukhogo*. 2005;(3):25–29. (In Russ.)
13. Fedosha D. V. Optimal design of power system. *Elektrotehnika i Elektroenergetika*. 2012;(1):57–61. (In Russ.)
14. Stepanov V. M., Kosyrikhin V. S. Methodology of calculation and design of electric networks of system of industrial power supply. *Izvestiya Tula State University. Technical Sciences*. 2014;(8):215–222. (In Russ.)
15. Romanova V. V. The program for determining the optimal location for installation of symmetry facilities in 0.4 kV power supply systems with a motor-drive load. *Journal of Siberian Federal University. Engineering and Technologies*. 2020;13(5):643–651. <https://doi.org/10.17516/1999-494X-0253>
16. Yakovkina T. N., Starodubtsev A. A., Chekhovskiy S. N. Designing the power supply system for the sulfate soap decomposition department of the "ILIM" Group Branch in Bratsk. *Proceedings of Bratsk State University. Series: Natural and Engineering Sciences*. 2018;2:68–72. (In Russ.)
17. Dobrodey A. O., Voronovich A. A. Automation of calculations in the designing of power supply systems of residential buildings. *Agrotehnika i Energoobespechenie*. 2018;(1):35–46. (In Russ.)
18. Savchuk I. V., Smolin N. I., Serov A. I. Automation of short-circuit current and voltage loss calculations in power supply systems and integration into a CAD system. *AgroEkoInfo*. 2023;(5). (In Russ.) <https://doi.org/10.51419/202135539>
19. Volkov N. A. The introduction of BIM technologies in the process of designing power supply networks. *Scientific Technical and Economical Cooperation in Asia-Pacific Countries in the 21st Century*. 2024;2:19–23. (In Russ.)
20. Pichuev A. V., Gribkova O. S., Burmatova E. K. Assessment of energy efficiency of alternative power sources in independent power supply systems of mining and processing plants. *Energy Safety and Energy Economy*. 2024;(4):43–49. (In Russ.)



21. Sofronov M.A., Petrov V.L. Prospects for solar power plants in electricity supply systems in mines. *Mining Informational and Analytical Bulletin*. 2024;(10):152–165. (In Russ.) https://doi.org/10.25018/0236_1493_2024_10_0_152

Information about the authors

Vadim L. Petrov – Dr. Sci. (Eng.), Vice-Rector, Professor of the Department of Energy and Energy Efficiency of the Mining Industry, University of Science and Technology MISIS, Moscow, Russian Federation; ORCID [0000-0002-6474-5349](https://orcid.org/0000-0002-6474-5349), Scopus ID [8919065900](https://scopus.org/8919065900), ResearcherID [P-9984-2015](https://orcid.org/P-9984-2015); e-mail petrovv@misis.ru

Elizaveta K. Burmatova – Design Engineer of the Electrical Engineering Department, Promstroy Engineering LLC, Moscow, Russian Federation; e-mail: burmatova.elz@gmail.com

Alexander V. Pichuev – Dr. Sci. (Eng.), Professor of the Department of Energy and Energy Efficiency of the Mining Industry, University of Science and Technology MISIS, Moscow, Russian Federation; ORCID [0000-0001-7457-5702](https://orcid.org/0000-0001-7457-5702), Scopus ID [57209798580](https://scopus.org/57209798580); e-mail allexstone@mail.ru

Received 02.09.2025

Revised 11.10.2025

Accepted 17.10.2025